AD-A083 014 NAVAL UNDERWATER SYSTEMS CENTER NEWPORT RI F/G 8/3
THE WINDWAVE AND TURBULENCE OBSERVATION PROGRAM (WAVTOP). THE M--ETC(U)
MAY 79 MIPR-Z-70099-7-71825-A
UNCLASSIFIED USCG-D-68-79 NL

1 OF 2
AD A083014

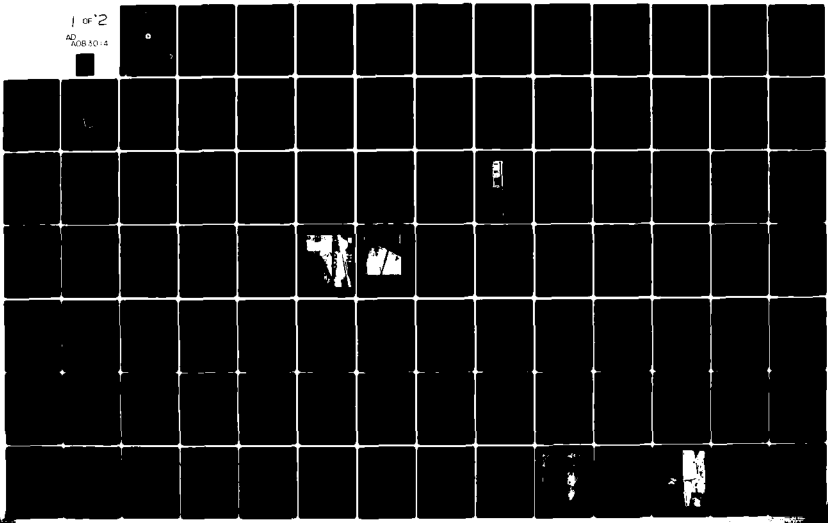

LEVEL II

(12)

REPORT NO. CG-D-68-79

THE WINDWAVE AND TURBULENCE OBSERVATION PROGRAM (WAVTOP)

The Measurement of Parameters Controlling Downward Mixing of Oil From the Sea Surface

David H. Shonting
Paul Temple
John Roklan

Naval Underwater Systems Center
Ocean Technology Division
Newport Laboratory, Newport, RI 02840

ADA083014

JULY 1979

FINAL REPORT

Document is available to the U.S. Public through the National Technical Information Service, Springfield, Virginia 22161

PREPARED FOR

US DEPARTMENT OF TRANSPORTATION
UNITED STATES COAST GUARD
OFFICE OF RESEARCH AND DEVELOPMENT
WASHINGTON, D.C. 20590

Technical Report Documentation Page

1. Report No. 19
CG-D-68-79

2. Government Accession No.

3. Recipient's Catalog No.

4. Title and Subtitle
The Windwave and Turbulence Observation Program (WAVTOP). The Measurement of Parameters Controlling Downward Mixing of Oil From the Sea Surface.

5. Report Date 11
May [redacted]79

6. Performing Organization Code
DOT/USCG

7. Author's 10
David H. Shonting, Paul R. Temple [redacted]
John Roklan

8. Performing Organization Report No.

9. Performing Organization Name and Address
Ocean Technology Division
Naval Underwater Systems Center
Newport, RI 02840

12 103

10. Work Unit No. (TRAIS)

11. Contract or Grant No. 15
MIPR [redacted]-Z-70099-7-71825-A

12. Sponsoring Agency Name and Address
Office of Research and Development
United States Coast Guard
Washington, D.C. 20590

13. Type of Report and Period Covered 9
Final Rep[redacted]t.
1 May 77 - 22 Jul 79

14. Sponsoring Agency Code
G-DMT-4

15. Supplementary Notes

16. Abstract

Wind-generated whitecaps have been identified as providing the key mechanism by which an oil slick is fragmented and injected beneath the sea surface. Ambient motions of the wind waves and smaller-scale turbulence then mix the oil further downward, to an extert dependent upon the kinetic energy of the motions.

The wave anc turbulence observation program (WAVTOP) has developed instrumentation and techniques to gather field data of the wind-generated motions in the upper ocean. The sensor package (BLT) includes small fast-response impellers and a capacitance wave staff system to measure particle velocity components and free surface elevation to determine shear, kinetic and potential energy content, and Reynolds stresses in the upper 5-10m. The battery-powered recording system utilizes a microprocesser digitizer programmable for data sampling.

Preliminary measurements were made with the BLT mounted on the AESOP Stable Spar Buoy and from a fixed boom on Gould Island. Results portray kinetic energy attenuating exponentially with depth and correlating with the local wind speed. The vertically integrating energy appears to correlate with the cube of the wind speed with a 15-20 min time lag.

Auto-spectra of the velocity data display narrow peaks demonstrating the monochromaticity of small wind waves. The spectra verify the attenuation of the wave energy with depth. Higher frequency (wave number) energy persists at deeper depths suggesting the presence of ambient turbulence. Reynolds stresses show fluctuations with time but display downward momentum flux and range from 1-2 dyne/cm^2 for winds from 4-5 m/sec.

17. Key Words
WIND WAVES, WAVE TURBULENCE, WAVE ENERGY MOMENTUM FLUX, WIND STRESS, IMPELLER METERS, OIL MIXING, WAVE MOTIONS

18. Distribution Statement
Document is available to the public through the National Technical Information Service, Springfield, Virginia 22161

19. Security Classif. (of this report)	20. Security Classif. (of this page)	21. No. of Pages	22. Price
Unclassified	Unclassified	103	

Form DOT F 1700.7 (8-72)

Reproduction of completed page authorized

METRIC CONVERSION FACTORS

Approximate Conversions to Metric Measures

Symbol	When You Know	Multiply by	To Find	Symbol
	LENGTH			
in	inches	*2.5	centimeters	cm
ft	feet	30	centimeters	cm
yd	yards	0.9	meters	m
mi	miles	1.6	kilometers	km
	AREA			
in^2	square inches	6.5	square centimeters	cm^2
ft^2	square feet	0.09	square meters	m^2
yd^2	square yards	0.8	square meters	m^2
mi^2	square miles	2.6	square kilometers	km^2
	acres	0.4	hectares	ha
	MASS (weight)			
oz	ounces	28	grams	g
lb	pounds	0.45	kilograms	kg
	short tons (2000 lb)	0.9	tonnes	t
	VOLUME			
tsp	teaspoons	5	milliliters	ml
Tbsp	tablespoons	15	milliliters	ml
fl oz	fluid ounces	30	milliliters	ml
c	cups	0.24	liters	l
pt	pints	0.47	liters	l
qt	quarts	0.95	liters	l
gal	gallons	3.8	liters	l
ft^3	cubic feet	0.03	cubic meters	m^3
yd^3	cubic yards	0.76	cubic meters	m^3
	TEMPERATURE (exact)			
°F	Fahrenheit temperature	5/9 (after subtracting 32)	Celsius temperature	°C

*1 in = 2.54 (exactly). For other exact conversions and more detailed tables, see NBS Misc. Publ. 286, Units of Weights and Measures, Price $2.25, SD Catalog No. C13.10:286.

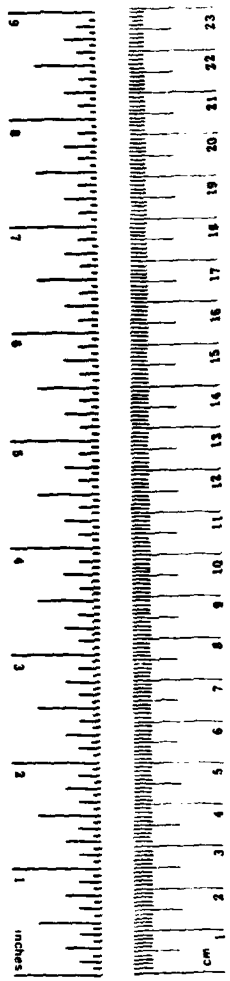

Approximate Conversions from Metric Measures

Symbol	When You Know	Multiply by	To Find	Symbol
	LENGTH			
mm	millimeters	0.04	inches	in
cm	centimeters	0.4	inches	in
m	meters	3.3	feet	ft
m	meters	1.1	yards	yd
km	kilometers	0.6	miles	mi
	AREA			
cm^2	square centimeters	0.16	square inches	in^2
m^2	square meters	1.2	square yards	yd^2
km^2	square kilometers	0.4	square miles	mi^2
ha	hectares (10,000 m^2)	2.5	acres	
	MASS (weight)			
g	grams	0.035	ounces	oz
kg	kilograms	2.2	pounds	lb
t	tonnes (1000 kg)	1.1	short tons	
	VOLUME			
ml	milliliters	0.03	fluid ounces	fl oz
l	liters	2.1	pints	pt
l	liters	1.06	quarts	qt
l	liters	0.26	gallons	gal
m^3	cubic meters	35	cubic feet	ft^3
m^3	cubic meters	1.3	cubic yards	yd^3
	TEMPERATURE (exact)			
°C	Celsius temperature	9/5 (then add 32)	Fahrenheit temperature	°F

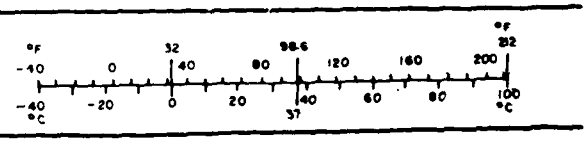

PREFACE

This report is submitted to the U.S. Coast Guard by the Naval Underwater Systems Center (NUSC) in completion of "Field Measurements Study of Turbulence and Waves" (MIPR - No. Z-70099-7-71825-A). The object of this work was to make measurements in the ocean of parameters controlling the downward mixing of oil in the surface layer. This required review of theory and recent laboratory wave tank studies, definition of parameters, and development of a system for their measure, and finally, making a series of field observations followed by analysis.

This work is one of four related programs sponsored by the U.S. Coast Guard to identify the sea state threshold beyond which containment and recovery of an oil slick is impractical because of the intensity of wind wave and turbulent mixing. The other programs are (1) A preliminary theoretical study by Arthur D. Little Inc., (2) A laboratory study of the properties of oil slicks and their dispersion by the Massachusettes Institute of Technology (MIT), and (3) An experimental laboratory study of turbulent dispersion in wind waves by Flow Industries, Inc.

During 1978-1979 research on the WAVTOP project was presented at the following meetings:

1. Oil Spill Conference, Newport, RI - Feb/78.
2. Tenth Annual Colloquium On Ocean Dynamics at University of Liege (Shonting and Temple, 1978), Liege, Belgium - Jun/78.
3. 1979 Oil Spill Conference, Los Angeles, CA. - Apr/79.
4. Workshop on the Physical Behavior of Oil in the Marine Environment. Princeton University, Princeton, NJ - 8-9/May/79 (Shonting, Petrillo, and Temple, 1979).

This NUSC study was conducted by Dr. David Shonting (Principle Investigator) of the Ocean Technology Division with assistance from Mr. John Roklan of the Exploratory Development Division (NUSC) who designed and directed assembly of the data logging system and associated software, and Dr. Paul Temple of the Graduate School of Oceanography, University of Rhode Island (URI) who assisted in field observations, analyses and report preparation.

Field assistance was provided by Mr. Anthony Petrillo of the Department of Ocean Engineering, URI and Mr. William Ryan of the Exploratory Development Division (NUSC) who was instrumental in assembling and testing the microprocessor systems. The efforts of Ms. Dale Licata and Ms. Robin Robertson both of the Department of Ocean Engineering (URI) in the field experiments and for analyzing data are gratefully acknowledged. Thanks is also owed to Mr. Angelo Mazarreli, Captain of the R/V BROWN, and Mr. Michael Kinane, president of Sheilco Corp., for assistance in field work and instrument fabrication. Early planning and calibrations were ably assisted by Mr. A.T. Massey of the Ocean Technology Division (NUSC) and Mr. Gary Peterson, president of Peterson Engineering, Seattle. Special gratitude is owed to Ms. Eileen Domingos, our group secretary, for her untiring patience in manuscript typing and, in general, helping to minimize the entropy inherent in the report preparation.

This research was monitored by Mr. Richard A. Griffiths of the U.S. Coast Guard. We gratefully acknowledge his support in the form of stimulating discussions and cheerful and enduring patience throughout the course of this study.

List of Symbols Used in Text

a = wave amplitude (cm).

D = depth (cm or m).

D_E = frictional dissipation of fluctuating motions (erg/cm^{2}s).

D_m = frictional dissipation of mean flow (erg/cm^{2}s).

Fo = vertical net oil flux from mixing by wave motions (gm/cm^{2}s).

Fx, Fz = frictional components in x and z directions (dyne/cm^3).

g = gravitational acceleration ($\sim$ 980 cm/s^2).

$KE(z)$ = kinetic energy of fluctuating motions as a function of depth (erg/cm^3).

p' = fluctuating dynamic pressure (dyne/cm^2) associated with wave motions.

T = averaging or total record time (s).

$u(t)$ = horizontal velocity component in the direction of wind wave propagation (cm/s); a function of time t.

$v(t)$ = horizontal velocity component parallel to wave crests (cm/s).

$w(t)$ = vertical velocity component; positive upward (cm/s).

x = direction of wave propagation (positive).

y = direction of wave crests.

z = vertical axis positive upward and having its origin at the mean free surface level of the ocean.

z_T = wave trough depth (cm).

$(\bar{\ })$ = mean value of ( ).

$(\ )'$ = fluctuation about $(\bar{\ })$; such that $(\bar{\ })' = 0$.

$\eta(t)$ = level of the free surface (cm) measured at a location (x,y).

ρ = mass density (gm/cm^3).

ω = circular frequency (rad/s).

TABLE OF CONTENTS

I. INTRODUCTION

A large tanker collision or grounding can quickly release large volumes of oil to the sea, producing an immense slick which under most conditions produces disastrous results. To predict the fate of this slick poses a difficult, if not an intractable, problem. Consider the possibilities. At best, the surface oil is advected by a mean current or blown by local winds which disperse it laterally over the open sea (as occurred with the ARGO MERCHANT disaster in 1977). Less favorable conditions of wind and current can cause a high oil deposition on a coast. Perhaps the worst effect is when oil, churned up by high seas, is mixed downward and, in shallow regions, causes oil penetration into the bottom sediments as was seen in the AMOCO CADIZ disaster (ENDECO, 1978). (In this case it was believed that the high turbulent energy conditions caused much bottom sediment to become suspended and combine with the vertically mixed oil; the resulting resettling carried the oil-sediment mixture to the bottom.) In short, horizontal advection can flush away surface and volume distributed oil, but oil contaminated sediment caused by vertical mixing may reside for months or years, having disastrous effects on sea life near and at the bottom.

Millions of dollars are being spent to design and test oil recovery equipment to function on the open seas, where, during high wave energy conditions, the clean-up problem is formidable. Practically all equipment and techniques being devised are for recovery of surface floating oil, a relatively simple problem as compared to trying to purge oil which has been vertically mixed within the water column. It is thus important that we attempt to understand the mechanisms by which oil is mixed vertically, knowledge which is necessary to devise systems and techniques to combat the

spread and vertical mixing of surface oil. It is also important that we obtain the ability to assess the energy and intensity of mixing as it is related to the sea state in order to judge at what point it is impractical to utilize oil containment and recovery techniques.

The Wave and Turbulence Observation Program (Project WAVTOP) was initiated by the Naval Underwater Systems Center (NUSC) with its purpose to define and make measurements of dynamic parameters which promote the vertical mixing of spilled oil on the open sea. The Project WAVTOP is designed to complement Coast Guard sponsored studies of oil spill dynamics which include wave tank modeling of breaking waves in an oil slick (Lin et al, 1978), theoretical studies of the relation of sea state to the dispersion of oil spills (Raj, 1977) and studies of oil mixing properties and breaking waves in a tank (Milgram et al, 1978). It is the necessary welding of theory, laboratory experiments, and actual field measurements from which it is hoped that we can forge workable predictive models of the behavior of oil slicks under various wind and sea conditions.

During these WAVTOP studies from 1/May/1977 to 1/December/1978, we have developed and calibrated a new system to measure the dynamic properties of wind generated surface motions (waves and turbulence), made several preliminary field observations, and summarized the data. This report reviews the WAVTOP effort and suggests future studies.

(This report includes results drawn from a large amount of recorded wave motion data. Field data of wave motions is available as tabulations and on magnetic tape. These data could be made available upon request to: Dr. D. Shonting, Ocean Science Branch, Naval Underwater Systems Center, Newport, RI 02840.)

II. PARAMETERS ASSOCIATED WITH OIL MIXING IN THE UPPER LAYER

The calm ocean exhibits a minimal effect upon an oil slick; a mean current may advect the oil, spreading it laterally. The only waves present per se may be swells from a distant storm that produce essentially irrotational motions which transmit no oil or, for that matter, produce little vertical momentum flux.

The onset of wind, stressing the sea surface, produces a variety of new surface motions. The initial response is the generation of capillary waves which in turn appear to feed momentum into the sea surface to form progressively larger wind waves that are accompanied by a mean horizontal wind-generated current and a mean vertical shear. The waves increase in size with wind speed and form whitecaps when the wind speed exceeds 6-7 m/s. It is in these conditions that we begin to observe vertical mixing of an oil slick.

What specific parameters or mechanisms govern vertical transfer of oil through the sea surface and into the surface layer? Recent studies shed light on this question:

A. Raj (1977), *in summarizing oil mixing parameters, as related to wind and sea states, specified the depth variations of the mean square velocity fluctuations, the integral scale of turbulence, and the energy spectrum of the free surface elevation.*

B. Milgram, et. al. (1978) *determined from observations of breaking waves in a tank that the most significant influence on the dispersion of oil into submerged droplets is that of breaking waves. Thus, the oil film is fragmented by the high energy breaking turbulence and is injected beneath the free surface as droplets. The motion of these droplets is then determined by the balance of the buoyancy of the oil droplets (upward) and the*

Reynolds stresses tending to mix the oil (downward). The scales of the mixing motions may be much larger than the breaking turbulence. In fact, they may be of the scales of the surface wave motions themselves.

C. *Lin et. al, (1978) observed from wind and wave flume measurements, that wave breaking initially introduces oil vertically as a "strong vertical burst motion like a plume plunging downwards below the water surface" penetrating about one wave height. Spectra of the motions show a dominant peak at the wave frequency with a "Kolmogorov" ($-^5/_3$) fall-off for two decades of frequencies. Oil concentration resulting from the wave breaking was exponentially distributed with depth.*

From the above results, it appears that the vertical transfer of oil through the sea surface is a two-step process. First, breaking whitecaps supply large "point" concentrations of high wave number turbulent stress which overcome the surface tension and break or fragment the oil into globules and spew them downward (Figure 1A). Second, after the oil globules are scattered beneath the sea surface they will be mixed downward by those internal motions which are rotational and transfer stress. The motions existing in the upper layer are basically orbital or "orbital related" motions of the wind waves themselves, having scales from a few centimeters to the orbital diameters associated with the largest wind waves present. The vertical extent of the oil mixing is directly related to the mean kinetic energy of the local orbital motions of the waves, found to decrease exponentially with depth (e.g., Shonting, 1967). Thus, the combined net effects of both whitecaps and the subsurface wave motions will create a steady state vertical oil gradient (Figure 1B).

Oil mixing is thus associated with surface wave motions which transfer stress and kinetic energies. Figure 2 is a contrived spectrum depicting

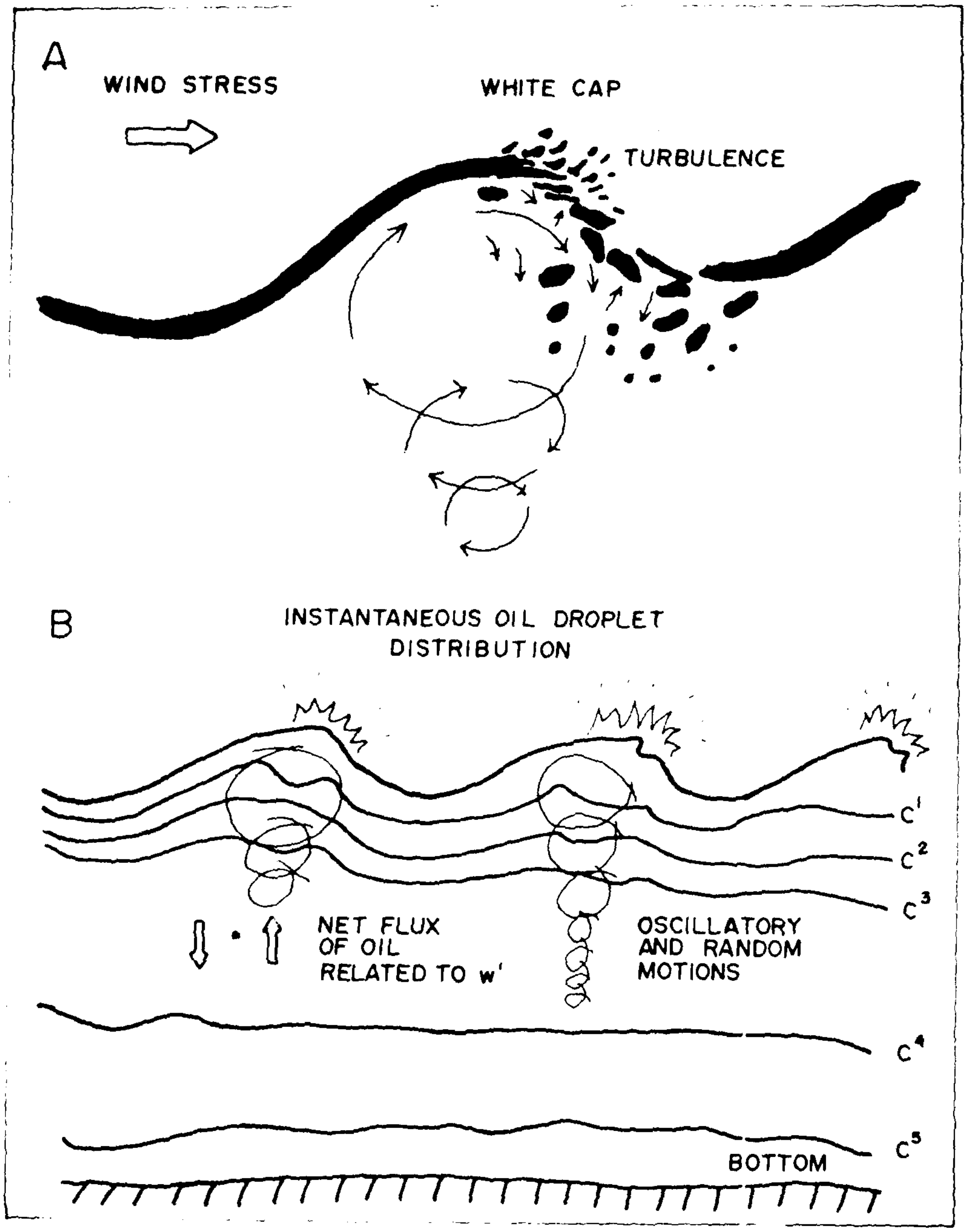

Figure 1: A) Oil slick (black boundary) is fragmented by breaking wave turbulence which overcomes surface tension of both water surface and oil layer. B) Continuous subsurface mixing by the rotational components of the wave motions distributes oil downward producing an oil concentration gradient from the "plane source" at the surface.

the types of wind generated motions of interest. Calm conditions (heavy line) have little energy in the scales or frequencies of our "mixing motions" (orbital scales and smaller). The "windy" spectrum up to the breaking wave peak delineates the energy bands producing stress and mixing (beyond, scales become so small and isotropic that little net stress and oil transfer should occur). From Figure 2, it appears that our measurements should concentrate on motions whose scales fall in the hatched regions.

Very few (if any!) measurements have been made in the open sea for verification of the effects of breaking waves and kinetic energy intensity upon oil mixing. Ideally, observations should be made in an oil spill area first in uncontaminated open sea conditions to obtain baseline data and then similar observations made in situ in an oil spill environment. This latter study may be over-ambitious since oil spills are not often provided specifically for such studies. Moreover, the occurrence of an accidental major oil spill results in a chaos in which the conducting of scientific experiments is likely not to be given high priority.

At the time of this wiriting, the Northern Cherbourg Peninsula of France is still recovering from a disastrous oil spill resulting from the wreck of the 200,000 ton oil tanker, AMOCO CADIZ. After the spill, persistent high winds and rough seas served to mix and spread the light crude oil over a wide coastal zone. On-scene measurements were made by ENDECO (1978) of the vertical concentration of oil at stations along the coast and in a brackish estuary. Sections made from 7 km offshore to the shoal beaches indicated high concentrations of oil dispersed 3-4 m downward offshore, but, nearer the beaches where waves were breaking, the oil was totally distributed throughout the water column from 5-12 m. These results indicate that the oil distribution within the water was very dependent upon

Figure 2: Contrived ocean spectra of calm conditions (heavy line) and windy conditions which produce rotational mixing motions (hatched spectra). High frequency (or wave number) turbulence (dissipation region) builds up in windy conditions but its energy is so small it is ineffective for vertical mixing.

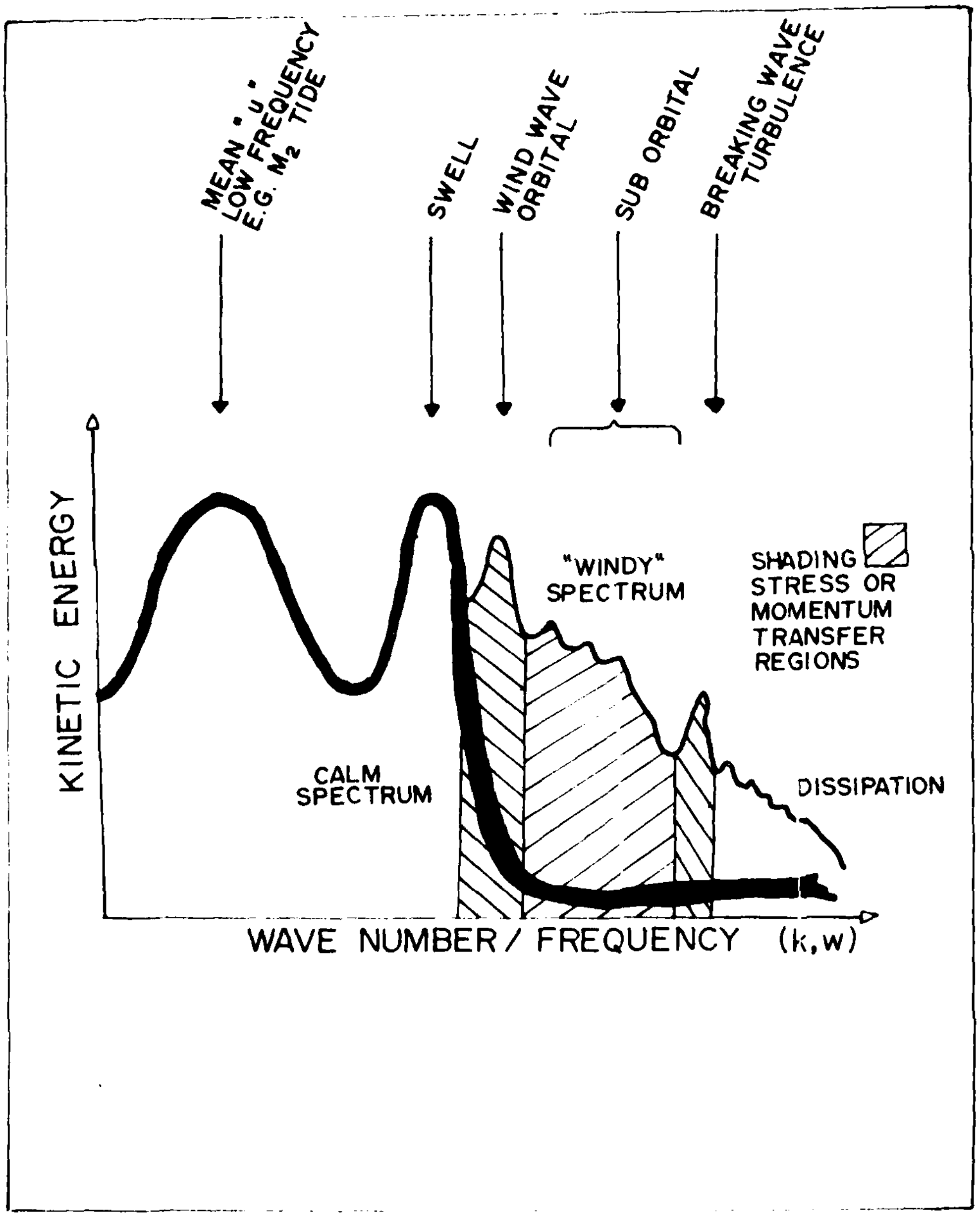

the presence of breaking wind waves, a verification of the laboratory results cited above.

One objective of our study is to determine the energetics associated with the wind wave motions and relate it to the character of the wind itself. In the following section, we construct a theoretical framework to relate the variables measured to the physical concepts of momentum and energy fluxes.

III. ON THE ENERGETICS OF WIND WAVE MOTIONS: WHAT TO MEASURE

Since the parameters related to oil mixing are dynamic quantities related to momentum and energy it is instructive that we define oil mixing as it relates to basic conservation concepts applied to the sea surface region. We shall formulate expressions for the time rate of change of energy and momentum related to wind wave motions in terms of measurable quantities within the upper layer. The analysis follows that of Starr (1968) who has utilized the Reynolds formulation of fluxes from covariance relationships of fluctuating quantities to better understand a wide variety of transport phenomena in the atmosphere, oceans and even spiral galaxies (Starr and Newell, 1963).

We consider the upper 10 m layer of the ocean (Figure 3) within which we wish to measure motions associated with wind-generated surface waves. In the presence of the waves, the physical measurement of these motions, for practical reasons, must be made at or below the level z_T which is the wave trough level (i.e., a region occupied by water at all times). The x axis, defining the z_T level, points positive in the direction of the progressive wind waves and the z axis points positive upward having its origin at the mean free surface. For our formulations we make the following assumptions:

1. We consider motions only in the x and z directions, neglecting cross wave velocities, i.e., parallel to wave crests.

2. Motions occurring at speeds producing particle displacements associated with gravity waves are virtually unaffected by Coriolis forces.

3. The mean sea surface is essentially horizontal, and the local density is assumed constant. Therefore, no mean horizontal pressure gradients are present in the water other than those associated with a slowly varying barotropic tide.

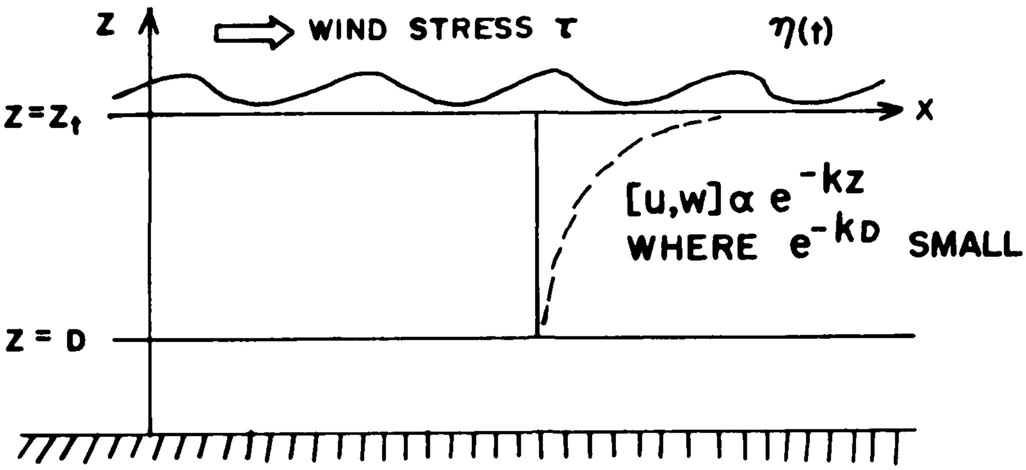

Figure 3: A two-dimensional ocean from which we estimate the time variation of mean and eddy kinetic energy. The layer above z_T is where the wind stress is directly applied. Velocity measurements are made from $z = z_T$ to $z = D$ where the motions become negligible.

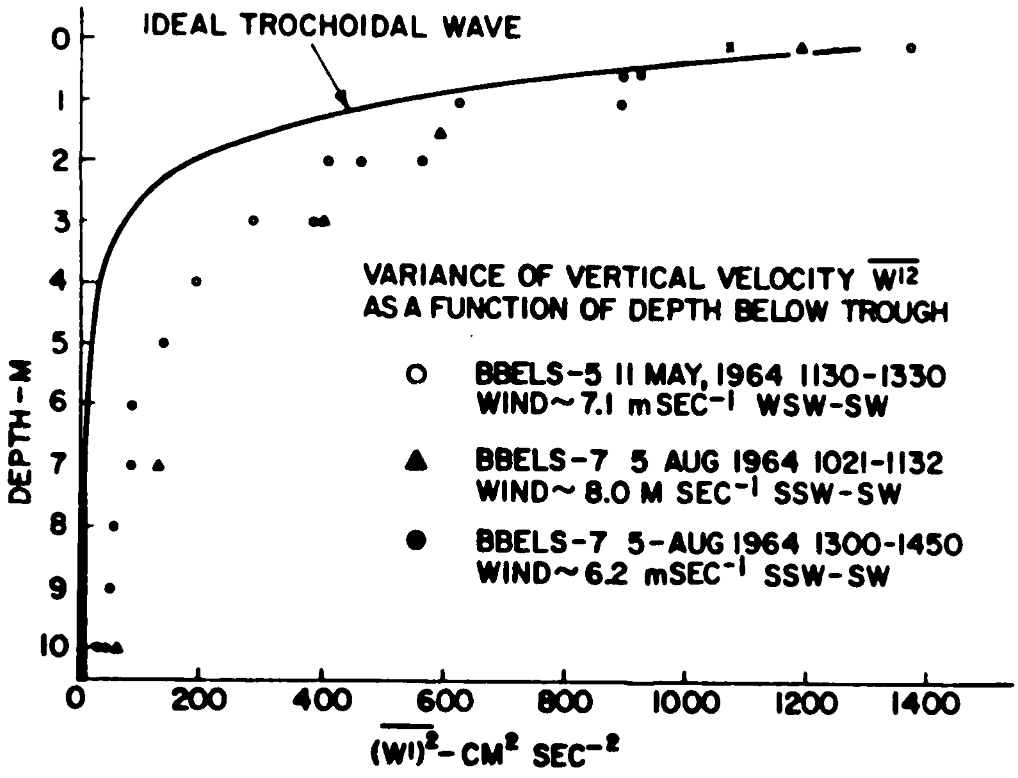

Figure 4: Variance $\overline{w'^2}$ estimated as a function of depth below for z_T for three different wind and sea states from the Buzzards Bay Entrance Light Station. The kinetic energy of the vertical motions appears to fall off somewhat more rapidly than does the energy of the ideal trochoidal wave model. Also, there appears a residual amount of kinetic energy remaining constant with depth below 5 m.

4. The statistical properties of the velocity and pressure fluctuation are homogeneous in the horizontal over the local area, as is the mean horizontal current. These properties may, however, undergo changes much slower than the periods of the wave motions (in fact, these changes, such as are associated with wind variations, are of principle interest).

5. Motions are associated only with wind-generated waves, propagating in the +x direction and the mean tidal flow; no standing waves being present.

The momentum equations for the u and w motions in the x and z directions, respectively, may be written as

$$\rho\frac{du}{dt} = -\frac{\delta p}{\delta x} - F_x \tag{1}$$

$$\rho\frac{dw}{dt} = -\frac{\delta p}{\delta z} - g\rho - F_z \tag{2}$$

where ρ is density, p is pressure, t is time, F_x and F_z are frictional retarding forces per unit volume in the x and z directions and g is the acceleration of gravity, assumed constant. With the aid of the two dimensional continuity equation

$$\frac{\delta\rho}{\delta t} + \frac{\delta\rho u}{\delta x} + \frac{\delta\rho w}{\delta z} = 0 \tag{3}$$

and by multiplication of equations (1) and (2) by the respective velocity components expanding of the total derivatives, and invoking assumptions 1-5 we form the kinetic energy relation

$$\frac{\delta}{\delta t}\left(\rho\frac{u^2+w^2}{2}\right) = -\left[\frac{\delta}{\delta x}\left(\rho\frac{u^2+w^2}{2}u\right) + \frac{\delta}{\delta z}\left(\rho\frac{u^2+w^2}{2}w\right)\right] - \left(\frac{\delta pu}{\delta x} + \frac{\delta pw}{\delta z}\right) - g\rho w - uF_x - wF_z \tag{4}$$

We average equation (4) with time over a region of ocean where we invoke assumption 4 above. We then define the measured variables in the form

$$u(t) = \bar{u} + u', \; w(t) = \bar{w} + w \text{ and } p(t) = \bar{p} + p' \qquad (5)$$

for example where $\bar{u} = \frac{1}{T} \int_0^T u(t)\, dt$ and then by definition $\bar{u}' \equiv 0$.
The period of averaging T is much greater than the periods of the surface wind waves and in spite of the slowly varying tide level we may safely assume $\bar{w} = 0$.

We have thus, after the appropriate averaging,

$$\frac{\delta}{\delta t}\left(\rho\frac{\bar{u}^2}{2} + \rho\frac{\overline{u'^2+w'^2}}{2}\right) = \frac{\delta}{\delta z}\left(\rho\overline{u'w'}\ \bar{u}\right) + \frac{\delta}{\delta z}\left(\rho\overline{\frac{u'^2+w'^2}{2}w'}\right) + \frac{\delta}{\delta z}\left(\overline{p'w'}\right)$$
$$-\bar{u}\, F_x - \overline{u'F_x} - \overline{w'F_z} \qquad (6)$$

This relation is a balance of mean and wave (eddy) kinetic energy. To the mathematician, the time derivatives of the barred terms may be troublesome. Since we aren't mathematicians we won't be troubled since the partial time derivative is meant to assess the change over time intervals large compared to the wind wave periods. Thus, the wave periods may range from 0.5-10 s while we wish to consider kinetic energy changes in response to wind stress changes which occur from tens of minutes to several hours.

To obtain the energy balance of horizontal mean motion, we multiply equation (1) by u and form

$$\frac{\delta}{\delta t}\left(\rho\frac{\bar{u}^2}{2}\right) = \frac{\delta}{\delta z}\left(\rho\overline{u'w'}\ \bar{u}\right) + \rho\overline{u'w'}\ \frac{\delta u'}{\delta z} - \bar{u}F_x \qquad (7)$$

By subtracting equation (7) from (6) we obtain

$$\frac{\delta}{\delta t}\left(\rho\frac{\overline{u'^2+w'^2}}{2}\right) = -\frac{\delta}{\delta z}\left(\rho\overline{\frac{u'^2+w'^2}{2}w'}\right) - \rho\overline{u'w'}\ \frac{\delta u}{\delta z} - \frac{\delta}{\delta z}\overline{p'w'} \ -\overline{u'F_x}\ -\overline{w'F_z} \qquad (8)$$

which is the balance of wave (eddy) kinetic energy.

Note that all terms on the right, in both (7) and (8) (except the viscous dissipations) involve vertical spatial derivatives and covariances,

both being indicative of transport properties of a fluid. Since the equations indicate the change occurring at a point it is of interest to also integrate the relation vertically since our concern is the energetics of a finite water column and how surface wind stress imparts momentum and energy throughthe level z_T. We thus integrate equations (7) and (8) from the trough level z_T down to a depth D. All integrands, which are partial derivatives with respect to z, need be evaluated only at $z = z_T$ since at $z = D$, all fluctuations vanish (Shonting, 1967).

The integrated forms of (7) and (8) are

$$\frac{\delta}{\delta t}\int_D^{z_T} \rho\frac{\bar{u}^2}{2}\, dz = \int_D^{z_T} \rho\overline{u'w'}\, \frac{\delta\bar{u}}{\delta z}\, dz - \rho\overline{u'w'}\, \bar{u}\,\Big|_{z_T} - D_m \tag{9}$$

and

$$\frac{\delta}{\delta t}\int_D^{z_T} \rho\frac{\overline{u'^2}+\overline{w'^2}}{2} dz = -\int_D^{z_T} \rho\overline{u'w'}\, \frac{\delta\bar{u}}{\delta z}\, dz - \rho\overline{\frac{u'^2+w'^2}{2}w'}\Big|_{z_T} - \overline{p'w'}\Big|_{z_T} - D_E \tag{10}$$

The quantities D_m and D_E denote the frictional dissipation of the mean flow and of the eddy kinetic energies, respectively, for the unit water column between z_T and D.

The first integral on the right of (9) and (10) represents the transformation term between the two types of kinetic energy or, in other words, energy transferred from the mean motion by the turbulent shear stresses to produce turbulent energy (Hinze, 1959) in the water column of unit cross-section and z_T D meters high. The second term in equation (9) is the boundary transport of mean flow kinetic energy between the layer of direct forcing and the region below. This is what Hinze (1959) refers to as convective diffusion of the kinetic energy by turbulence. This effect is due to the Reynolds stress acting in the direction of the mean flow.

The second term of (10) is a boundary transport of eddy kinetic energy across the surface z_T caused by the net flux associated with the covariance between w' and the eddy kinetic energy components (note that this is sum of two triple product correlations). Finally, the third term of (10) is the covariance of pressure and vertical velocity evaluated at depth $z = z_T$. It provides a second boundary flux of eddy kinetic energy across the surface by virtue of the work done by pressure force p' acting over the displacement w'. The sum of the vertical terms in equation (10) is thus the transport of eddy kinetic energy for the u' and w' velocity components.

From a practical point of view, we should note that wave observations have been made in Narragansett Bay where the tidal currents (i.e., values of $\bar{u}$), depending upon the tidal phase and location, vary in speed from 0-100 cm/s. Clearly, for a vanishing mean current, equation (9) becomes identically zero. Equation (10) on the other hand, simplifies to

$$\frac{\delta}{\delta t}\int_{D}^{z_T} \rho\frac{\overline{u'^2}+\overline{w'^2}}{2}dz = -\rho\frac{\overline{u'^2+w'^2}}{2}w'\Bigg|_{z_T} -\overline{p'w'}\Bigg|_{z_T} -D_E \qquad (11)$$

Now there is no mean eddy energy conversion term. However, we still have the advection terms of kinetic energy and pressure. This perhaps suggests the importance of assessing the ratio

$$\frac{\bar{u}^2}{\overline{u'^2}+\overline{w'^2}} = f(t) \qquad (12)$$

for a given set of observations which allows estimating the relative amounts of mean versus eddy or turbulent energies at a given depth and under specific wind and wave conditions.

The above derivations allow the observed parameters to be evaluated in the context of balanced energy equations. Specifically, the variances and Reynolds stresses can be used to calculate the order of magnitude of terms in equations (9) and (10). The Reynolds stress component $\tau_z = -\rho\overline{u'w'}$ defines a flux of horizontal momentum $\rho u'$ transported downward by the covariance between u' and w'.

These same concepts can be applied to the vertical mixing of oil. Considering again Figure 1, we could define a vertical oil transport term analagous to the Reynolds stress as an oil concentration fluctuation (oil)' correlating with w' i.e.,

$$F_0 = \overline{(oil)'w'} \tag{13}$$

Thus, in an actual oil spill, one could measure at a point in the ocean the time variation of oil concentration (possibly by use of a fluorometer system) and w' simultaneously to determine the flux F_0.

It is clear that our observational problem must first measure and gather simple statistics of wind wave motions from the largest wave orbital diameters down to scales of breaking wave turbulence. Analysis should include:

1. The kinetic energy (variances) of the motions.
2. The dominant energy-containing scales from the spectral density versus frequency and the spatial correlations.
3. Covariances between horizontal and vertical velocity components.

These statistical properties should be assessed in relation to depth, the local wind conditions, sea state (observed from free surface elevation statistics) and whitecap occurrence, since these data have been shown to be relevant to oil mixing.

We wish to measure the vertical distribution of kinetic energy from the sea surface down to a depth where the wave induced motions vanish. We assume that the motions u' and w' defined by Equation (5) are strictly wave orbital motions of deep water type (wavelength less than twice the depth) and can be represented as fluctuations at a fixed horizontal position by

$$u' = a\omega\ (\exp \omega^2\ z/g)\ \cos \omega t$$

and

$$w' = a\omega\ (\exp \omega^2\ z/g)\ \sin \omega t$$

where a is amplitude, and ω is circular (radian) frequency, and g is gravity. Then by eliminating the trigonometric terms and multiplying by $\rho/2$ we obtain

$$ke = \rho/2\ (\overline{u'^2} + \overline{w'^2}) = a\omega\rho/2\ (\exp \omega^2\ z/g)$$

which becomes the kinetic energy at depth z associated with a two dimensional progressive wave in the x-z plane.

Now if we integrate in the form

$$\int_D^{\eta(t)} ke\ (z)\ dz$$

we obtain the total kinetic energy of the wave motions in the water column between the free surface $\eta(t)$ and the depth D where the u' and w' motions are negligible (say 1% of their surface value). A problem occurs in the interpretation of the energy integral at the surface. It is clear, since we desire the average kinetic energy, we shall integrate from the upper limit $\overline{\eta}(t) = 0$ by definition.

One aim of our field measurements is to evaluate the energy density term ($\rho\overline{w'^2}$) and vertical integral by use of actual values of $\overline{u'^2}(t)$ and

$\overline{w'^2}(z)$. These variances, however, are obtained only at discrete depths of instrument placement; usually, for the WAVTOP measurements, the uppermost instrument was placed 10-20 cm below the estimated wave trough level. The uppermost region must be measured as accurately as possible since the energy is an exponential function increasing to the surface.

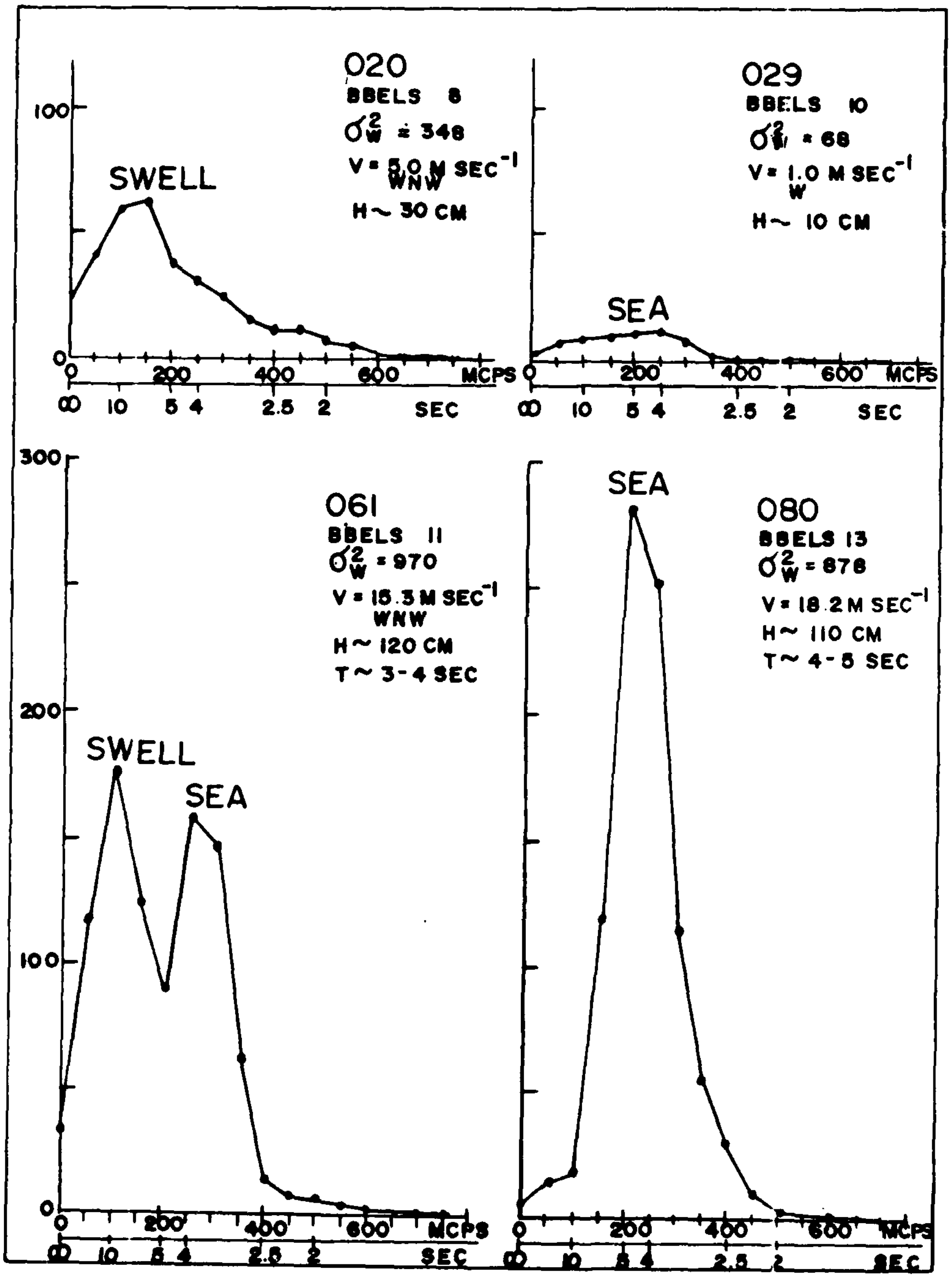

Figure 5: Auto-spectra of the vertical velocity w', observed at one meter below the level z_T for four different wind and sea conditions at the Buzzards Bay Entrance Light Station. The spectra clearly indicated the character of the ambient surface wave conditions; i.e. compare the shape and values of the spectra with the indicated variance (α ke), wind speed and estimated wave parameters, H (Height) and T (Period).

IV. PREVIOUS OBSERVATIONS OF WAVE MOTIONS

Experiments were made to measure some of the quantities in equations (7) and (8) by the writer between 1963-1966. Some degree of success was achieved in measuring orbital motions u' and w' at several depths and in various sea conditions from a fixed tower (see Shonting, 1964 and 1967). The sensor systems were ducted impeller system which were relatively crude and were limited to scales of 10-20 cm and frequencies of less than 2 Hz. Orthogonally and linearly spaced (in the vertical) ducted meters were rigidly supported on a vertical rod which was suspended by support guys maintaining the sensors at fixed depths beneath the trough depth z_T. The system was mounted on the windward (waveward) side of the Buzzards Bay Entrance Light Station (41°23.8' N and 71°02' W) where the water depth is 15 m. Sea state, wind velocity, and currents were monitored during the wave measurements.

Results of these measurements (Shonting, 1968 and 1970) indicate the following:

1. The kinetic energy of the fluctuations (proportional to the variables $\overline{u'^2}$ and $\overline{w'^2}$) decreases nearly exponentially with depth and scales reasonably well with a trochoidal wave model (see Figure 4).

2. Kinetic energy estimated for the wave motions appears equal to the potential energy of the waves (estimated from the variances of the free surface elevation $\eta'(t)$).

3. Auto-spectra show the wave types present, and energy changes of growth and decay (see Figure 5).

4. Reynolds stresses $-\rho\overline{u'w'}$ estimated over intervals large compared to wave periods are consistently positive in wind-wave field, indicating

a downward transport of horizontal momentum through the upper layer. Individual waves show scatter ranging up to 20-30 dyne/cm^2 near the wave trough level for winds of the order of 7-12 m/s. From the above observational results it is clear that it is indeed feasible to register wind wave induced orbital and turbulent motions in the upper 5-10 m layer. Such measurements require the use of: (1) fast responding and accurately calibrated velocity sensors and (2) a stable platform from which to support such instruments. The following section reviews the development of the system to measure wave motions.

V. INSTRUMENTATION

The Eulerian measurement of wind wave motions requires that our chosen instrumentation must contain specific attributes. The sensing system must register both the mean and fluctuating velocity components in the water column. Moreover, the instruments should have a sufficiently fast response to measure smaller scale velocity fluctuations, yet have a long enough recording capacity to evaluate slow variability and stable mean values. Further, the systems must be capable of being arranged geometrically for simultaneous measurements at different depths. Based upon the above considerations, an instrument package for the WAVTOP observations was developed consisting of three basic components: the sensors, electronics and energy supply, and pressure cases.

A. The Sensor Systems

The sensor system (Figure 6A) is a ducted impeller device designed by Smith (1978) at the University of Washington. The plastic impeller, which is mounted with jewel bearings, contains two small magnets mounted on its edge. As the impeller spins in response to the fluid flow, the field of the magnets interacts with a "Hall effect" crystal pickup mounted inside the tip of the stainless steel support rod. With passage of the blade magnets, a charge separation occurs in the Hall effect device forming a pulse which is amplified, shaped into a square wave by a Schmidt trigger, and coded by a sequence of short/long or long/short pulses indicating the sense of rotation. The Hall effect pickup offers a minimum magnetic force field which otherwise could slow the spinning impellers through interaction of the magnets. Thus, the combination of a neutrally buoyant impeller and the Hall effect pickup provides a low velocity threshold response.

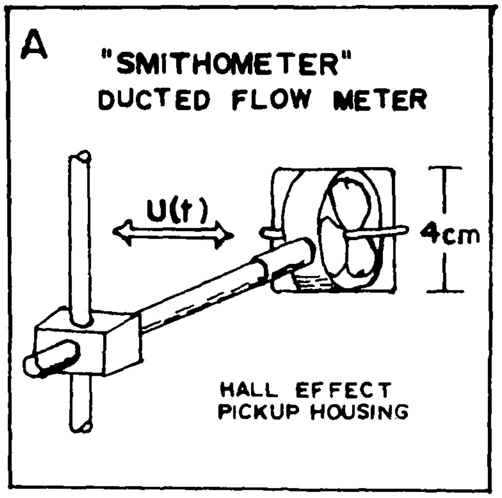

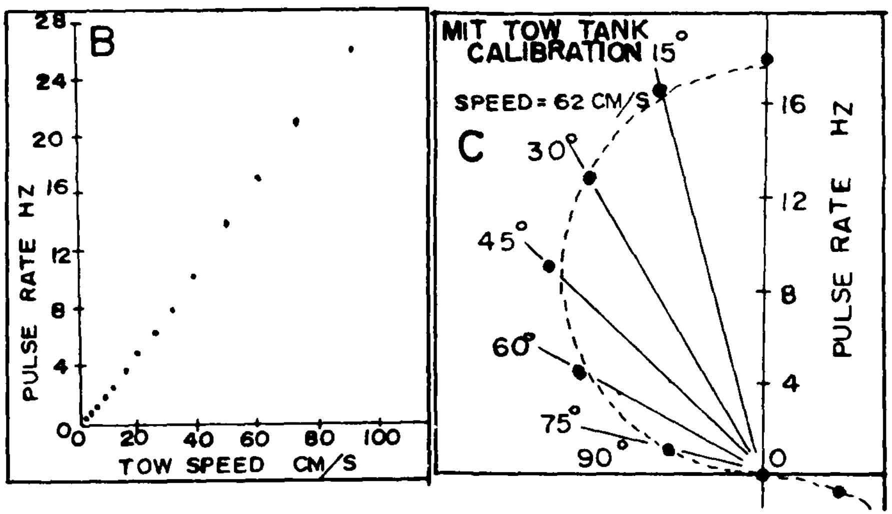

Figure 6: A) Ducted impellor (Smithometer) system. The spin axis is to record the horizontal velocity component u. B) Typical calibration curve for the towed sensors in the MIT towing tank. The calibration curve of angular velocity (pulse rate Hz) proves a very linear relation to speed even down to 5 mm/s. C) Off angle response calibration at 62 cm/s tow speed. Actual data are the black dots and the dashed circle is the cosine relation.

The lower limit of the scales of motions measured is defined by the dimensions of the "Smithometer" impeller sensor relative to the spatial variability along the instantaneous axis of flow. The 4 cm diameter impeller limits our detectable scale size of an eddy motion to about 10 cm. The response limit of the Smithometer impeller sensor is about 5 Hz (Smith, 1978). This is equivalent to our chosen sampling frequency of 0.2 s which gives a Nyquist frequency of 2.5 Hz, the upper frequency limit from which we could expect any spectral information. It is noted that a sample rate of 0.20 s. is sufficiently short enough to properly sample even the smallest wind generated gravity waves, i.e., those having heights of 10-20 cm, wave lengths of 50-100 cm and periods of 0.4-1s.

For two sets of observations, a wavestaff system was used to obtain free surface records simultaneously with the velocity measurements. The wavestaff used was Coastal Data Services model WS500-3 which operates on a capacitance principle relying on a linear relationship between wave height and capacitance. A 12-volt power supply was used which gave a calibration content of 0.373 m/v. The wavestaff, 3 m in length, was placed in the water with the top 0.5 m above the mean water level and approximately 0.5 m horizontally from the velocity meters.

B. Calibration of Smithometer Sensors.

A series of calibrations of the Smithometers was performed in the Massachusetts Institute of Technology (MIT) ship-towing tank of the Department of Ocean Engineering. Examination was made of the linearity of impeller angular velocity with flow speed, the off-angle response from axial flow, and the threshold velocity.

For these MIT tests, the units were towed with their spin axes parallel

to the relative flow, forth and back over the 30 m tank at speeds from 1-90 cm/s. The output response (see Fig. 6B) was very linear to within a few percent at all speeds greater than 1.5 cm/s. The uncertainty in the sensor-observed velocities decreased from 5% to 1% as the velocity was increased to 50 cm/s. The sensor-observed velocities also differed from the selected tow tank velocities by +5%. No estimate of accuracy may be made, as the uncertainty of the tow tank velocities was not known.

To examine the Smithometers ability to resolve velocity vectors, the units were towed at several speeds at angles off-axis between 0^o and 90^o in 15^o increments. Figure 6C shows the typical response of the sensors indicating near cosine response which may be used for all seven sensors with a maximum error of 2-3%. The latest calibration at MIT indicated the best cosine response occurred at the highest towing speeds. The most deviation (~ 5%) from a cosine response curve was found at small towing speeds (< 10 cm/s).

Threshold speeds were measured between 0.4 and 0.5 cm/s in the first calibration, an order of magnitude lower than for conventional rotor devices. Observations during the last calibration test showed the new sensors have a threshold velocity of about 0.8 cm/s; the threshold velocity had approximately doubled after a year's use. A possible explanation for the decrease in static balance is slight misalignment of the axes because of normal handling in the field.

C. The Electronics and Microprocessor Systems

The microprocessing data logger system utilizes solid state electronics incorporating recent developments in microcircuitry. The system contains a microcomputer which performs functions including sampling raw signals, averaging, digitizing and recording.

The system (shown schematically in Figure 7) utilizes a Z80 8 bit microprocessor. The Z80 Central Processing Unit (CPU) follows instructions contained in a nonvolatile Read Only Memory (ROM). This can be changed (reprogrammed) to provide flexibility so as to modify data sampling and recording instructions.

Outputs from six ducted meter systems are monitored by the Z80 CPU on an "interrupt basis" via a parallel input-output (PIO) chip. When a meter requires service (interrupts) the Z80 CPU inputs the state of the timing chain through the PIO. The data is stored in the Random Access Memory (RAM) which is related to the instrument which causes the interrupt. Between interrupts, the CPU processes the displacement data to calculate frequency and sense of rotation for each sensor in a sequential manner, this produces a time series of vector components which are digitized at a preset rate and outputted into the digital cassette recorder. The velocity fluctuations (which are generally much higher frequency than the digitizing rate) are integrated (averaged) over the sampling (digitizing) period.

Switches are used to select various data acquisition times and the time between acquisitions. During wait cycles, only CMOS circuits are energized; this yields a considerable power saving. These switches can be used to:

1. Input a time delay which is initiated from battery plug-in time.
2. Specify length of data acquisition and waiting time, e.g. 15 min. sample then 45 min. wait.
3. Provide low voltage protection to prevent battery drain. When the main B+ voltage attains the minimum threshold value, the

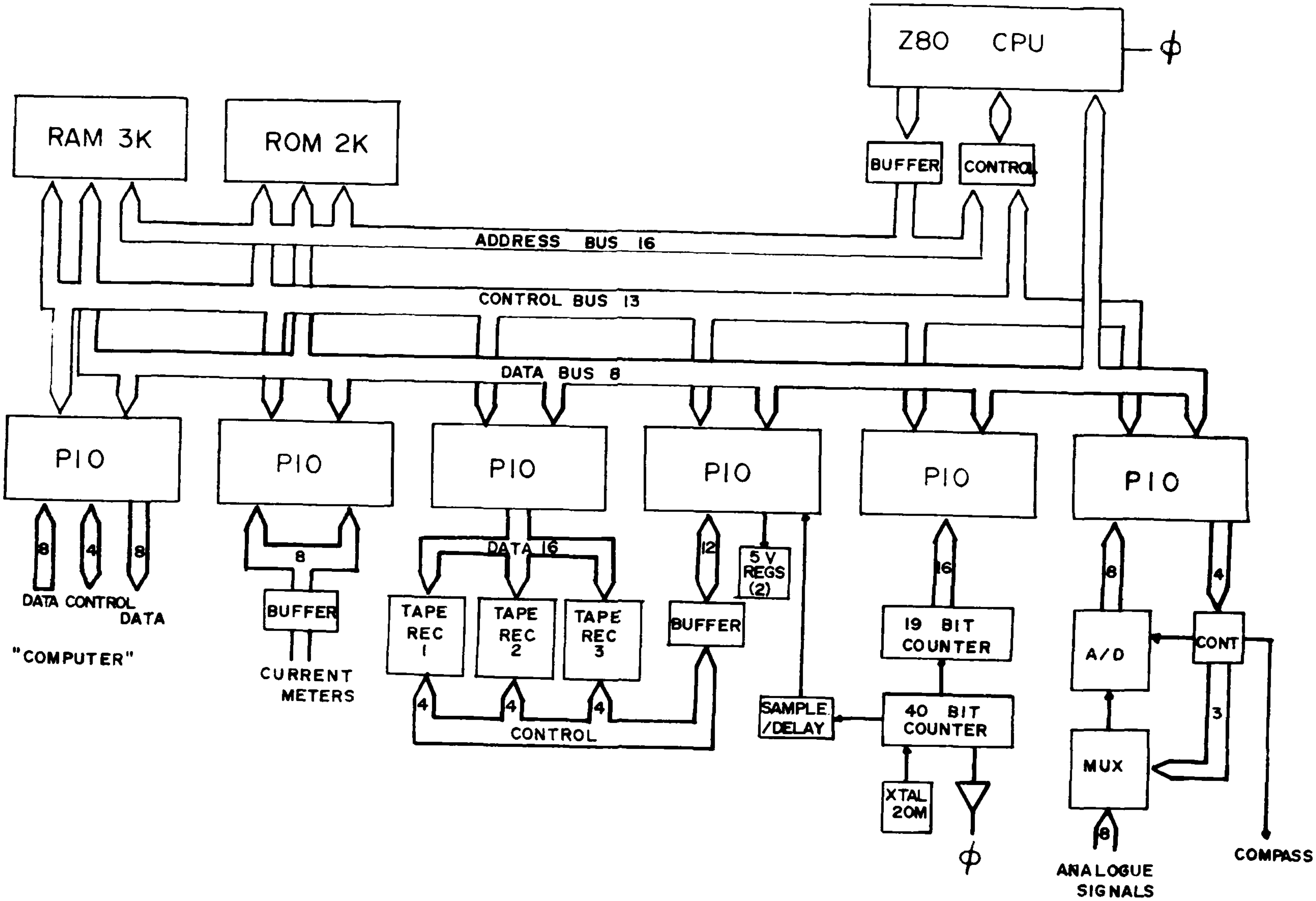

Figure 7: Electronics block diagram of BLT microprocessor-data logger. (See text for explanation of functional components.)

system automatically shuts down; this avoids batteries becoming flat and unrechargeable

Figure 8 shows the assembly with the microcomputer board (left) and the three Memodyne incremental cassette recorders (right). The electronics and battery packs are enclosed in twin aluminum pressure cases equipped with bulkhead connectors and "O" ring seals. To absorb the moisture, small dessicant packages are placed in the pressure case. The batteries consist of 12 General Electric sealed lead-acid cells usable in any orientation.

Programs are written in Z80 assembly language. A crossassembler, which is coupled to a Honeywell 316 minicomputer, is used to transform the assembly language program into Z80 machine language.

The machine language program is down loaded by the Honeywell into a Z80 development system which it supports. The data acquisition system with its ROM removed is connected to the development system. The program, which resides in the development system RAM, is run and debugged. With the exception of the ROM, all of the data acquisition system electronics are exercised. When the algorithm is debugged, it is placed in a ROM. The ROM is placed in the data acquisition system, which becomes a dedicated autonomous microcomputer.

The microprocessing data logger system inherently functions by the direction of programs stored within the ROM. Thus, the full capability of the data logger is, in a sense, evolutionary since we can constantly alter, improve, and expand its functions by reprogramming the ROM unit. Since the initial WAVTOP observations involved six Smithometer inputs, a program to sample the pulses from six meters plus one analog to digital channel was written and debugged. The data is organized into records consisting of

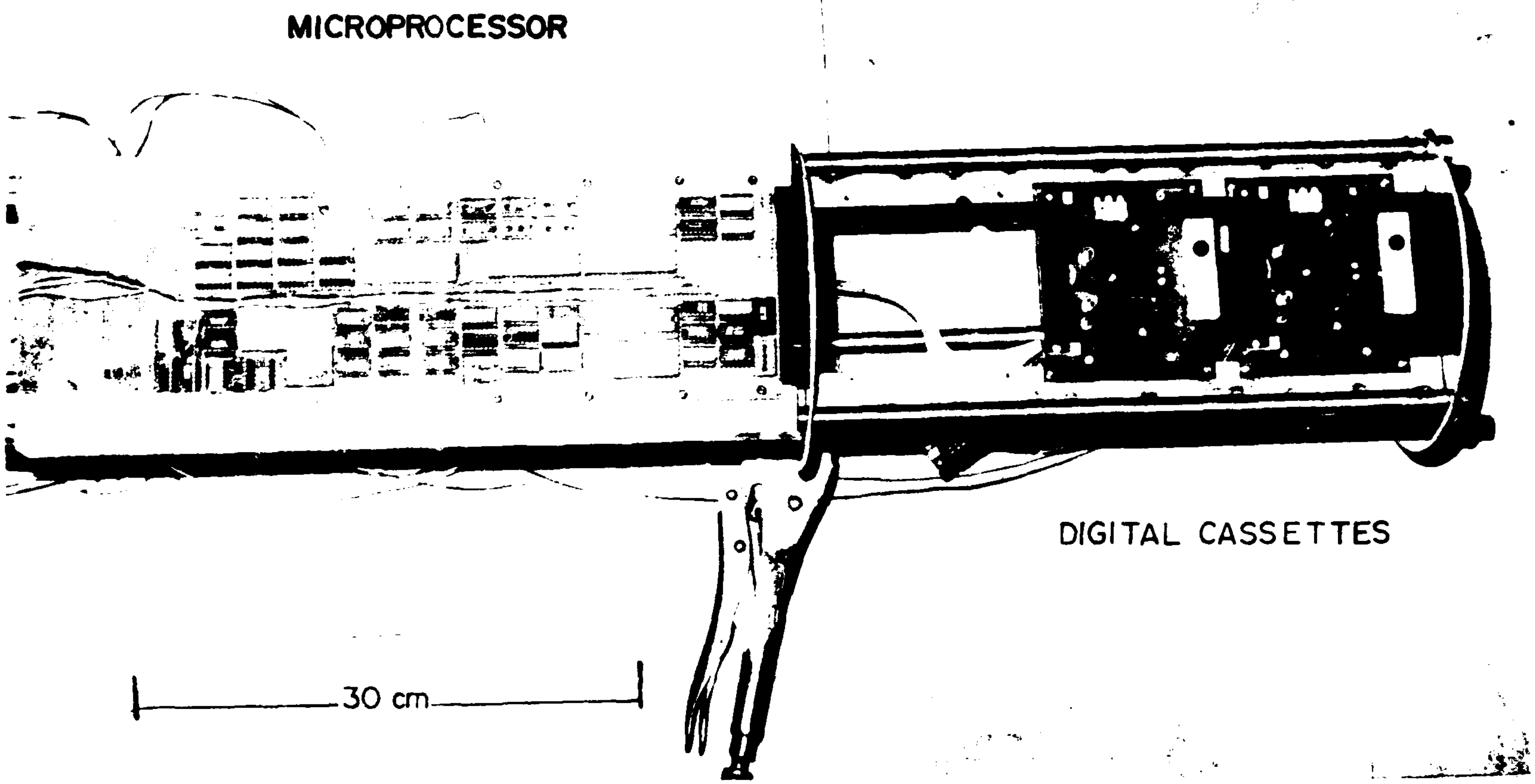

Figure 8. BLT hardware assembly. Left side shows the array of various micro circuit chips. At far lower left are a few identifiable electronic components termed capacitors, thermistors and resistors. At right shows two of the three Memodyne digital cassettes which register the processed data.

a one byte (8 bits) record counter, a one byte data acquisition set counter, 8 bytes of a/d data, and 64 bytes for each Smithometer used. A hexadecimal dump of two records is shown in Figure 9. In this display, the two left-most columns are dump program parameters; the first number is a count of the number of records read from the cassette; the second number is the count within the record of the next work displayed. Note the data is displayed as 2-byte words. In this example, the system was programmed to monitor four current meters, of which only the first two were used.

Normally six current meters are monitored, and data is reconstructed at a 5 Hz rate. This yields 394-byte records which contain 12.8 s of data (64X0.2 s).

Since a Memodyne incremental recorder accepts data at 11 to 21 bytes/s, three recorders are needed. Record N is recorded on cassette A, record N + 1 on cassette B, record N + 2 on cassette C, record N + 3 on cassette A, etc. Note in Figure 9 the record number has increased by three. A program in the Honeywell reads the cassettes and merges them into a single time series which is stored on an IBM compatible 7 or 9 track tape. The data is now ready for processing on a large computer. For WAVTOP observations, the maximum expected velocity range is $\pm$ 50 cm/s. This range is set in the software program giving a relationship between data counts and flow speed as is shown in Figure 10. Thus, the pulsed frequency (counts) varies directly with positive speed up to 127_{10} (i.e., to the base 10) or $7\,F_{16}$ (to the base 16), overflow results at 128_{10} (80_{16}), and then at the 129_{10} (81_{16}) negative speeds take over, flipping the relation to -50 cm/s and decreasing to zero by 255_{10} (FF_{16}).

The combination of the unique Smithometer sensors and the versatile

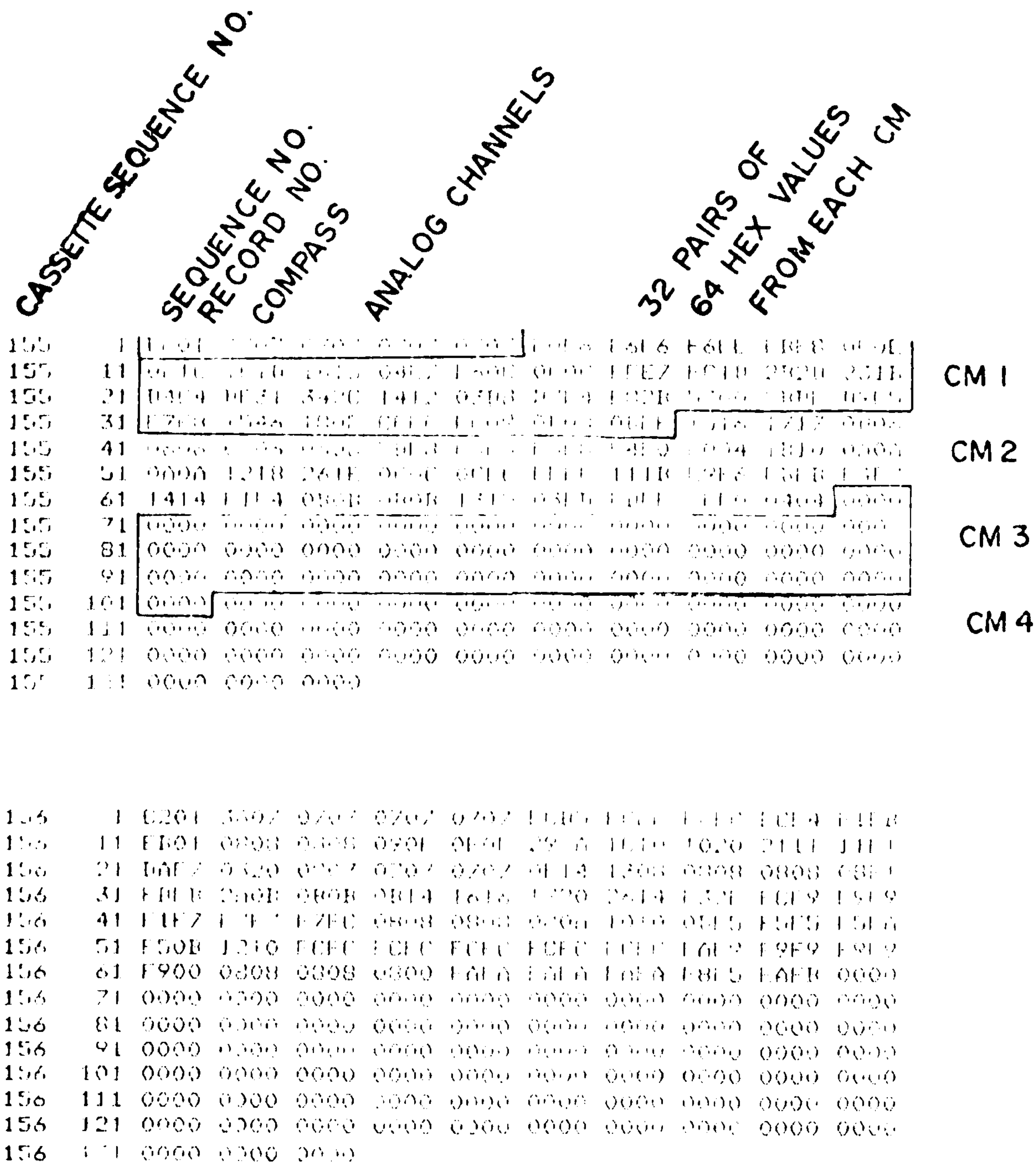

Figure 9. The data format of hexadecimal numbers as it is written on the Memodyne digitial cassettes. Here is contained one analog record (magnetic compass bearing of the AESOP bouy) and four Smithemeter outputs, wherein channels 3 and 4 were unused and read as zeros.

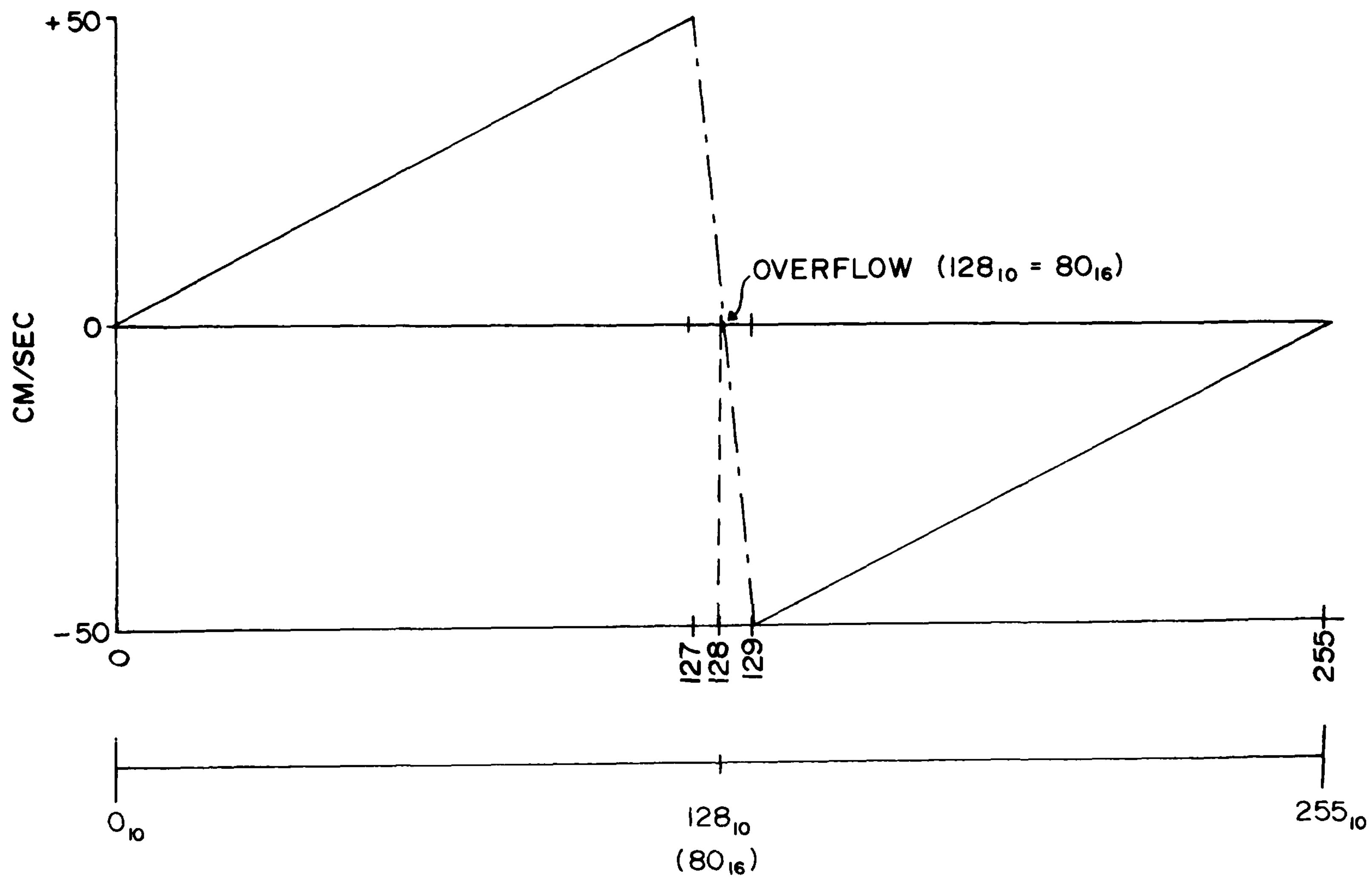

Figure 10. The analog relationship for transforming the Smithometer pulse rate into flow speed (cm/s). For this measurement the maximum recordable speed is 50.4 cm/s. This value is registered for all speeds equal to or exceeding it. For observations in faster currents, the maximum speed may be doubled; this reduces the resolution of individual values by 0.5 since each channel is limited to 64 bytes to register speed.

microprocesser data logger renders the composite system a unique and versatile oceanographic tool. The Smithometer System and Data Logger, packaged for mounting on various platforms, can be used to measure motions in upper or bottom ocean boundary layers; hence, it is called the Boundary Layer Thing (BLT). A summary of the systems sensing characteristics is given in Table 1.

TABLE 1

Characteristics of BLT/Ducted Flow Meter System

Diameter Impeller	4 cm
Response Distance	3 cm
Frequency Response	5-10 Hz
Threshold Speed	3-5 mm/s (depending on rotor axis alignment)
Linearity	Within 3-5% (One curve can be used for all systems)
Cosine Response	Good; 10-15% Maximum error at angles approaching 90^{o},-12 to + 12 volt.
Smithometer Signal Output	Nominal pulses whose duration to period ratio indicates flow direction
Maximum Depth of Use	Impeller units tested to 20 atm (200 m)

D. Sensor Mounting and Platforms

Preliminary observations in Narragansett Bay were made using the AESOP stable platform (Shonting and Barrett, 1971) from which to mount the BLT system (Figure 11). The AESOP buoy is 18.9 m long and weighs 76 kg in

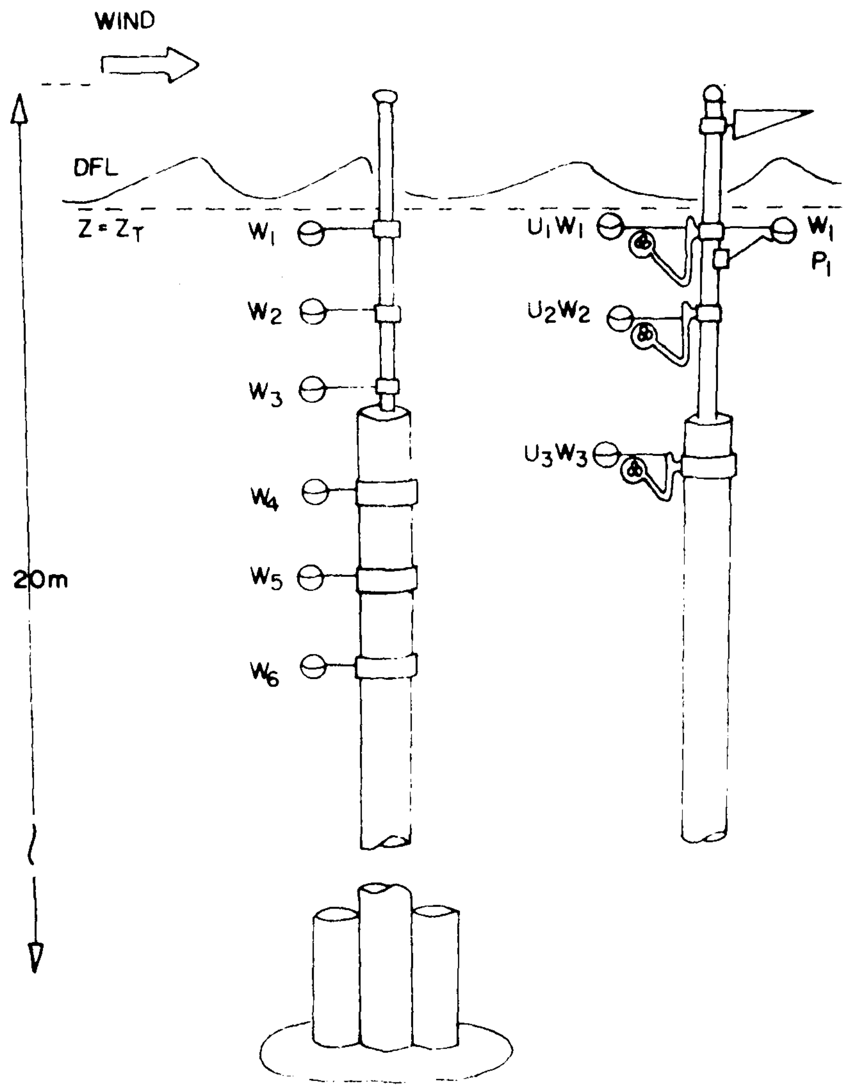

Figure 11. Schematic diagram of the AESCP bouy with the Smithometer configured (Left) for measurements of w' at six vertical collinear depths, and (Right) for measurement of u' and w' components at three depths. At the right on the topmast is a sensor for registering w' with the dynamic pressure p'. The vane atop the topmast keeps the AESOP oriented at a fixed direction with respect to the wind.

air with a combined ballast and payload weight of 65 kg. The buoy consists of buoyant sections that are easily assembled and dismantled and may be varied in number to alter the buoy's overall length, draft and payload. Tests in deep laboratory tanks show that, when the buoy is coupled to a damping disc at its base it has a natural period to heave in excess of 30 s and can be used as a stable platform in the presence of surface waves with periods up to 8-9 s and heights up to 2 m.

The Smithometers were configured to provide vertical line spacing of six instruments to determine the motions at six depths simultaneously as a function of wind, sea state, and whitecap conditions (Figure 11 left diagram). An alternative configuration (Figure 11 right diagram) is to register orthogonal components u and w, as pairs in order to calculate the Reynolds stress ($-\rho\overline{u'w'}$). This requires monitoring the heading of the AESOP buoy with a built-in compass signal which was recorded along with the velocity components.

The microprocessing electronics and battery pack case are fitted to the base of the AESOP buoy just above the damping disc. The AESOP platform is loaded to the side of the research craft. The Smithometers are then placed upon the upper topmast at the desired vertical spacing. The precise equilibrium position of the buoy in the vertical after launching, is controlled by adding or removing small 200 gm shackles on a tether line running from the damping disc up to a small cherry float. The tether line is made to exceed the water depth to insure AESOP retrieval in case of accidental sinking.

Preliminary AESOP observations were made in Narragansett Bay in an area 1-2 km north of the Newport Bay bridge (broken-line rectangle in Figure 12). The water depths range from 20-30 m, sufficient for the 18 m

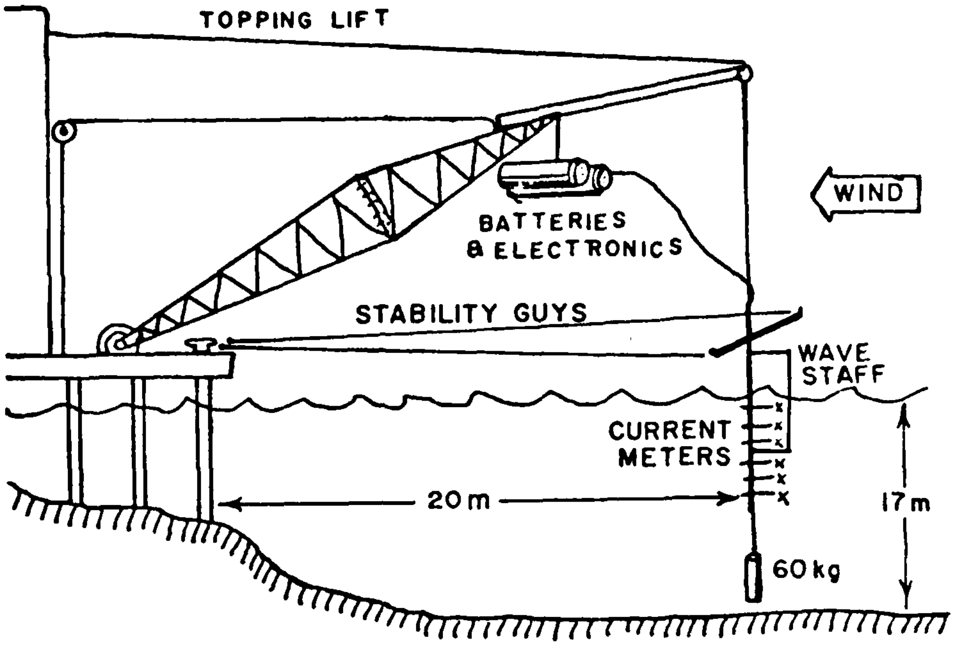

Figure 12. Experiment arrangement for wave observations at the Gould Island pier in Narragansett Bay. The pier faces west allowing observations of the prevailing southwest sea breezes and northwest winds associated with high pressure fronts. The heavy weight and support guys provide a maximum stability.

AESOP draft. Because of tidal currents of 35-60 cm/s maximum, observations were made during slack periods, and the AESOP was positioned to allow for tidal drift such that the buoy did not run aground within the observation period.

A second series of WAVTOP observations was made from the Gould Island facility in Narragansett Bay which has a 70 m long pier facing the west (Figure 13). The water depth within a 400 m western sector off the pier exceeds 12-16 m which for wavelengths up to 25-30 m we can classify such as a "deep water type." The BLT System with the Smithometers and a wavestaff are suspended from a stiff boom unit at pier side (Figure 12). For observations, the boom was fitted with an Al "I" beam extension to place the entire BLT wavestaff system at some 15 m away from the pier.

The prevailing winds are westerly except for the occasional "northeaster" cyconlic lows which generally pass over Nantucket giving strong SE to NE winds and precipitation. In the warm months, a southwest sea breeze builds up by 1500 hours to 7-9 m/s (14-18 knots). Throughout the year, the strongest steady winds come from the northwest associated with passages of highs which follow a cyclonic low pressure system. The Gould Island pier is situated (Figure 13) with fetches which vary from 2-3 km to the SW to 7-12 km to the NW, making it ideal for observing short-fetch wave buildup.

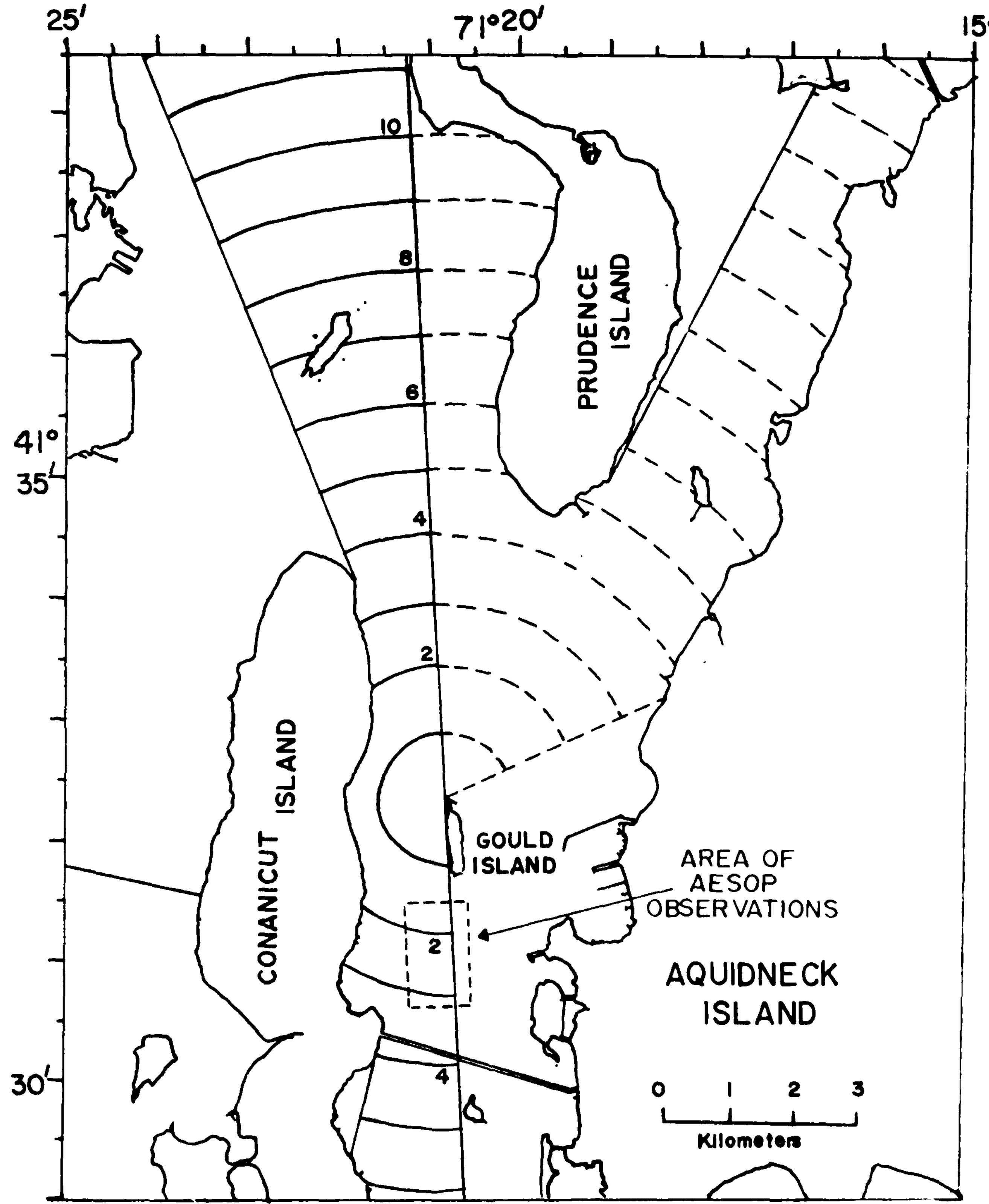

Figure 13: Lower Narragansett Bay showing fetches (solid arcs) available from waves generated by winds having a westerly component.

VI. OBSERVATIONS AND RESULTS

A. General Description of the Experiments and Results

The first set of field observations, designated as WAV-002, 003, 006, and 007, were made using the AESOP stable spar as a platform. These experiments were of preliminary nature to test the BLT electronics and the feasibility of making measurements with AESOP launched from a small research vessel. The R/V BROWN of the University of Rhode Island, Department of Ocean Engineering was utilized to work with the AESOP (Figure 14).

For these preliminary measurements, the Smithometers were oriented to register only the vertical velocity w' since the AESOP was not equipped with a directional holding vane system to maintain a fixed azimuth with respect to the wind and (or) wave direction, this being necessary for any measure of u' (horizontal component in the wave propagation direction). The observations of w' from the AESOP displayed some effects on the magnitudes because of small vertical fluctuations of the buoy; however, careful monitoring of the freeboard of AESOP during each observation indicated a high degree of stability (freeboard fluctuations less than $\pm$ 5 cm).

Observations 008, 010, 011, and 012 were made with the Smithometers mounted in a semi-rigid suspension from the stiff boom from Gould Island (see Figure 15). For records 011 and 012 the free surface elevation was continuously recorded with a capacitance wavestaff system.

An example of the Smithometer raw data outputs (to show that they actually record wave motion) is shown in Figure 16 (lower traces). Here the u and w are seen to oscillate about zero and are approximately $\pi/2$ (90^0) out of phase as they shouldbe.The flat parts or steps in these velocity signals are caused by the quantization of the signal which is in 0.4 cm/s

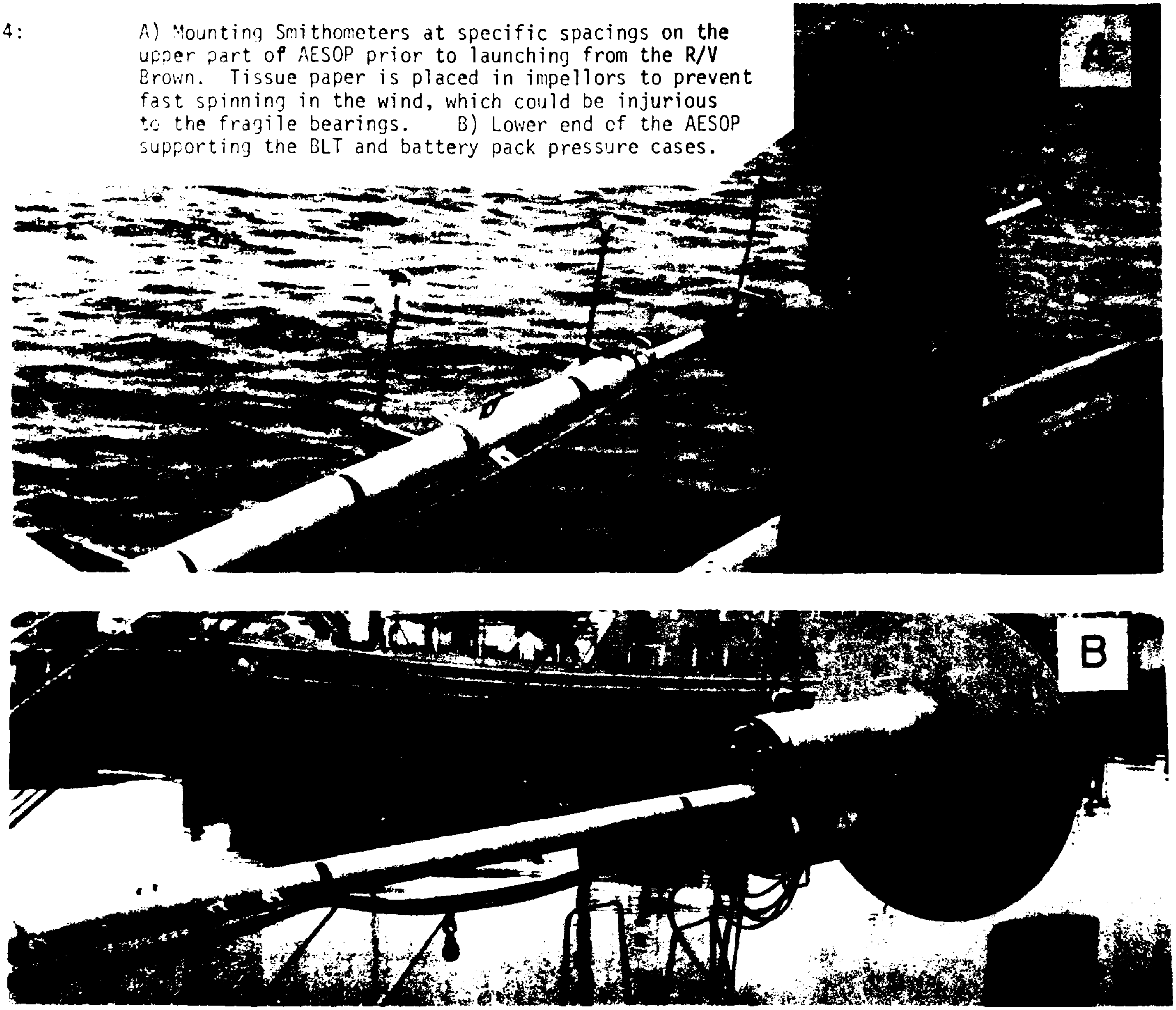

Figure 14: A) Mounting Smithometers at specific spacings on the upper part of AESOP prior to launching from the R/V Brown. Tissue paper is placed in impellors to prevent fast spinning in the wind, which could be injurious to the fragile bearings. B) Lower end of the AESOP supporting the BLT and battery pack pressure cases.

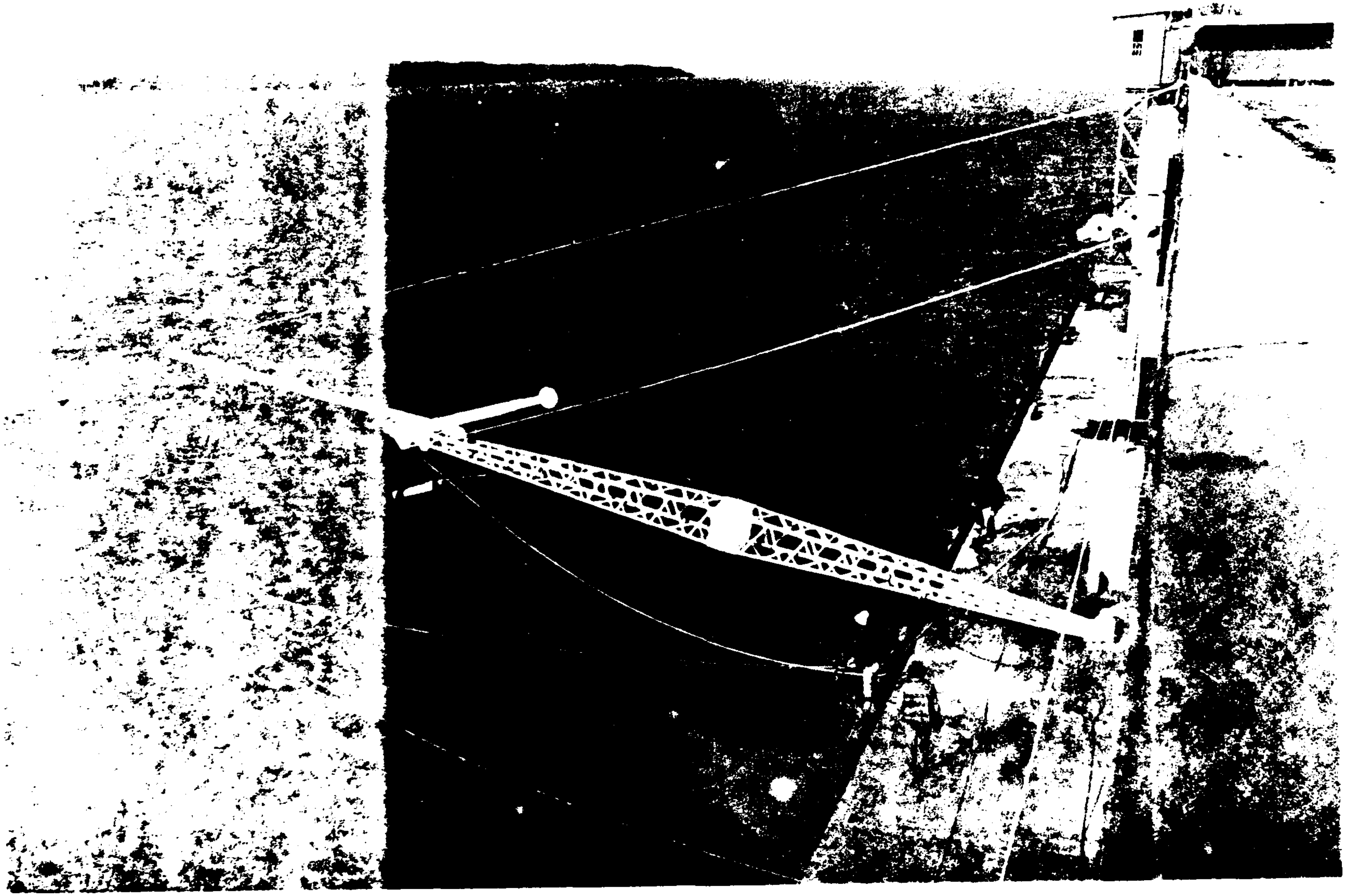

Figure 15: The Gould Island stiff boom system for supporting the BLT and Smithometer arrays.

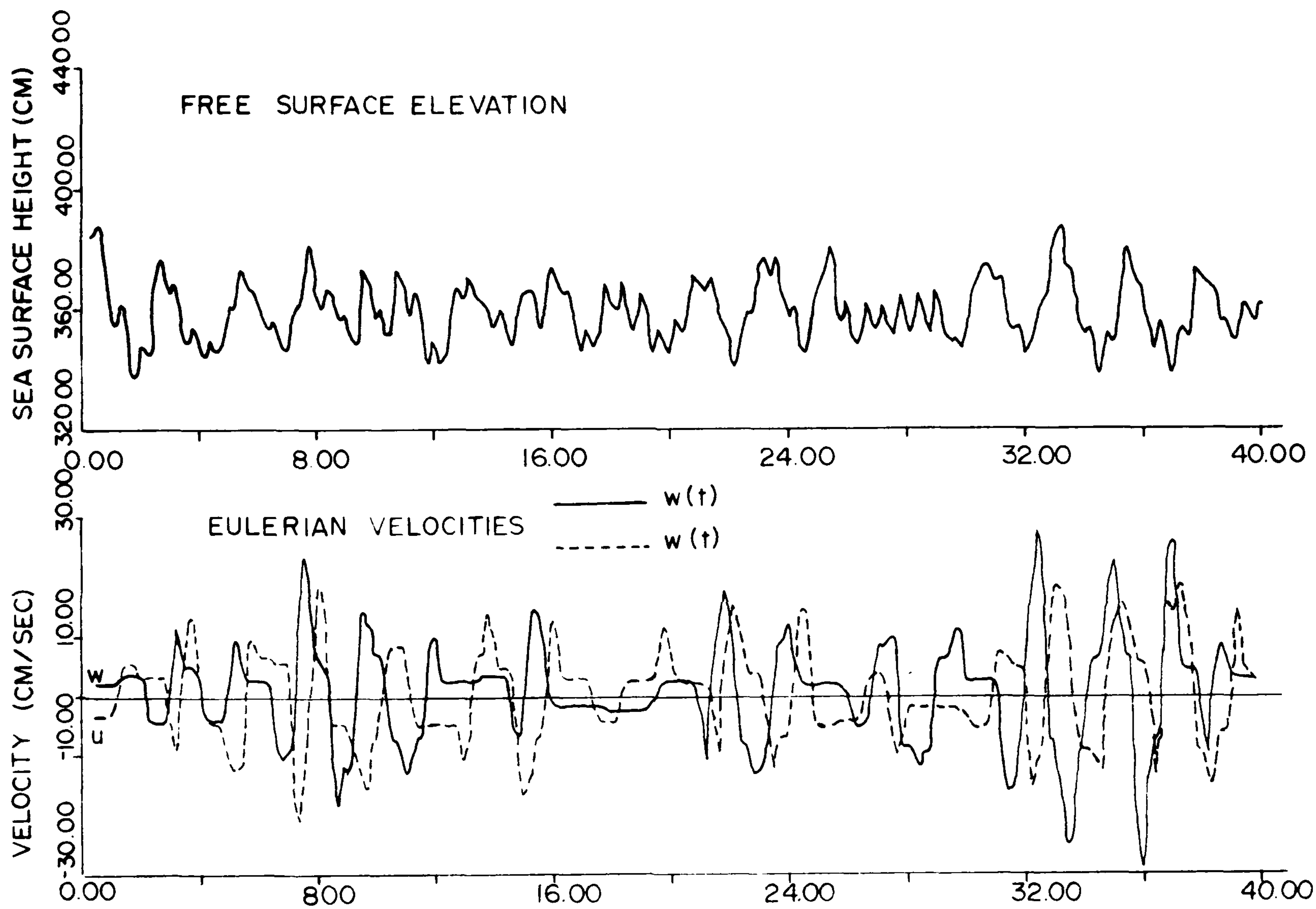

Figure 16: Raw data plot traces of the URI wave staff system (upper trace) and the u and w velocity components (lower traces) plotted against time.

increments. Amplitudes of the u appear to be slightly lower than those of w. The upper curve (Figure 16) is the data trace of the wavestaff where ordinate values (in cm) indicate wave heights (i.e., 2 x amplitude) of 30-50 cm. For these measurements, the wavestaff was positioned in a vertical plane which intersects the vertical line of current meters. Thus, if we assume the waves to be "long crested" (two dimensional) the wavestaff and meters are sensing the same wave at identical times.

In a single sinusoidal wave we have from equations (14) and (15)

$$u' \propto f(z) \cos \omega t$$

and

$$w' \propto h(z) \sin \omega t$$

where f(z) is an exponential decrease with z. These components are derived classically from the velocity potential given as

$$\phi \propto g(z) \sin \omega t$$

and the free surface variable $\eta(t)$ (registered by the wavestaff) is derived from $\delta\phi/\delta t$ evaluated at the surface where z = 0 to first order approximation.

From these relations we see that u'(t) leads w'(t) by $\pi/2$ (90°) and u'(t) is in phase with $\eta(t)$, relations which appear verified in Figure 16. The wavestaff data thus appears to be a realistic record of the sea surface oscillations. Furthermore, using a stopwatch, the observed waves had periods corresponding to those of the velocity and wavestaff records.

B. Kinetic Energy Variation with Depth and Time

The kinetic energy of the wave motions is fundamental to our study. A proper measure of this quantity insures the validity of our observations and lays the groundwork for better understanding of the mechanisms of wave generation, whitecap production and how the various velocity components promote mixing of oil or other surface pollutants.

We shall utilize the definition of kinetic energy E_k (as stated in section III) as being associated with a two dimensional motion defined by equation (14), i.e.,

$$E_k = \tfrac{1}{2}\rho\,(\overline{w'^2} + \overline{u'^2}) \sim \rho\overline{w'^2} = \rho\,\mathrm{var}\ w' \tag{18}$$

This assumes the w' and u' are primarily related to orbital motion in the xz plane. Clearly two sources of error occur; (1) waves are three dimensional since many of the smaller motion components will tend to be isotropic. Thus the y component u(t) may contribute energy, and (2) the u' term may have contributions from small scale horizontal flow not associated with gravity waves. This may be true, especially of flow around the Gould Island pier. To help minimize this effect, observations were made at, or near, slack tide.

The above sources of effort notwithstanding our estimate of kinetic energy of the vertical velocity component is used because it is the easiest component to measure, and a vertically oriented sensor is independent of azimuth i.e., wave or horizontal current direction. Thus, the variance, $\overline{w'^2}$, is used as an approximation of the state of the kinetic energy of the wind waves.

In the following summary we examine the depth variation of kinetic energy as a function of various wind and sea states. In observations WAVTOP 003, 008, 010, 011, and 012 the wind and wave conditions varied to such a small extent during the observational period that the forcing parameters are considered constant, i.e., these records are considered manifestly "steady state" conditions. However, in observations WAVTOP 002, 006, and 007, the winds changed markedly during the recording periods. Consequently, advantage was taken of this nonstationary condition and analysis was made of the

vertical kinetic energy distribution as a function of the wind and observed wave conditions, i.e., as they varied with time.

The following is a summary of the aspects the kinetic energy variations for each of the data sets:

WAVTOP 002 (24/Mar/78); Six Smithometers were supported from the AESOP spar buoy at depth below z_T of 10, 110, 210, 310, 410, and 610 cm. During the record, the wind speed increased from about 1 m/s to 9 m/s over the 110 min observation period.

The w' velocity component displayed pronounced changes related to the increased winds. Four series of variances (i.e., $\overline{w'^2}$) at each depth were calculated for 12 s intervals every 21 minutes (Figure 17). The increase in the wind speed from 4 to 8.5 m/s definitely increases the kinetic energy in the upper 3 m of the water column.

In order to better examine changes of energy with time,"running variances" were calculated (Figure 18). From the velocity data (recorded each 0.2 s) the means and variances were estimated for groups of 10 " records" (i.e., 128 s). Since the wave periods, as will be seen from the spectra, were of the order of 2 s this averaging time includes 50-60 wave periods - sufficient for a reasonable estimate of the energetics. The variance curves suggest the following:

1. The general trend of energy density follows the wind speed and varies by over an order of magnitude at all depths for the wind speed range of 2-9 m/s.

2. The energy remains exponentially distributed with depth as indicated by the similar vertical spacing with time on the semi-log graph.

3. Pronounced fluctuations in energy with periods of 10-15 minutes occur at all depths. Sometimes these pulses appear in phase with adjacent

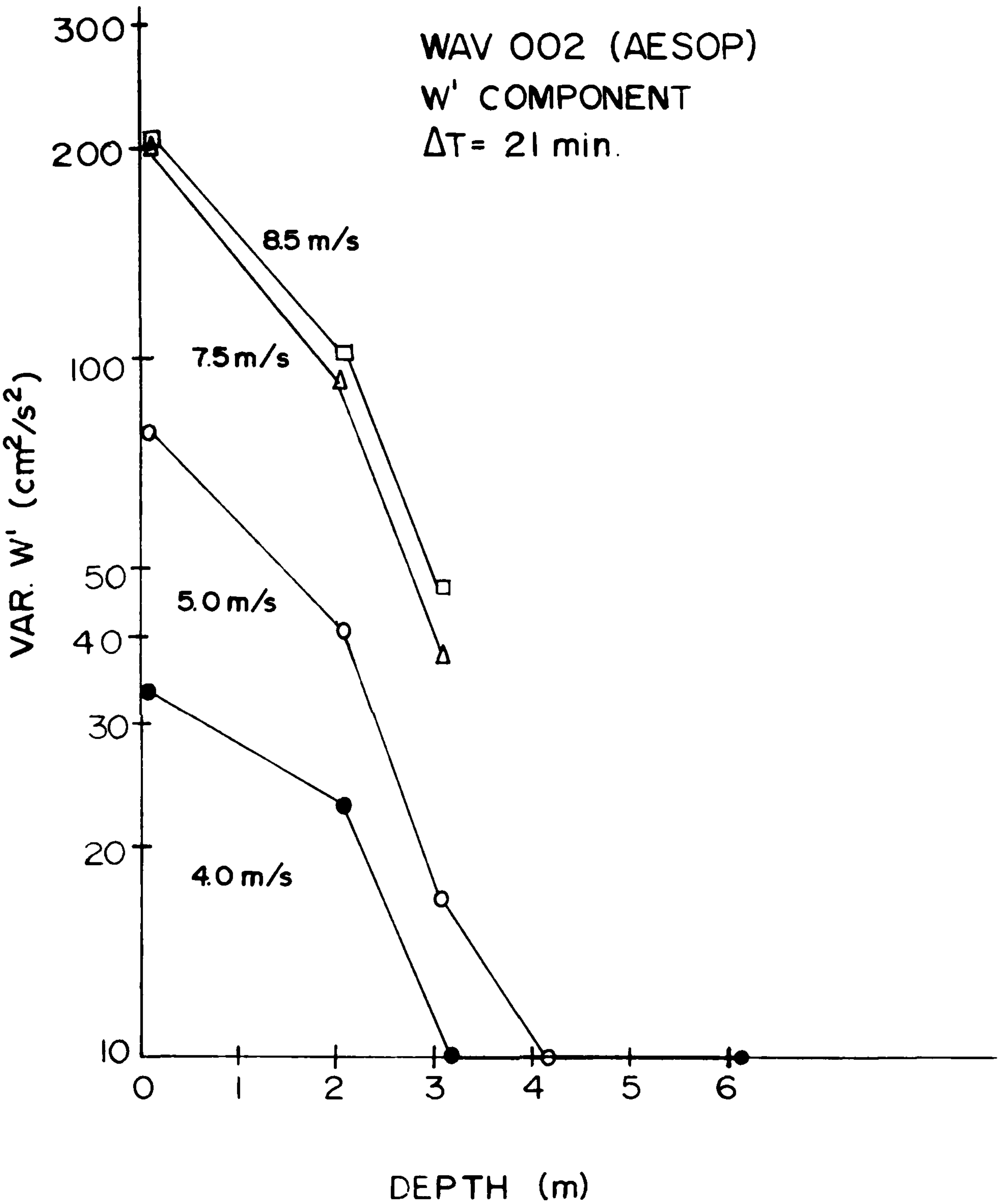

Figure 17: Variances of vertical velocity at various depth for different ambient wind speeds for WAVTOP 002. Values were estimated at intervals separated by 21 min.

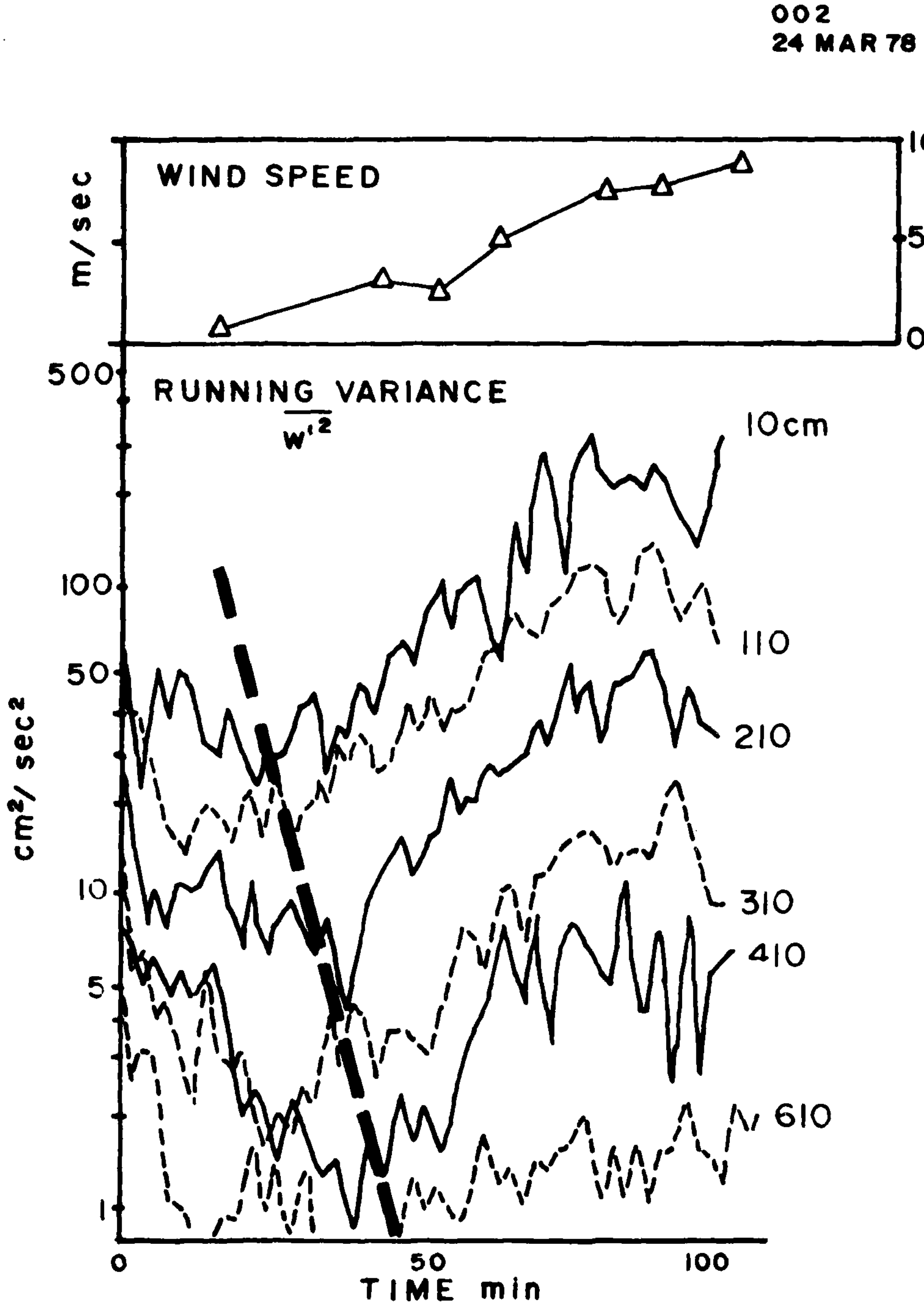

Figure 18. Running variances of the vertical velocity for Smithometers mounted on AESOP for WAVTOP 002. The diagonal line suggests a phase shift of response of the water column to wind stress. Thus, the energy level at, say 410 m appears to be 15-20 min later than the surface response.

records above and below, but at other times they appear random. The relative amplitudes appear independent of depth. There was no visible indication that the AESOP buoy was fluctuating vertically at these periods or even at its natural heave period of 26 s (Shonting and Barrett, 1971). It is tempting to speculate that these fluctuations are wave train packets which are generated by irregular wind stress pulses occurring upwind in the bay.

4. The variance traces all seem to be moving consistently downward at the onset of the record, probably due to a previous period of higher winds that the 1-2 m/s speeds registered at the beginning of the observation. The downward trend terminates at a pronounced energy minimum which appears in all records but appears time lagged progressively with depth. A broken sloped line (Figure 18) is drawn to suggest that a phase shift (lag) occurs whereby energy from the wind stress introduced takes a finite time to travel downward. The phase shift appears to be about 600 cm in 30 min, equivalent to a downward propagation rate of about 3 mm/s.

Different wind conditions (and, hence, sea conditions) cause different energy distributions to exist in the water column. The exponential decrease in kinetic energy with depth associated with motions of the surface waves would theoretically occur for a steady state system. Moreover, if new waves are constantly being wind generated then we should see a high concentration of energy at the surface. This is apparent in Figure 19 where two 12 minute averaged variances 70 minutes apart delineate the differences in kinetic energy distribution. For the higher wind speed, 8 m/s more total kinetic energy exists in the water column and this excess appears concentrated near the surface. This suggests that the energy-distributing process is not in a steady state as is shown by the nonexponential shape of the curve nearer the surface. The deeper values tend to converge, perhaps an indication that

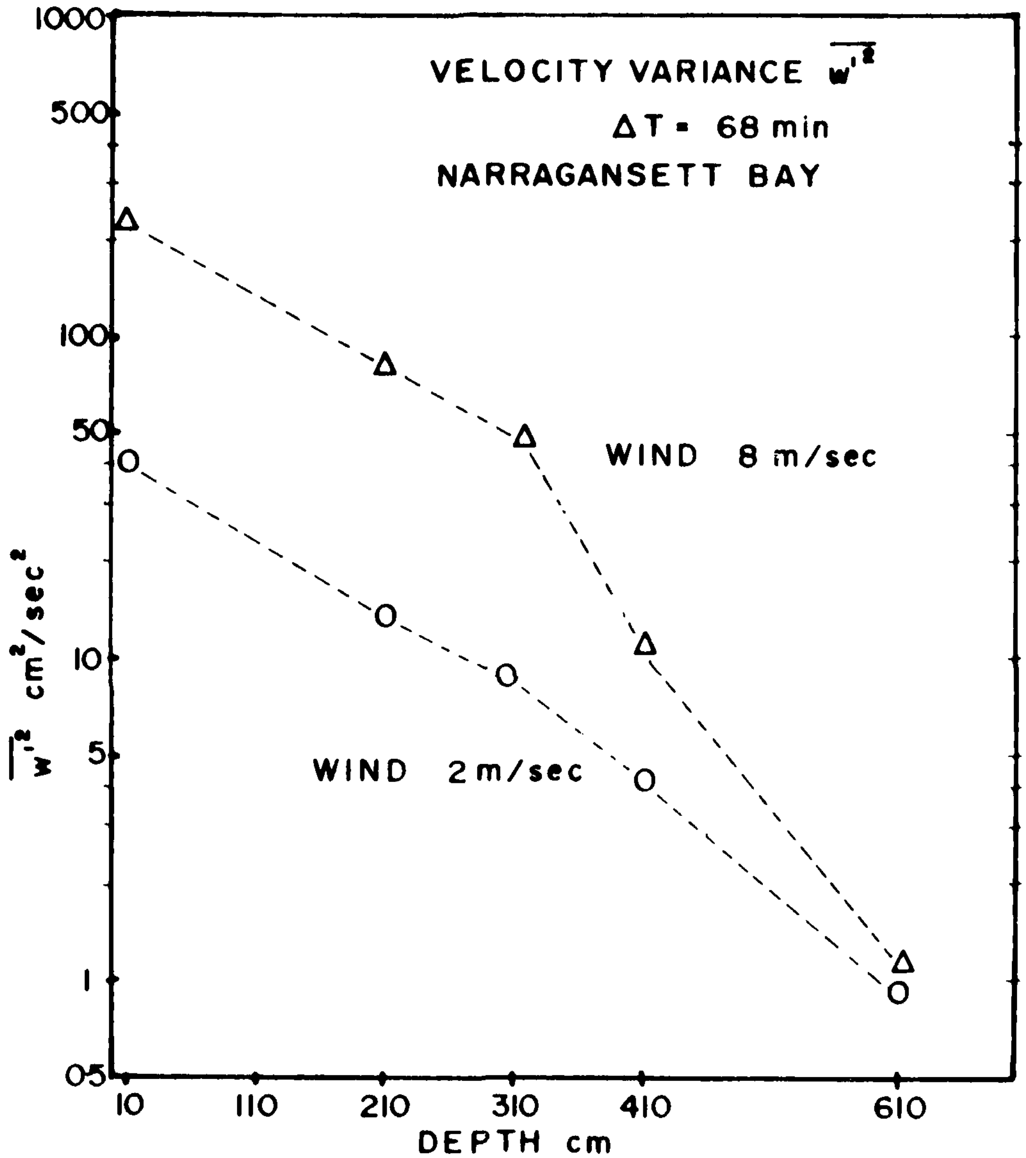

Figure 19: The vertical distribution of variance of the vertical velocity for two different wind speeds. For the delay of 68 min the increased wind stress apparently has only energized the upper 3-4 m. The deeper layers have not felt the influence of the wind stress.

surface energy has not reached to the deepest sensors.

The total wind wave kinetic energy in the water column is obtained by numerical integration of the relation

$$E_k = \int_D^{z_T} \overline{w'^2} dz \tag{19}$$

layer-by-layer over the depths of observation. This is shown in Figure 20 (solid curve) which represents four averages each over 1280 s (21 min). (Here the units are erg/cm^2 x 10^3 = 1 J/m^2.) Clearly, the energy content is increasing throughout the record.

Denman (1973) specifies the turbulent energy input by wind stress as

$$\tau = \rho_A C_A U_{10}^2 \tag{20}$$

ρ_A is air density, C_A is a drag coefficient and U_{10} is the wind speed observed at 10 m height above sea level. The rate of working by the wind stress (or power input) is given by

$$Ew = \tau U_{10} = \rho_A C_A U_{10}^3 \tag{21}$$

The plot of the cube of the wind speed (dashed curve in Figure 20) shows a positive correlation with the increase in the integrated energy content.

<u>WAVTOP 003</u> (14/Apr/78): Six Smithometers were mounted from the AESOP to register w(t) at 10, 50, 100, 150, 200, 300 cm below z_T. For this period the winds remained at about 7 m/s. The w' kinetic energies estimated at two intervals 21 min apart (Figure 21) are practically identical and quite exponential; suggesting that the vertical KE distribution had attained nearly a steady state.

<u>WAVTOP 006</u> (9/Aug/79): This experiment was made from Gould Island (Figure 13). The BLT system was positioned over 17 m water depth using the

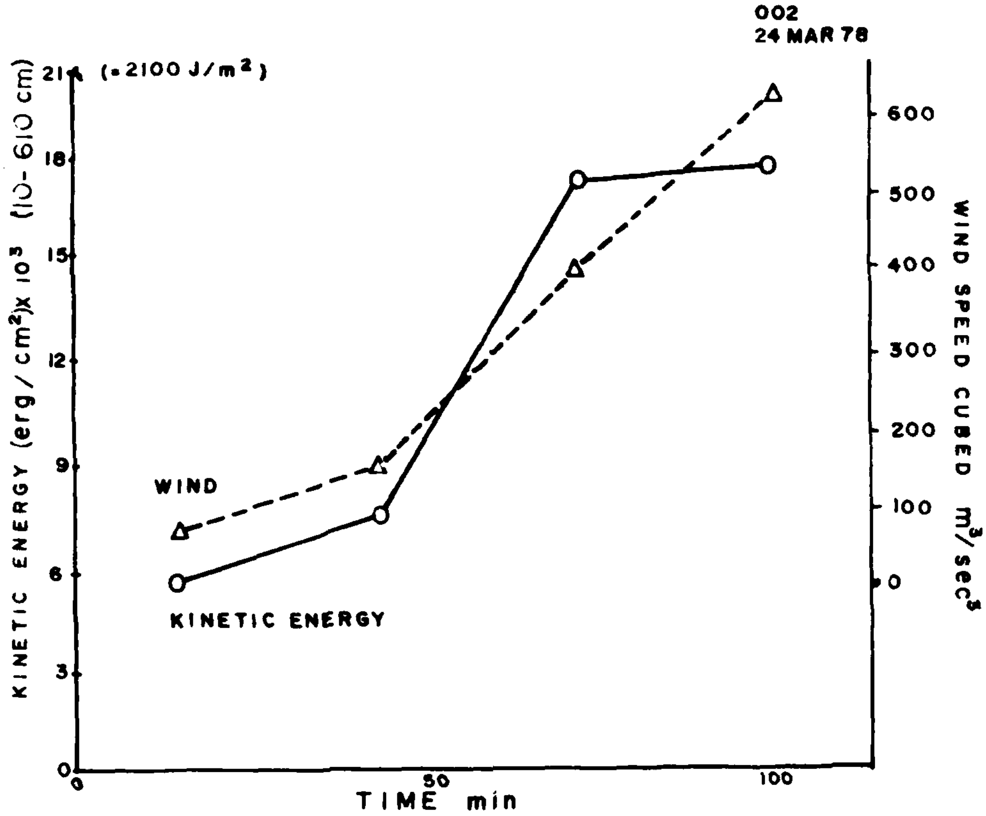

Figure 20: The vertically integrated kinetic energy and the cube of the wind speeds for WAVTOP 006 (observed from AESOP).

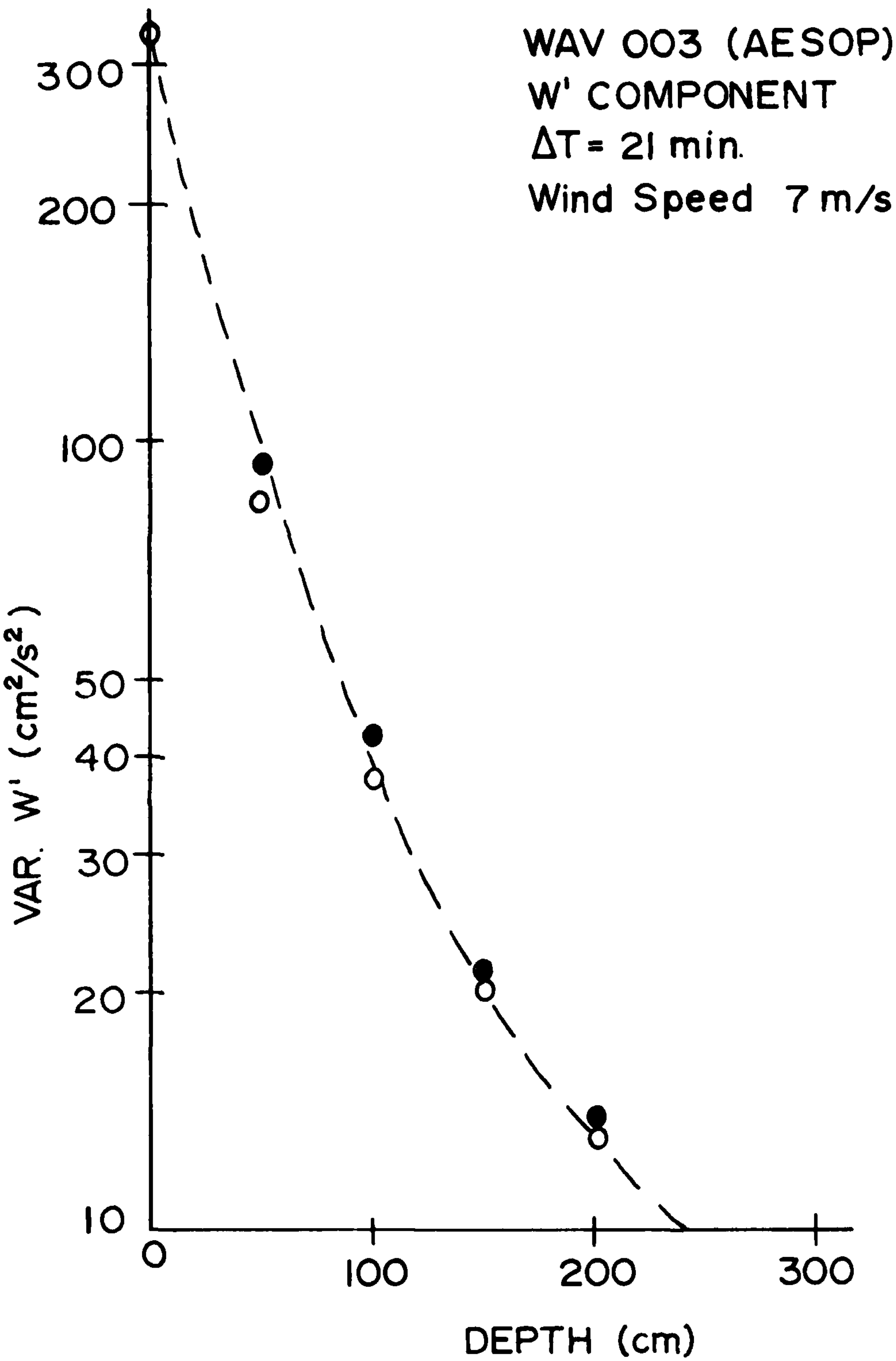

Figure 21: Variance as a function depth for WAVTOP 003 (observed from AESOP).

large stiffboom (Figure 15). Five Smithometers were suspended from the boom support to register w(t) at depths of 10, 50, 100, 150 and 200 cm below z_T. The winds were gentle northwesterly and varied in speed from calm to 3 m/s. The wind waves were small wave lengths 2-3 m and heights 10-15 cm, commensurate with the small wind stresses.

A summary of the energy distribution at various times during these "light air" conditions is given in Figure 22. The energies are very low but still detectable. The data clearly forms an envelope of curves which relate monotonically to the applied wind speed. The energy values at depths 10 and 50 cm change by an order of magnitude between calm and 2.7 m/s. The exponential relation vanished at 100 and 150 cm. Here is the apparent "noise level" where values are associated with the ambient (non-surface wave related) turbulence displayed in the Buzzards Bay (Figure 4). The running variances (calculated for a sequence of 128 s intervals) again show energy perturbations which exponentially decay with depth (Figure 23A - lower curves). The energy distribution also displays sensitivity to the fluctuating wind field. The drop in wind at approximately 15 min is reflected in the variances (even down to 200 cm) within several minutes. A clear increase of wind peaking at 3 m/s is followed, but at a 15-20 min time lag, by the variances at 10, 50, and 100 cm depths.

To examine again the relationship (21), a plot was made of the wind speed cubed versus the vertically integrated kinetic energy (Figure 23B). The wind speed cubed appears to vary as the energy but with a definite phase lead of about 20 min throughout the record which includes a peaking and a final tailing off of energy. Happily the wind, ostensibly the supplier of the surface energy input leads the energy content and not the reverse!

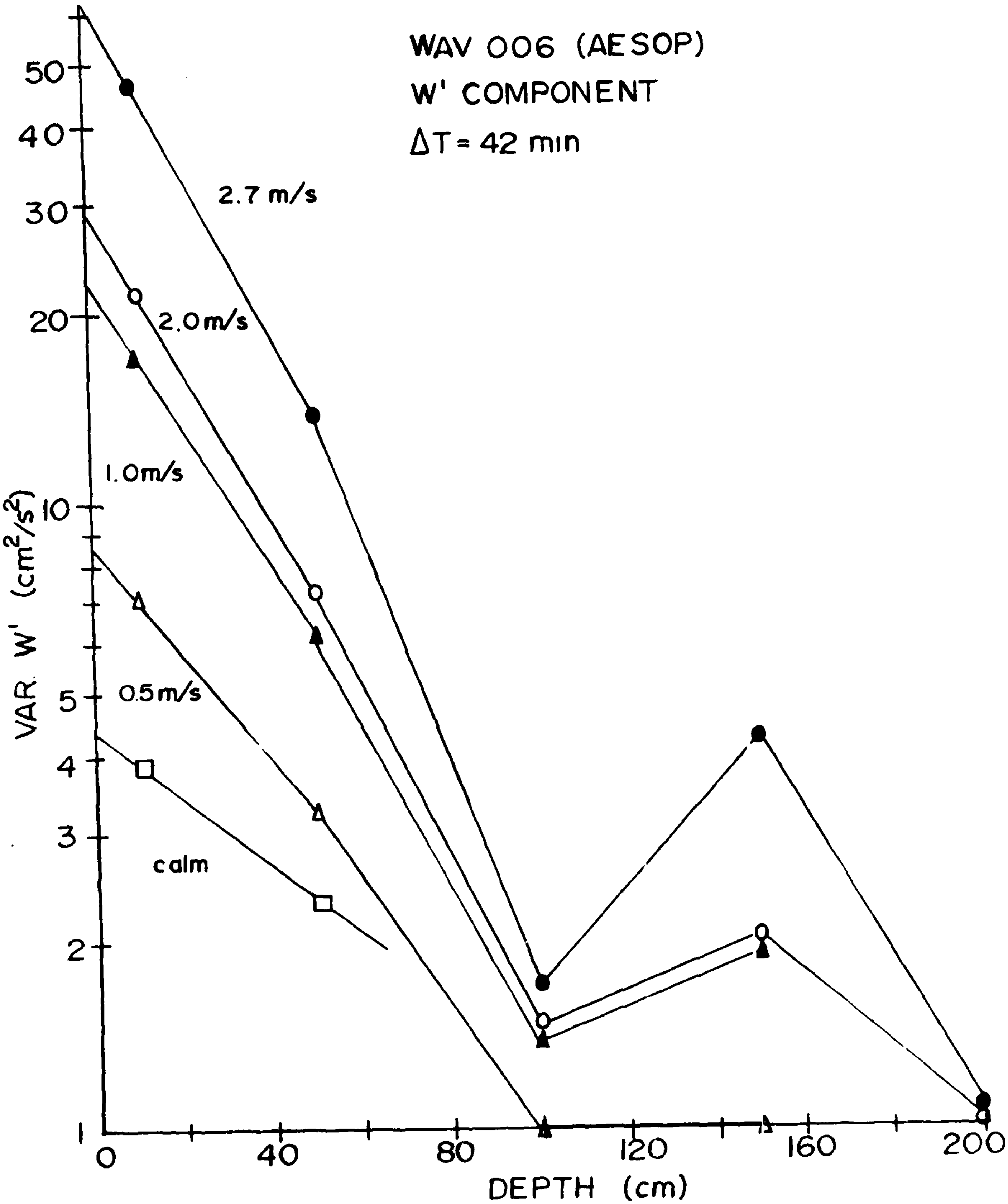

Figure 22: Variance as a function of depth for several wind speeds for WAVTOP 006 (observed from AESOP).

WAVTOP 007 (18/Aug/78): Five instruments registered at w' depths of 10, 50, 100, 150, 200, and 300 cm. Winds ranged from calm to 4 m/s. The energy distributions (Figure 24-triangles and squares) display a rapid decrease from 10 to 50 cm but below (as with WAVTOP 006) an ambient constant intensity occurs at 100 and 150 cm where the curves tend to flatten out in the region around 20 cm^2/sec^2.

WAVTOP 008 (6/Sep/78): Sensors were mounted at 10, 30, 50, 100, and 150 cm below z_T to register the horizontal velocity component u' sensed positively in the direction of the waves. This was the first opportunity to measure this component and to investigate the possible production of wind induced shear in the upper few meters. The SW wind was about 5.0 m/s and waves ranged 5-15 cm in height and 1-2 m wave lengths.

First we examine the running mean values (Figure 25) of the u', estimated from each 10 record sample (i.e., 128 s) for sensors at 10, 100, and 150 cm. The means vary from minute to minute; however, a vertical shear persists, as evidenced by the relative positions of the curves where (except for the 100 cm point at 15 min) $\overline{u}$ decreases monotonically with depth. These variations in $\overline{u}(t)$ could be associated with tidally advected eddies but more likely are due to accelerations from puffs of wind. Unfortunately, we do not have a continuous wind record for this period.

Running variances were estimated in groups of 10 records (120 s) and are plotted in Figure 26 for all depths. The 10 cm energy clearly maintains a higher level for the deeper depths. From 30 cm down, the curves are clustered and move along together.

Another way to examine the energetics is to compare the fluctuation kinetic energy with that of the mean motions. Sutton (1953) used the

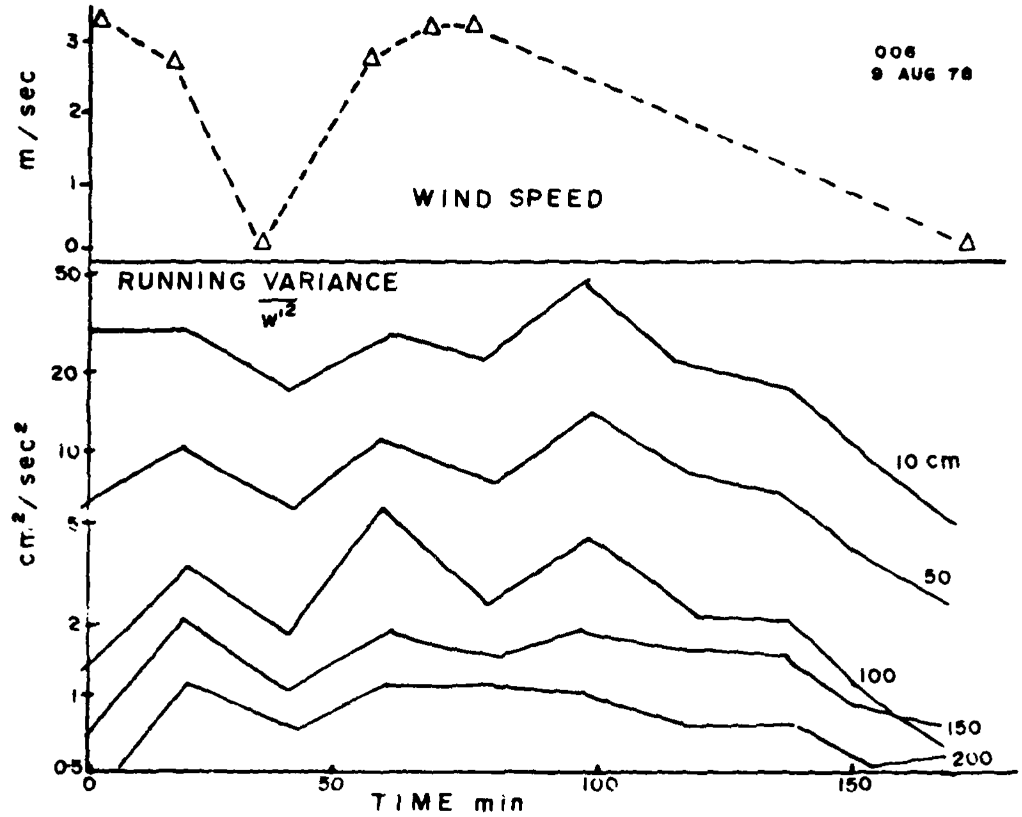

Figure 23: A) Running variances and wind speed.

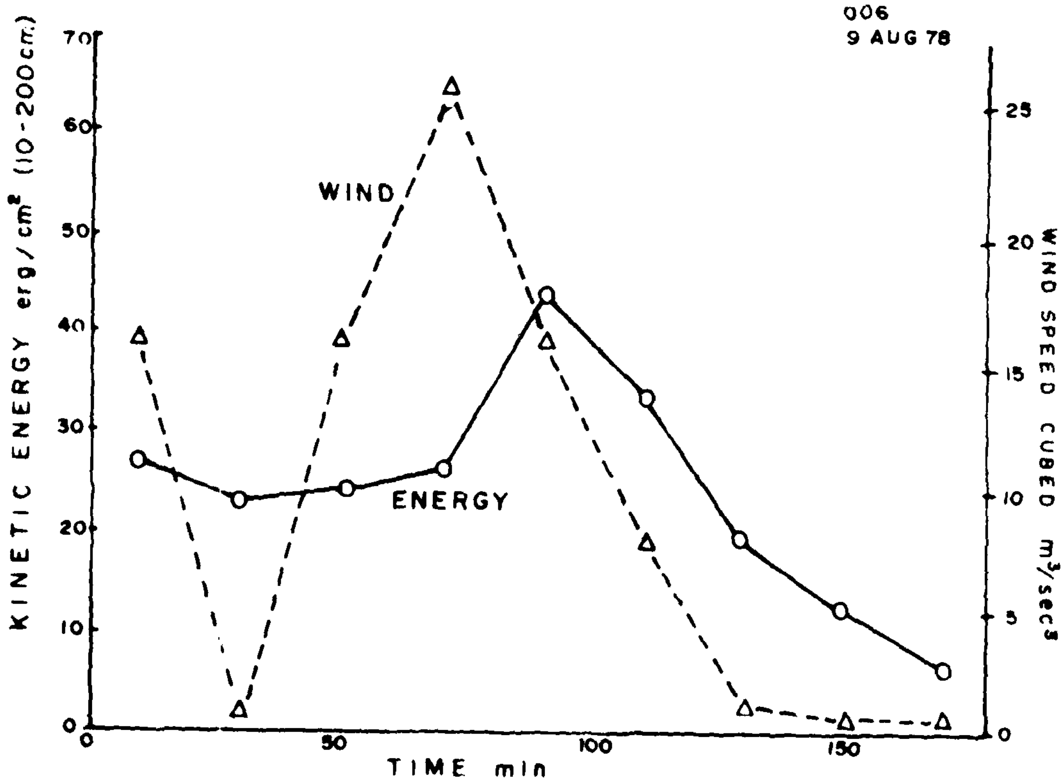

B) Vertically integrated kinetic energy and wind speed cubed: wind stress work leads the energy by 15-20 min.

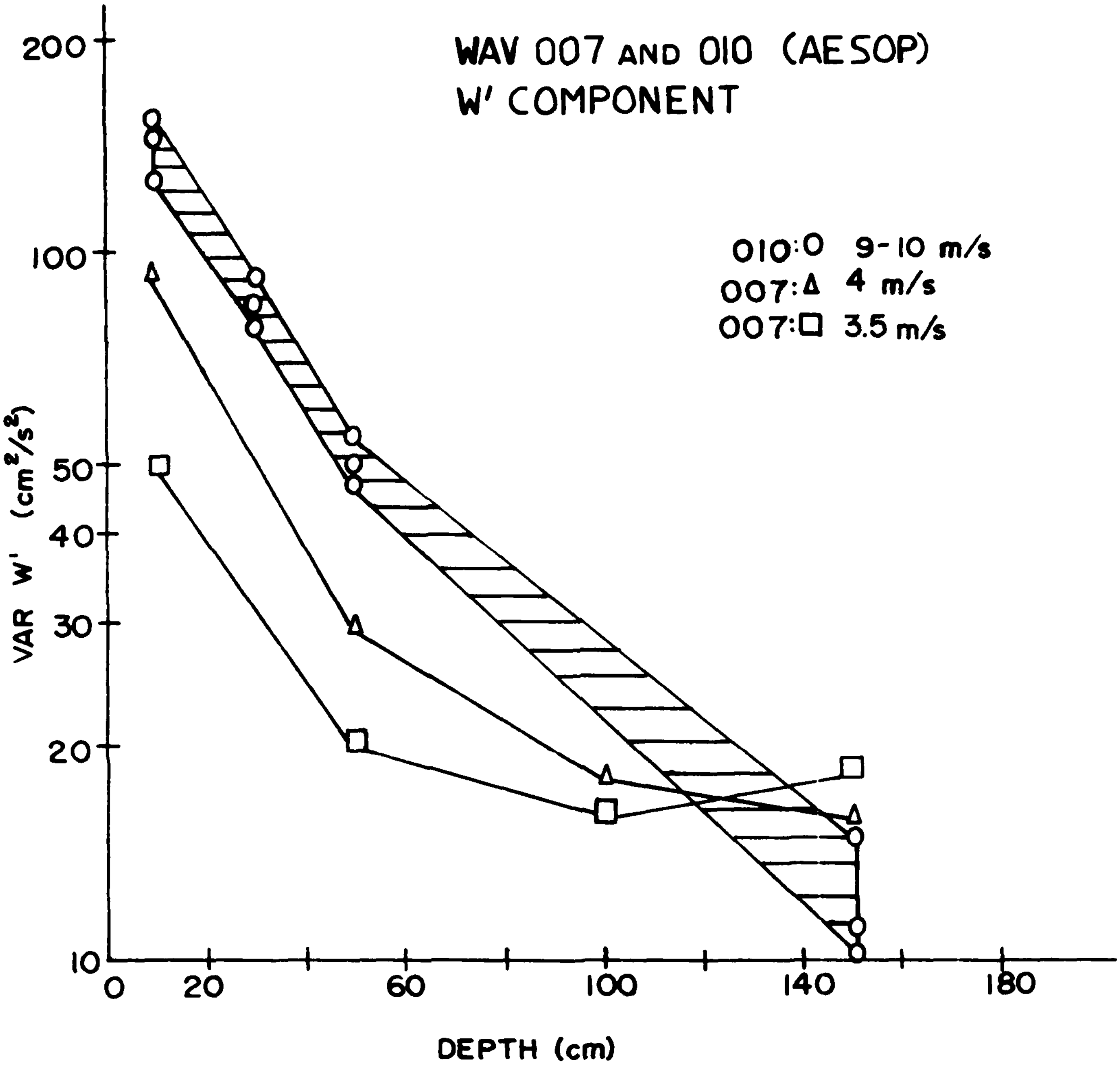

Figure 24: Variance as a function of depth and as a function of various wind speeds for WAVTOP 007 and WAVTOP 010.

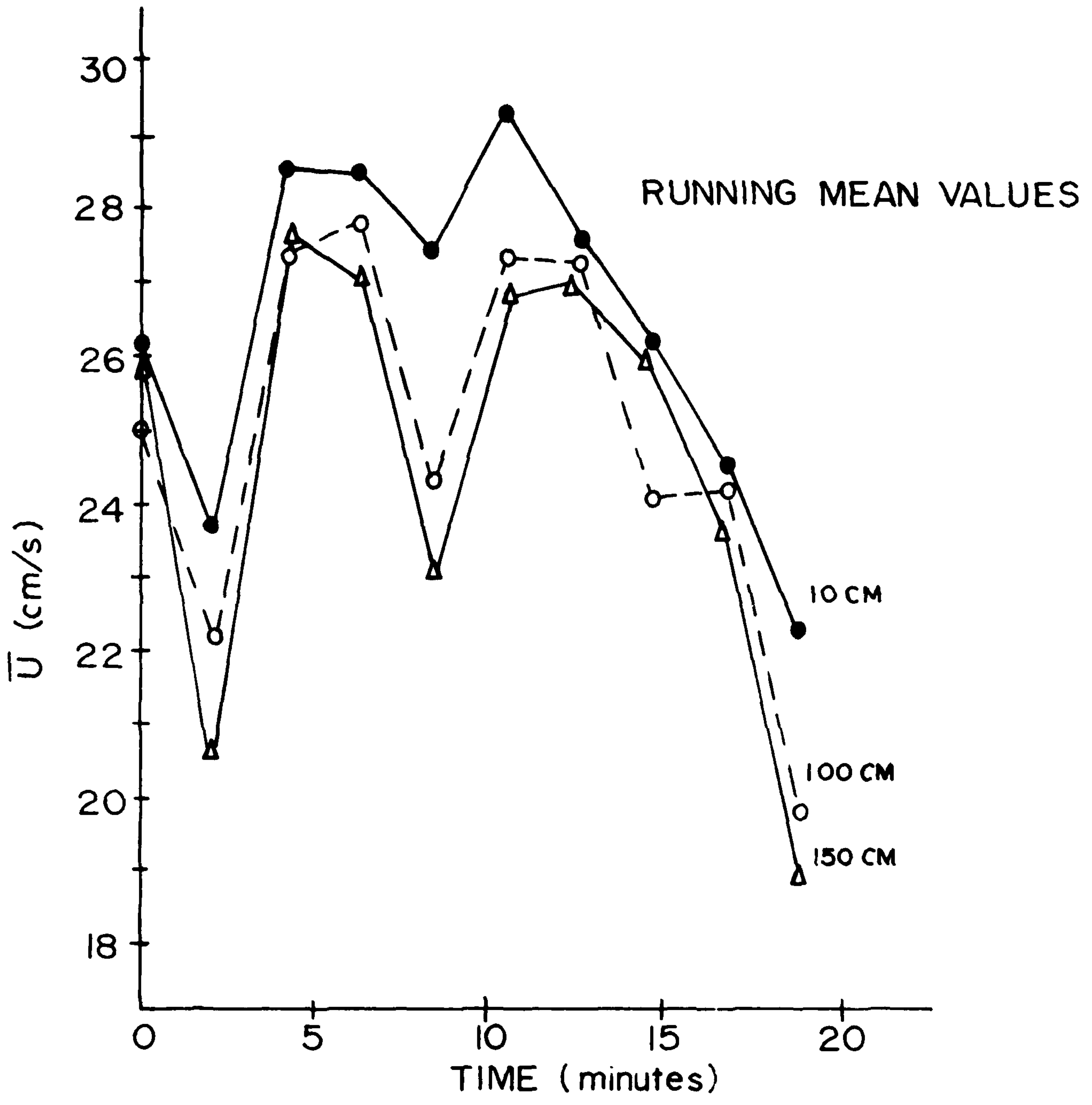

Figure 25: Running mean values for horizontal velocity for WAVTOP 008. These values indicate a mean shear existing between 10 and 150 cm.

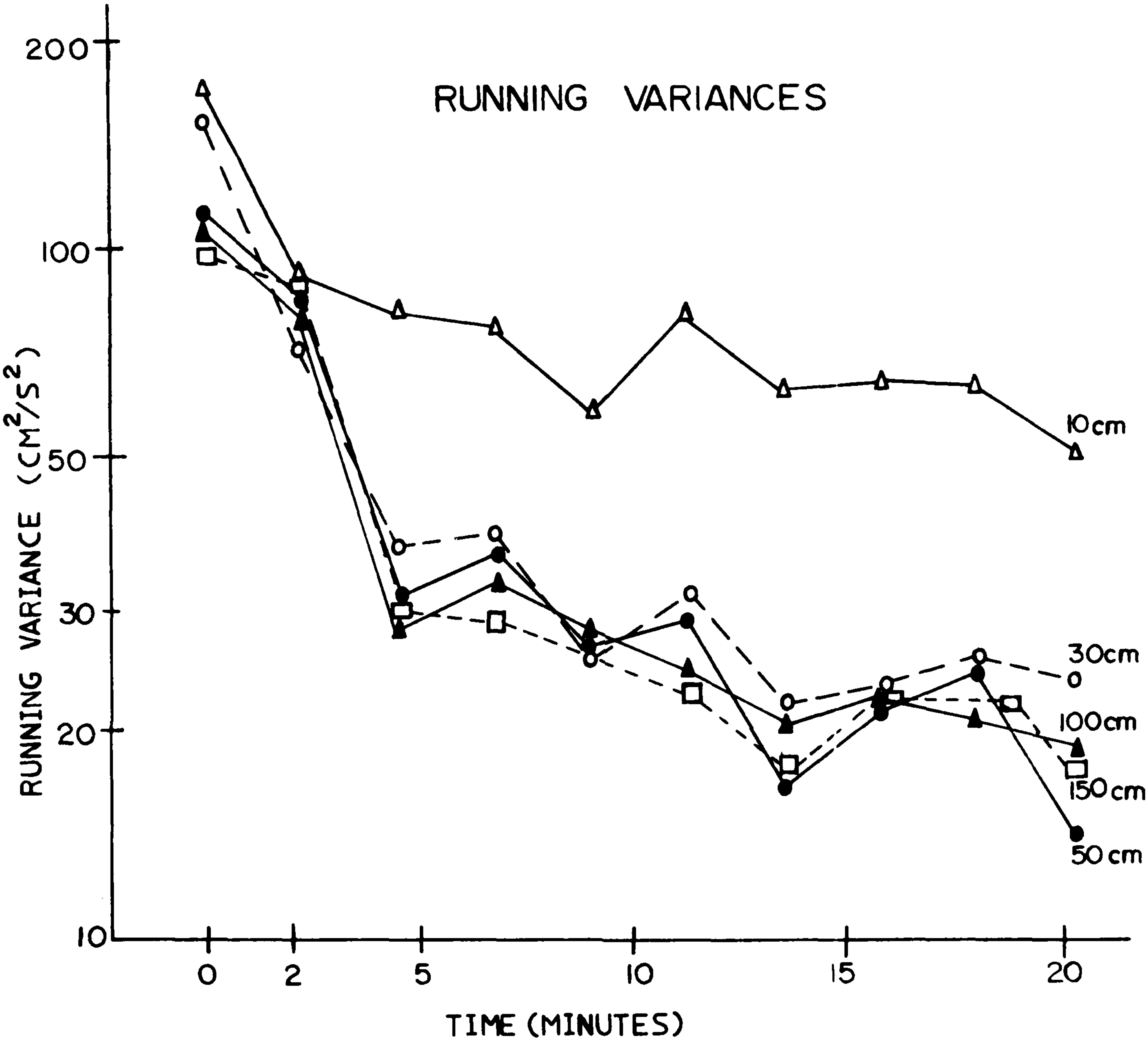

Figure 26: Running variances of u'(t). The wave motions appear confined to the upper 30 cm since the values at 30 cm and below appear quite similar indicating the presence of resident ambient turbulence independent of depth around 30-50 cm.

"gustiness factor" given by

$$G_x = \frac{\overline{u'^2}}{\bar{u}^2} \qquad (22)$$

The factors G_x are plotted for each depth (Figure 27), the numbers represent the sensor depth in decimeters. As with the variances, the 10 cm record is high in variability and the depths from 30 cm down result in highly clustered values, as if there exists a uniform turbulent level. It is noted that after tne initial drop in energy at 3-4 min into the record the remaining gustiness is about constant whereas from Figure 26 the fluctuating energy falls monotonically throughout the record.

<u>WAVTOP 010</u> (17/Oct/78): Smithometers were boom mounted from Gould Island to register the w' at 10, 30, 50, 100, 150 and 200 cm depths. The wind speed ranged from 9-10 m/s and the waves had estimated heights of 50 $\pm$ 5 cm and periods of about 2 s. Observations were made at Gould Island. Figure 24 shows the variances of w' as a function of depth. An exponential decrease in energy is observed down to 50 cm and at 150 cm the usual tail-off occurs. The clustering of data at 10, 30 and 50 cm indicates quasi-steady state conditions.

These energies at winds of 9-10 m/s are compared directly with the values of WAV 007 for 3.5-4.0 m/s, clarifying the relationship of kinetic energy distribution change with wind speed. It appears that the ambient turbulence level i.e., beyond 100 cm, was higher for WAV 007 although the surface energy was lower.

<u>WAVTOP 011</u> (19/Oct/78): Current meter pairs from Gould Island placed at 30 cm depth to register u' and w' and at 50, 100, 150, and 250 cm to record w'. Wave heights were small, 15 cm and wave periods 1.7 s for wind

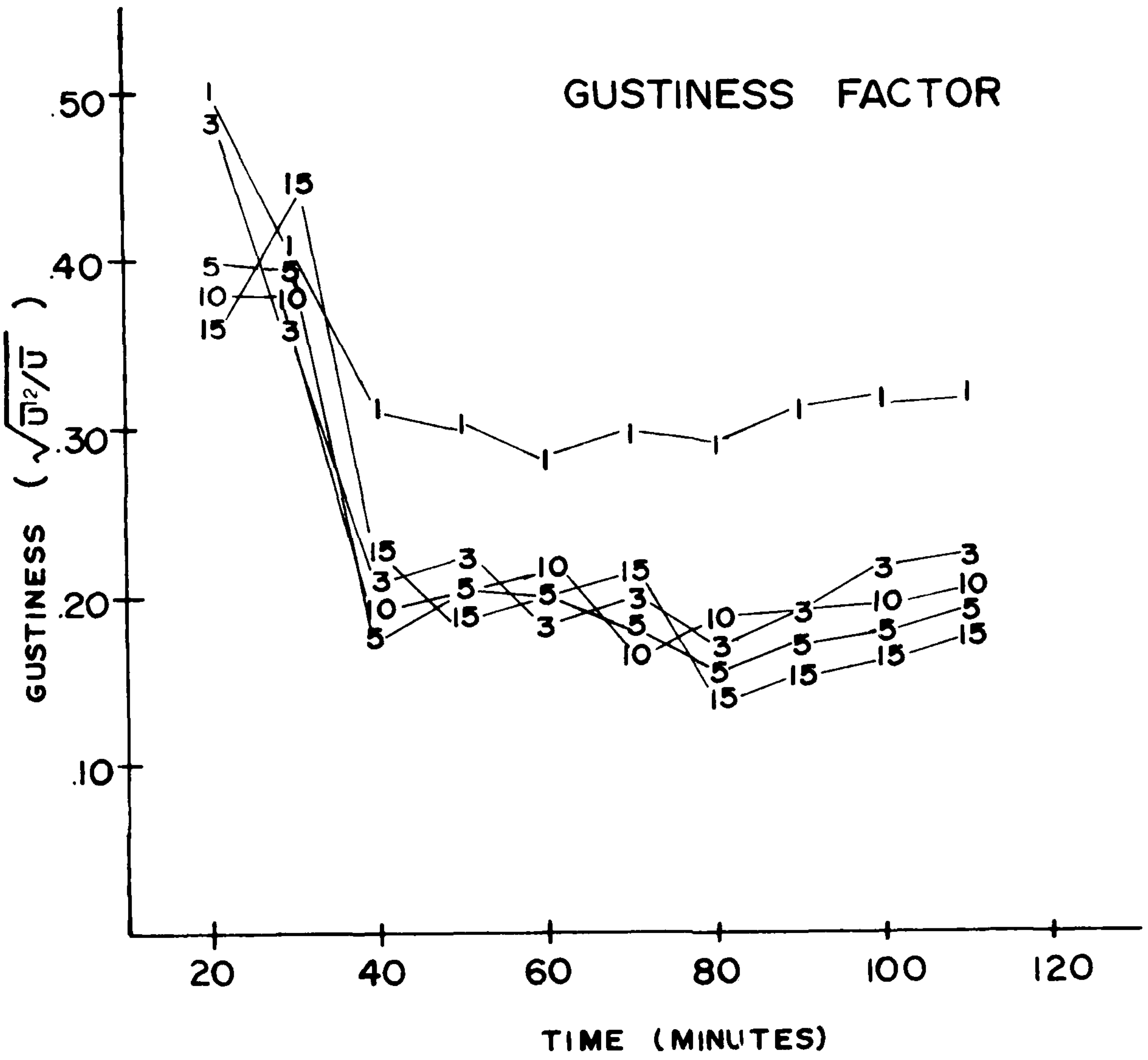

Figure 27: Gustiness factor plotted as afunction of time. The numbers refer to decimeter depth. The gustiness appears to have similar patterns as the variances. This again, as with Figure 26, suggests the existance of a uniform turbulent intensity.

at about 5 m/s. Figure 28 (open and closed circles) shows the typical exponential decay circles which flatten out at 150 cm depth as with previous records.

WAVTOP 012 (24/Oct/78): A sensor pair to register u' and w' was placed at 30 cm while w' recorded at 70 and u' at 110 cm; the wind speed was 5.5 m/s. The variances of both u' and w' as are shown in Figure 28 (triangles) indicate similar magnitudes and depth attenuation.

The variance (kinetic energy)-depth distributions for both WAV 011 and WAV 012 were observed under approximately the same local wind speeds, i.e., 5.0-5.5 m/s. The data from each record set, however, differ sufficiently to indicate that kinetic energy at a given depth is related to more than just the local wind speed.

These WAVTOP records of variances or kinetic energies observed with depth and time suggest the following:

1. Simultaneous measurements of velocity components at several depths in the wind wave field show an exponential decrease of amplitude and hence energy, with depth. These results suggest that the motions observed are primarily surface wave induced and hence follow approximately classical surface gravity waves. These results follow closely with those obtained in Buzzards Bay (Shonting 1967).

2. Changes in the vertical energy distribution and the total vertically intergrated energy correlate directly with the changes in wind and surface wave conditions. The kinetic energy (associated with the fluctuating wave motions) varies as the wind speed but displays a time lag or phase shift whereby the energy profiles reflect the downward propagation of energy as it "flows" from the surface. Moreover, the integral kinetic

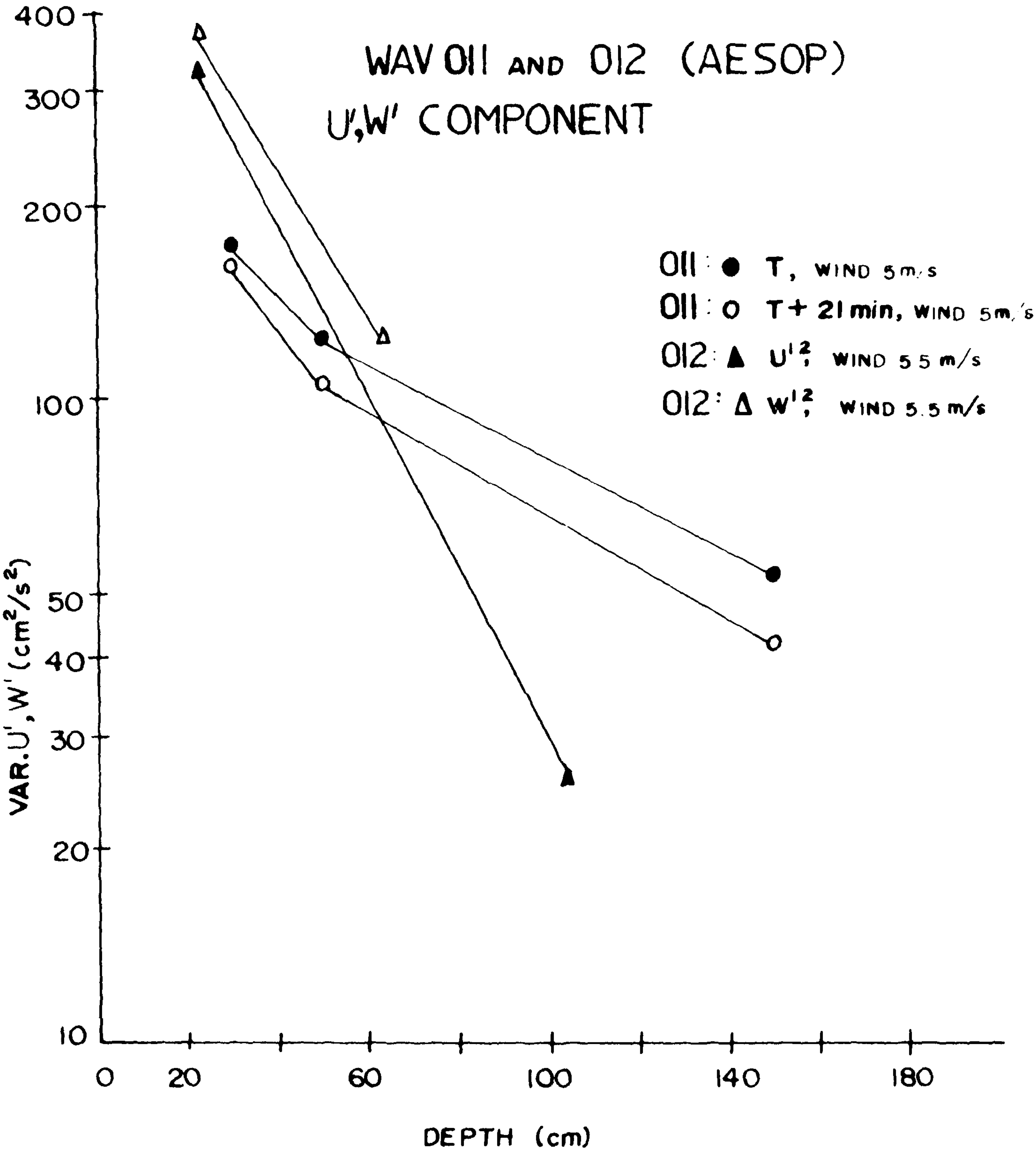

Figure 28. Variances of vertical velocity as a function of wind speed and as a function of depth for WAVTOP 011 and WAVTOP 012.

energy of the water column estimated at various times, during which the wind was accelerating or decelerating, displays phase lags of the order of 15-25 min. equivalent to downward propagation rates of energy of 2-5 mm/s.

3. Variances at various depths during both steady and accelerating wind conditions display strong fluctuations in wave energy which are generally in phase at all depths and vary by as much as a factor of two or three. The periods of fluctuations appear to be of the order of 3-10 min. (i.e. 40 to 140 times the wave period). This patchiness of kinetic energy appears associated with real inhomogeneities in the wind/wave field probably associated with gustiness, i.e., spatial variability in the wind field in the wave generation area.

4. Measurements of the horizontal wave velocity component at different depths in which the running mean is calculated display a true time variable velocity shear in which the velocity in the wind direction is highest at the shallowest sensor, decreasing roughly linearly with depth. These results, although very qualitative, suggest that we have recorded actual boundary shear generation.

It should be noted that much scatter occurs in the depth distributions of the velocity data. Some of this could be caused by noise associated with buoy motions (when AESOP was used) and spiking in the digitizing process. However, real deviations from exponentiality and the random scatter occur for at least two geophysical reasons;

1. The motions tending to be more random, i.e., turbulent as opposed to wavelike, may not obey an exponential law. These motions, which near the surface would be of low intensity compared to the waves, would arise deeper where their magnitudes exceed the attenuated wave motions. The net effect of this superposition of wave turbulent velocities would produce relations

where exponential fall-off occurs to a depth where the ambient turbulence displays scatter, precisely what is shown in Figures 22 and 27.

2. For the most part the wave measurements were made in situations where the waves generated were not equilibrated with the wind conditions, i.e.,not "fully developed". Thus, accelerating winds would produce small waves locally which are superimposed upon larger waves (miniature swells) propagating from an upwind region. The superposition of these motions would produce vertical energy distributions which would portray a complex mix of the energy undergoing constant redistribution. This situation is suggested by Figure 18. Furthermore, this transient insertion of energy from the accelerating wind of local smaller waves could provide an energy change depicted by Figure 19, where below 310 cm energy falls off and becomes indistinguishable with energy distribution of the previous level.

The kinetic energy data thus far obtained are preliminary in nature but the making of much more precise observations is possible with the present systems. To obtain better quantitative estimates of the vertical energy distribution and integral energy content and their relation to the wind field, will require careful monitoring of wind speed, fetch, duration and of the character of the local sea and swell.

C. The Relation Of "Surface" Kinetic Energy To Wind Speed

How best are we able to characterize the kinetic energy (ke) representative of that at the "sea surface"? Our analysis permits estimating the Ke at specific depths with respect to the mean free surface. Since the actual sea surface is moving it appears useful to extrapolate our measurements above the uppermost observation in order to deal with some defined mean surface.

The kinetic energy data in the form of the variance of the vertical velocity w'(t) clearly exhibits an exponential decrease with depth such

that we may conveniently extrapolate the data on the semi-log plots from the uppermost depth of measurement (usually 10 or 50 cm beneath the mean trough level) to zero on the depth scale which we have defined as the mean trough depth z_T . This allows us to intercompare data sets on a more systematic basis of the "surface" kinetic energy as related to the wind speed observed at the time of observation. Figure 29 shows a composite plot for several WAVTOP observations. The relation seems approximately linear, however, the scatter especially for the lower wind speeds, may be masking an exponential increase of surface kinetic energy versus wind. Actually this relationship is surprisingly clear, considering the inherent scatter in the data and also the likelihood that most of the observations were made in conditions which were quite transient, quite far from the ideal "steady state".

D. Auto-Spectra

In the previous section we portrayed the gross kinetic energy characteristics at various depths by the variances of the velocity components. The auto-spectra describes the kinetic energy as a function of the frequencies of the ensemble of various Fourier components of the observed motions. These statistics hence can detail the character of the windwaves being registered. Selected record sequences of various WAVTOP experiments were processed for energy spectral density estimates.

The general computer program used to calculate energy spectra is based on the Cooley-Tukey Fast Fourier Transform (FFT) algorithm (e.g. see Bendat and Piersol, 1971). A 10% cosine taper window is applied to the time series data to reduce side-lobe leakage. If necessary, zeros were added to the series in order to make the number of points equal to a power of two. After computing power spectra from the complete Fourier coefficients, one-sided spectra were plotted. For a given time segment, spectra were calculated at Smithometer position (spaced at different depths). Since the wind waves

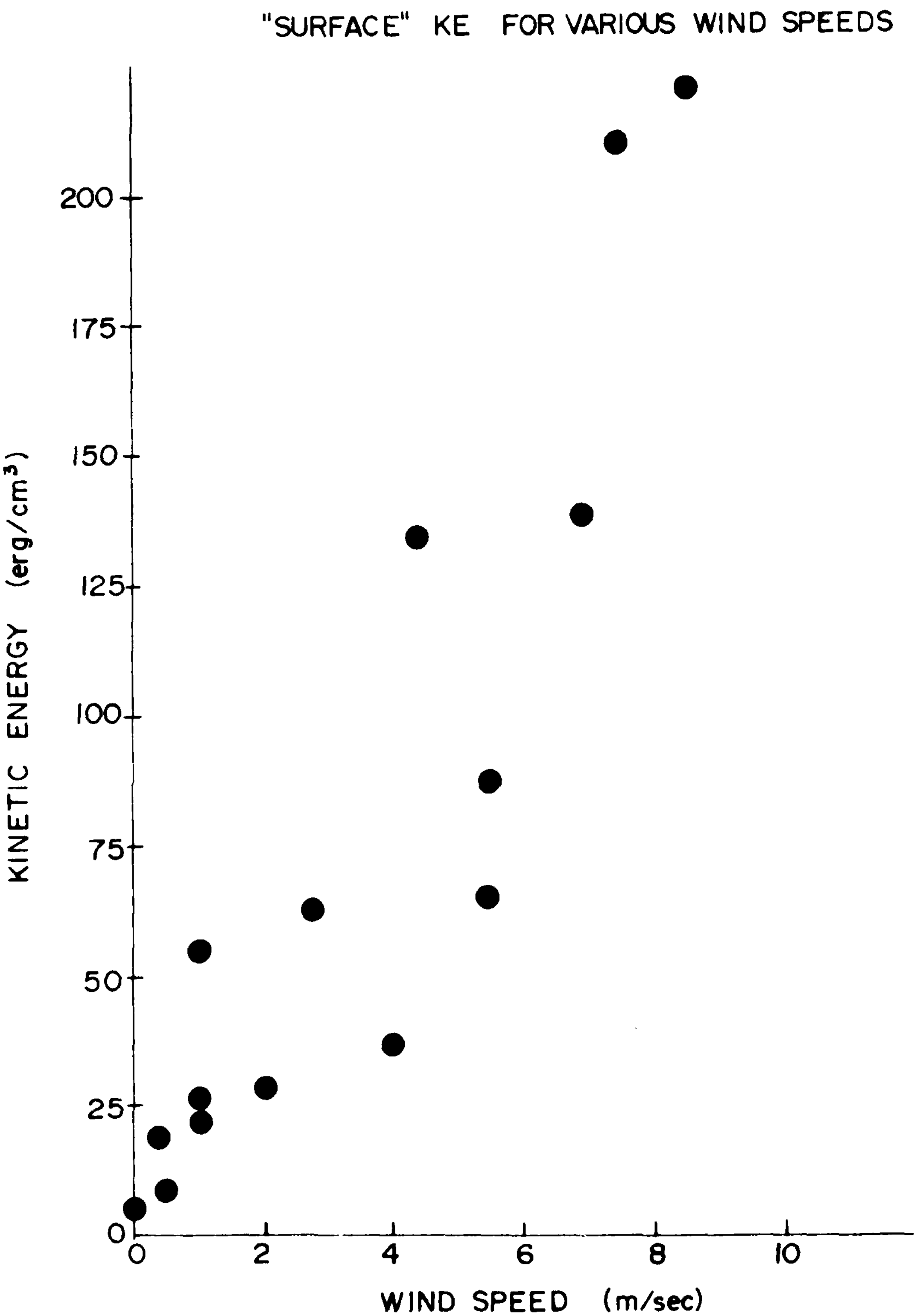

Figure 29: The kinetic energy at the "sea surface" estimated by extrapolation to zero depth of the variance/depth curves for various wind speeds. Values are taken for all WAVTOP records discussed.

of concern had periods of 1-5 sec, a sequence of 1024 data points was used in each spectral calculation. As each point represents 0.2 sec, the record length equaled 204 sec; a high enough sampling rate and long enough record to resolve and properly display the wind wave frequencies. In accordance with the sampling frequency, fluctuations of 2.5 Hz (the Nyquist frequency) are the fastest signals observable.

The frequency averaging provision of the computer program produced smooth spectra that had 10 degrees of freedom and a normalized standard error of about 0.3.

The velocity spectra provide a variety of interesting phenomena associated with the wave and turbulence motions. First is the attenuation of spectral density with depth as was grossly depicted by the variance with depth curves in section VI-B. Figure 30 shows three spectra of the vertical velocities for WAVTOP 010 simultaneously recorded at 10, 30, and 50 cm depth below the mean trough level. The winds were 9-10 m/sec blowing uniformly from the NW,producing quite uniform waves.

Several features of the spectra are noted:

1. The spectral peaks are very "monochomatic" with some 90% of the energy falling within 0.95 to 0.55 Hz bandwidth.

2. Clear energy attenuation occurs with depth with the dominant peak centered at about 0.5 Hz and the lesser peak at 0.65 Hz.

3. A slight but perceptible "red" shift of the peak occurs with depth.

4. There appears a "white" background motion from 0.0 up to about 1 Hz which persists at the three depths with the same energy levels.

The spectra of the motions like the gross energy,arethe result of complex interactions of wind stress acting on the sea surface both in the local time and space of the measurements and also to some degree a result of events taken place upwind (i.e., upwave) at an earlier time. For example,

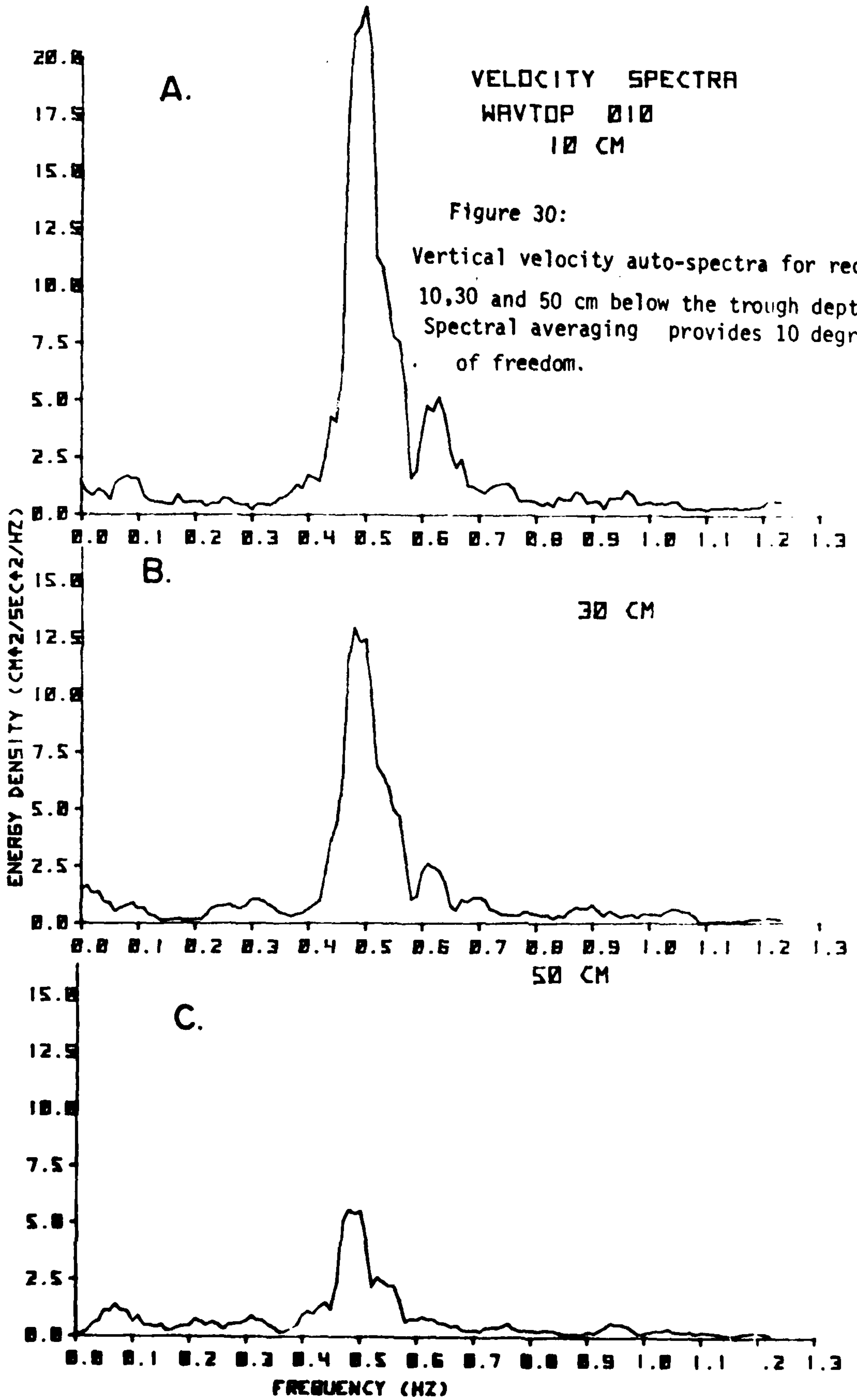

Figure 30:

Vertical velocity auto-spectra for records 10,30 and 50 cm below the trough depth. Spectral averaging provides 10 degrees of freedom.

Figure 31 A, B, and C shows three spectra from recordings of w'(t) obtained from a sensor mounted upon the AESOP at 10 cm depth. The data were estimated over 102 s intervals and are separated by 52 and 55 min. time intervals. The wind during this period varied from 2.5 to 3.0 m/s. The initial energy is highest and is concentrated at 0.5 Hz ($t = t_0$). Next at $t = t_0 + 50$ min the wave energy drops and the 0.5 Hz waves diminish also. Finally, at $t = t_0 + 107$ min the spectra have reddened with a lower frequency wave at 0.2 Hz dominating.

What we have observed is the likely result of a complicated mixture of Eulerian and Lagrangian events. Eulerian changes, because the stress input is varying at the immediate location of the experiment. Lagrangian changes, because the waves are moving across the bay plus the AESOP platform is also drifting with the tidal flow at about 3-5 cm/s. The peak at t_0 + 107 min is likely to be a wave train generated to windward which has arrived at our sensor in the form of a *miniature* "swell."

Spectra from WAVTOP 012 display the remarkable resolution of the Smithometer impellers in detecting wave motions. Figure 32 A, B, and C shows auto-spectra for three time series observations from sensors placed at 30, 50, and 100 cm depth. The trio of data extended over 102 s. The wind was 6.0 m/s NW and the ambient waves were observed to be quite regular in direction and having estimated periods of 2-3 s. The spectra of Figure 33 show their high degree of monochromaticity. The single spike at 0.4 Hz (or 2.5 s period) for the 30 cm deep sensor represents about 80% of the spectral density proportional to the variance of 111.4 cm^2/s^2. At 50 cm depth the motions still exhibit a vertical "line spectrum" which has diminished greatly from that of 30 cm depth, the variance having been reduced by 61%. The 100 cm depth spectral peak has almost but not completely vanished and the variance has been reduced by 94%.

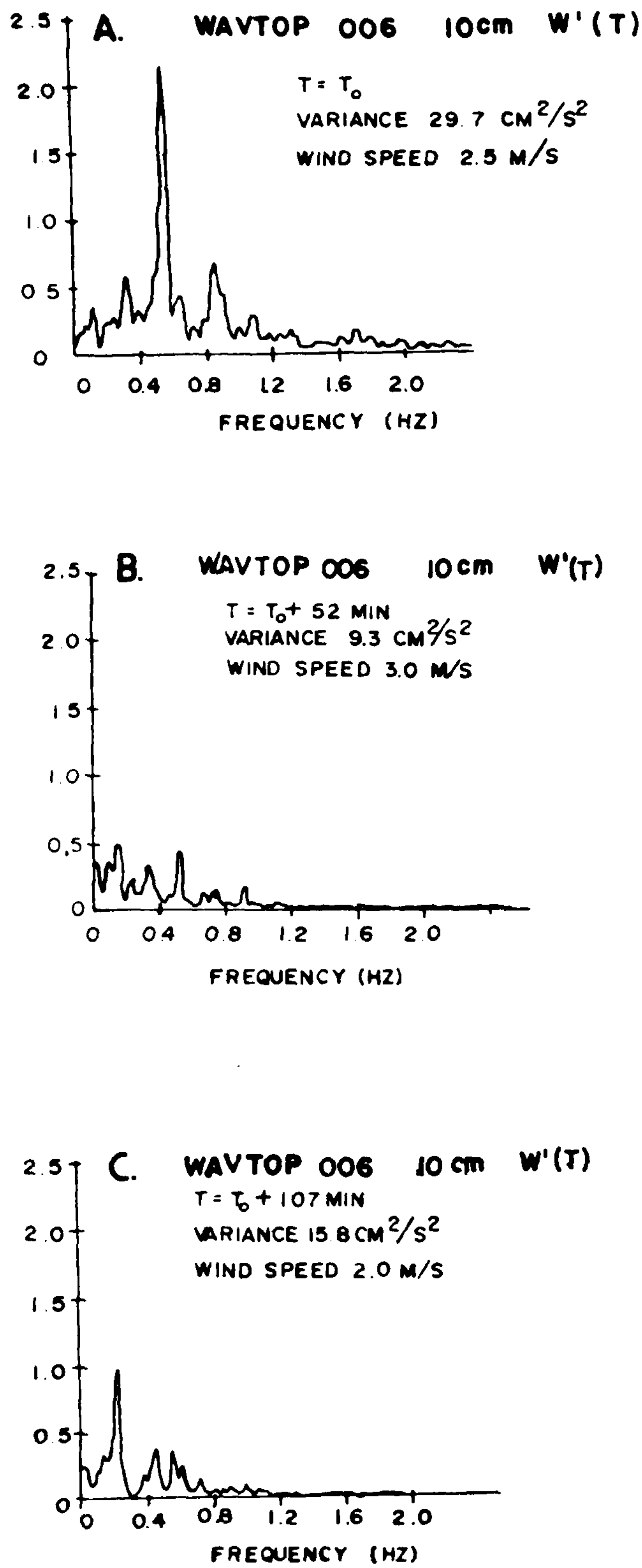

Figure 31: Three sequences of auto-spectra variation at 10 cm depth record.

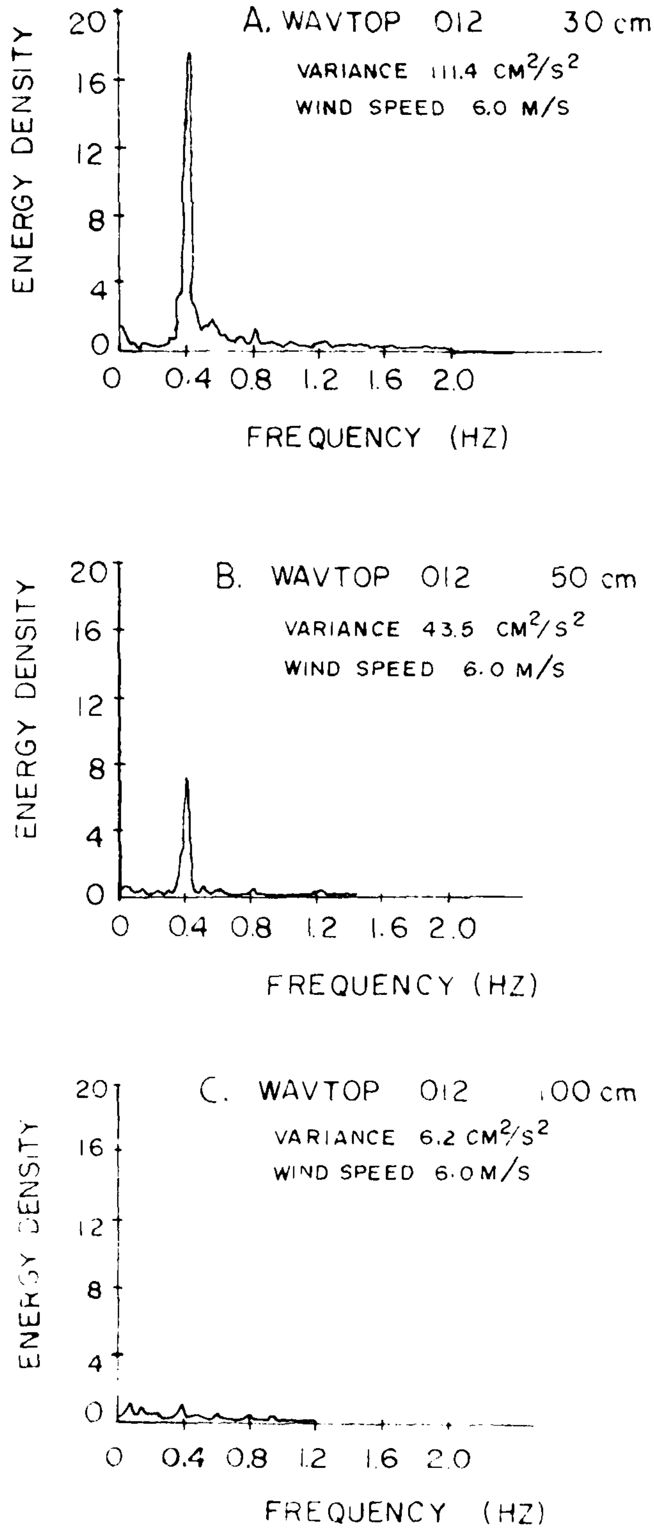

Figure 32: Spectra showing different distribution of energies at various depths for 30, 50 and 100 cm depths for WAVTOP 012.

The spectra of the velocity components, aside from its value to analyze the wave/turbulence structure, can be used as a check to monitor the stability of platform from which the Smithometer-BLT system is attached. For example, Figures 33A and 33B show spectra from $w'(t)$ components at 410 and 610 cm measured from the AESOP system. The 410 cm record displays two large peaks at periods of 12.5 s and 5.2 s. The former period is certainly too long to be characteristic of a wave in Narragansett Bay with a maximum fetch in the NW direction of only 7 km. The former peak is conceivable for a surface wave having traveled some distance down the Bay.

The 610 cm spectra of $w'(t)$ show the same 12.5 s peak which has about the same amplitude as that at 410 cm depth. However, the 5.2 s peak has all but vanished. Conclusion: our sensors have registered a resonant motion of the AESOP buoy which becomes more apparent at deeper depths where the surface waves are strongly attenuated.

E. Estimates of Reynolds Stresses

For WAVTOP records 011 and 012 simultaneous recordings were made of u' and w' at a depth of 30 cm beneath the mean trough level z_T. These data permitted estimating the Reynolds stress component given by

$$\tau_{xz} = -\rho\overline{u'w'} \tag{23}$$

This is the correlation (covariance) between u' and w' such that a positive value of τ_{xz} indicates a downward flux of horizontal momentum. Pairs of u' and w' sampled each 0.2 s were multiplied and then averaged over each "record length" of 12.8 s or 64 data pairs.

1. WAVTOP 011

The plot of the "running stresses" is shown in Figure 34 for 200 records covering 43 min. During this period, the wind was 5.0 m/s and the wave heights were approx. 15-20 cm with periods averaging 1.7 s. Waves

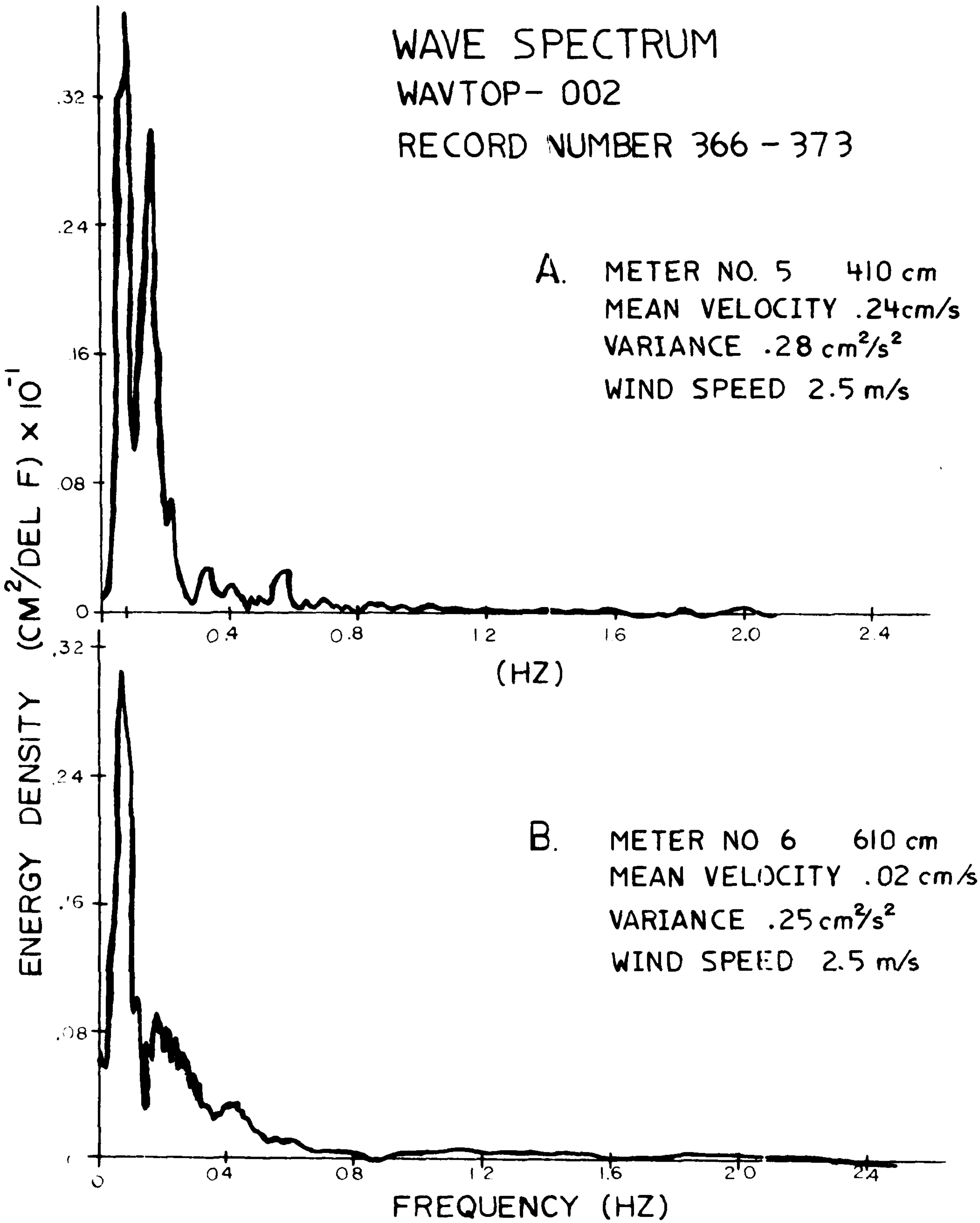

Figure 33: The 5.2 s peak attenuates strongly from 410 cm to 610 cm; clearly wind wave energy. The 12.5 s peak shows no attenuation and appears to be natural vertical AESOP motion.

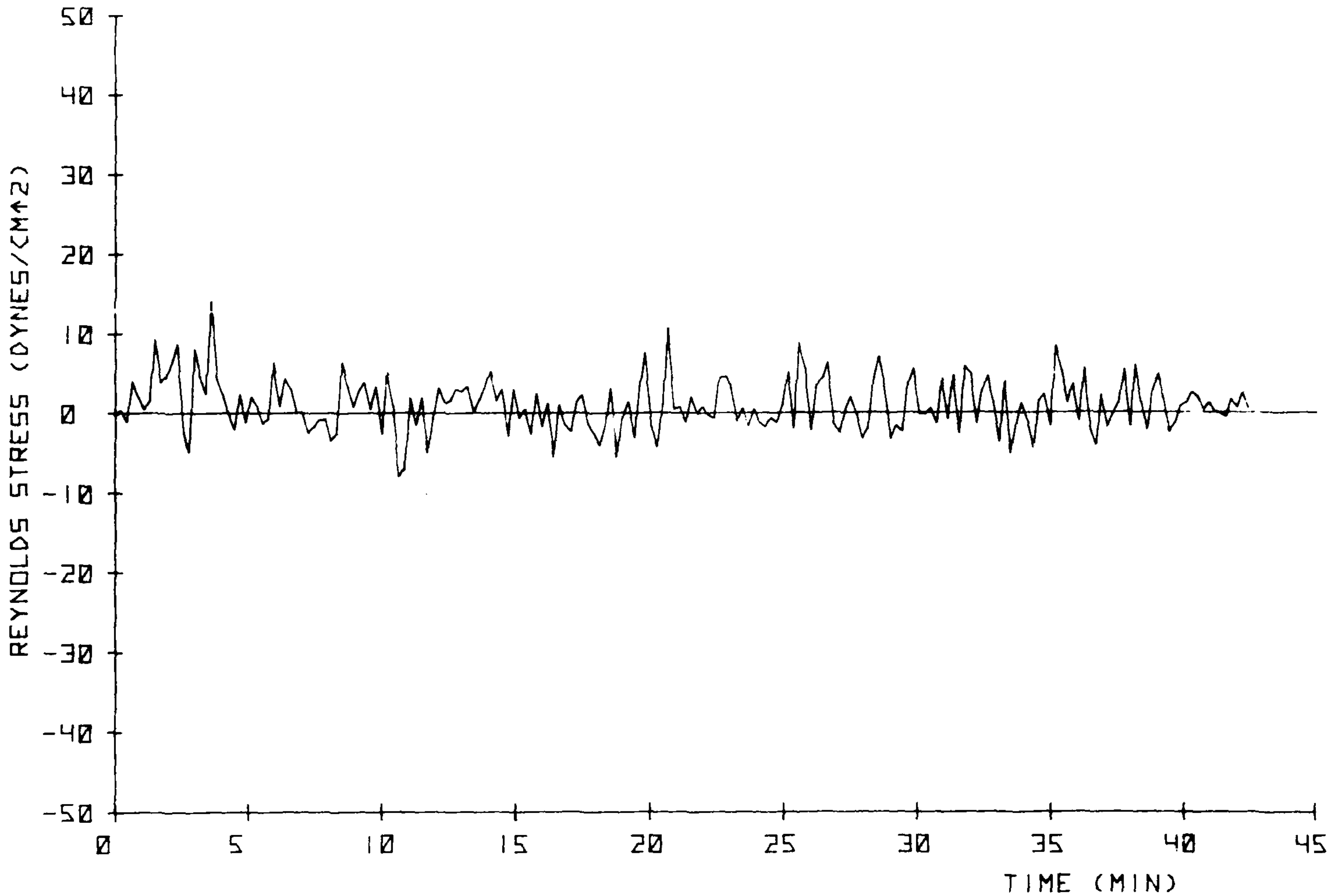

Figure 34: Raw data of the Reynolds stress estimates for WAVTOP 011. The stress average for the entire record was +1.06 dyne/cm^2 signifying downward momentum flux. The sharp peaks and valleys suggest that stress transfer to be highly nonlinear and that transient effects are highly important. For this record the wind speed averaged 5 m/s.

were observed arriving from the NW and also from SW, giving a complex wave field. The raw data record shows much variability with strong spiking giving ranges of stress from +5.5 down to -14.3 dyn/cm^2 and averages +1.06 dyn/cm^2. This positive value demonstrates a downward flux of +u horizontal wind imparted momentum.

The sharp peaks indicated a bursting effect which has sustaining periods of 10-50 s. These periodicities are not incommensurate with observed gustiness or pulses of wind over the water.

Since it is the mean stresses which have an overriding effect upon surface water transport, a filtering was done on the raw data record (Figure 35) in the form of a nine point equally weighted running filter. Here the immediate effect is to smooth the values and produce a generally positive persistent stress with small amplitude undulations.

2. WAVTOP 012

Figure 36 shows the running stress estimated from the raw data, but with much larger amplitudes than occur in WAVTOP 011. The average stress for the 200 point (43 min) sample was +1.52 dyn/cm^2. The wind during this period was more variable, averaging 5.5 m/s. The waves, however, were more fully developed and unidirectional. The pulsing is much more dramatic than for WAVTOP 011, especially during the first 12 minutes of the record. Here a periodicity seems to occur at 2-3 minutes again. This is suggestive of irregularities in wave trains as they pass the suspended instruments.

The nine point equally weighted filter again (Figure 37) smooths much of the character of the fluctuations with the initial imputs from 2-8 minutes supplying most of the momentum flux for the record.

The irregularity in the stress values points to the problem of obtaining stress values representative of a large ocean area. The Reynolds stress is a signed vector and spatially averaging it over large areas will generally reduce its magnitude (Shonting, 1970). Furthermore, the stress is

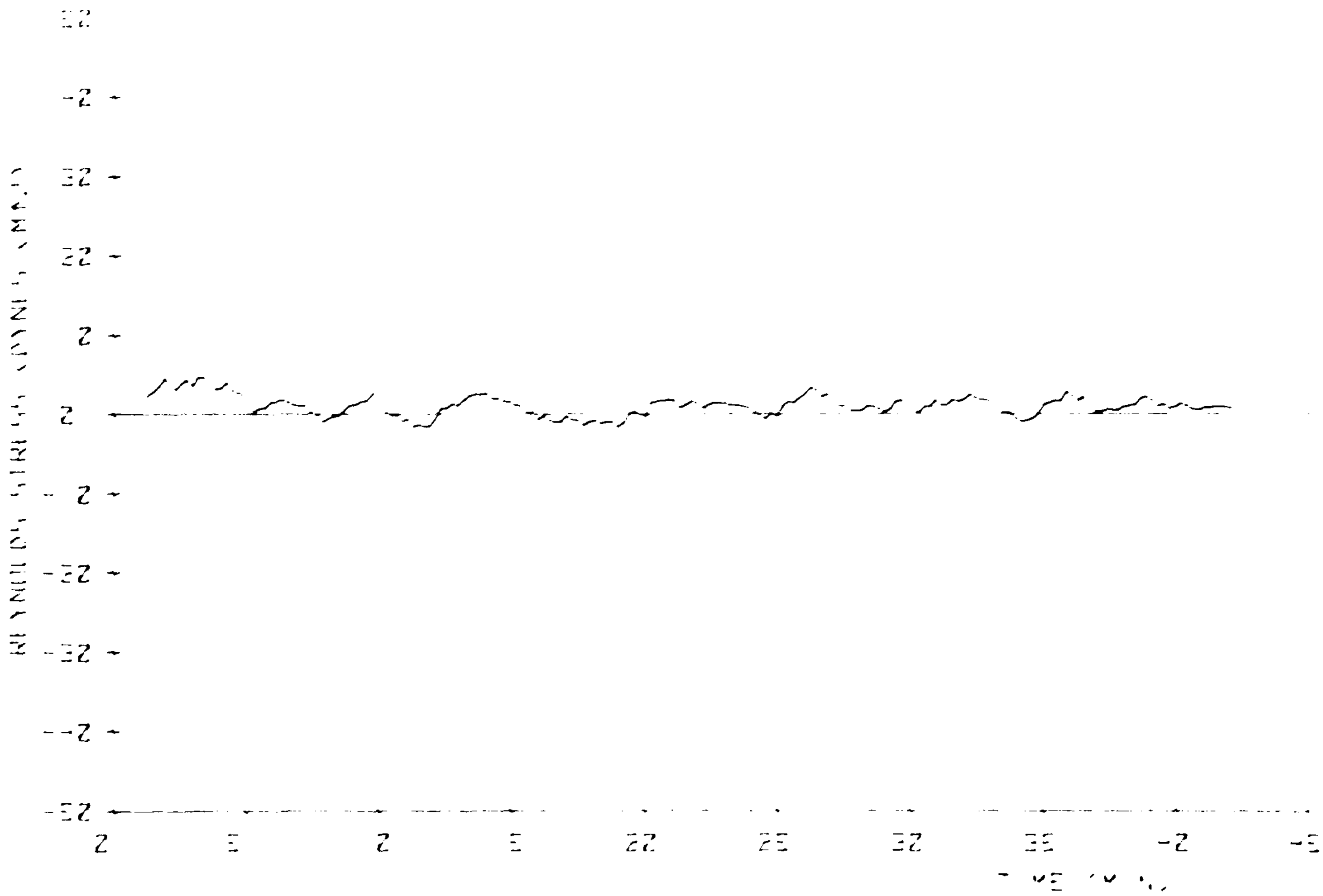

Figure 35: Filtered data of the Reynolds stress estimates for [illegible]

WAVTOP 012

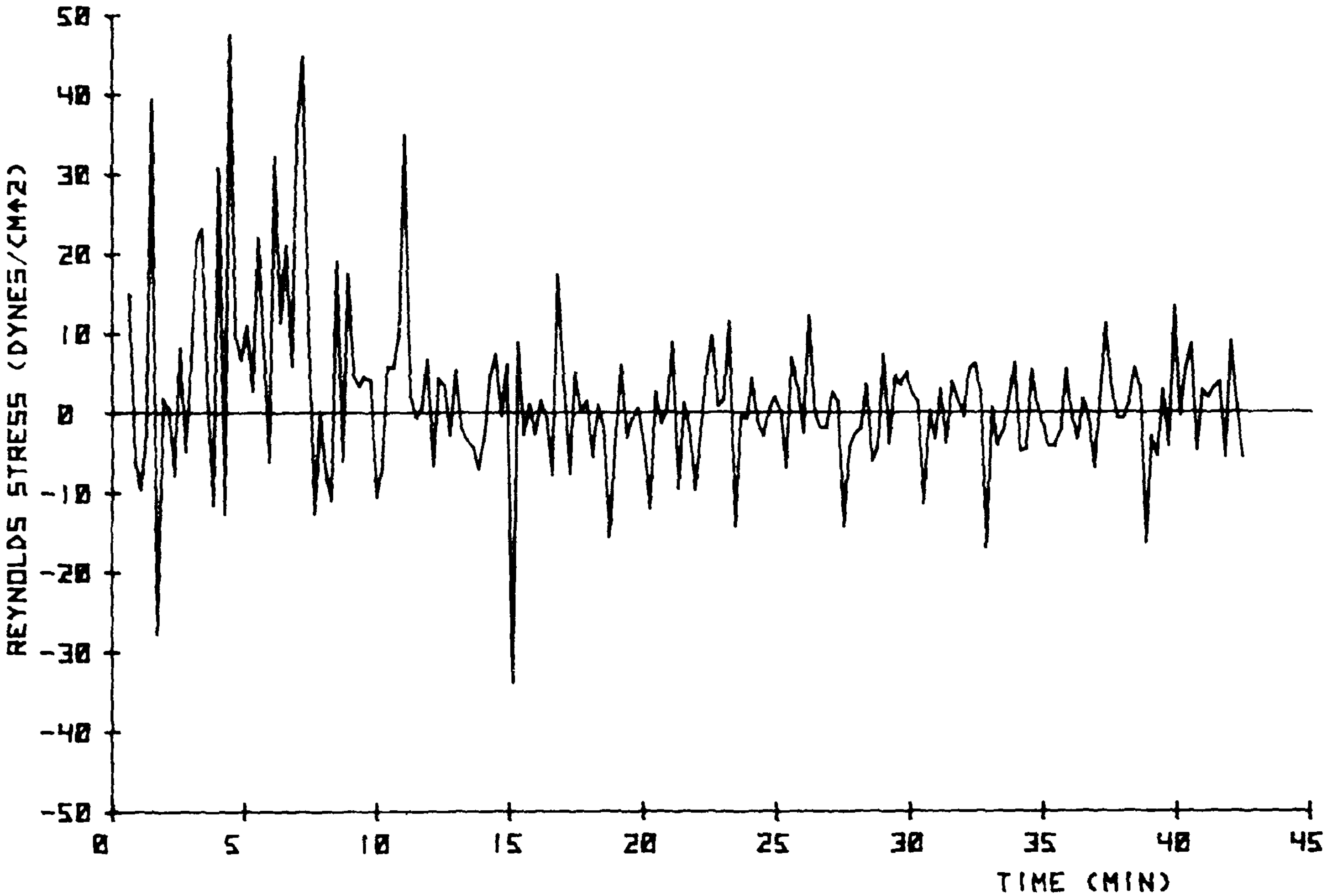

Figure 36: Raw data of the reynolds stress estimated for WAVTOP 012. The wind speed averages 6 m/s. For the entire record the mean stress was 1.52 dyne/cm^2 signifying downward momentum flux. Again as in WAVTOP 011 high frequency fluctuations in stress are registered.

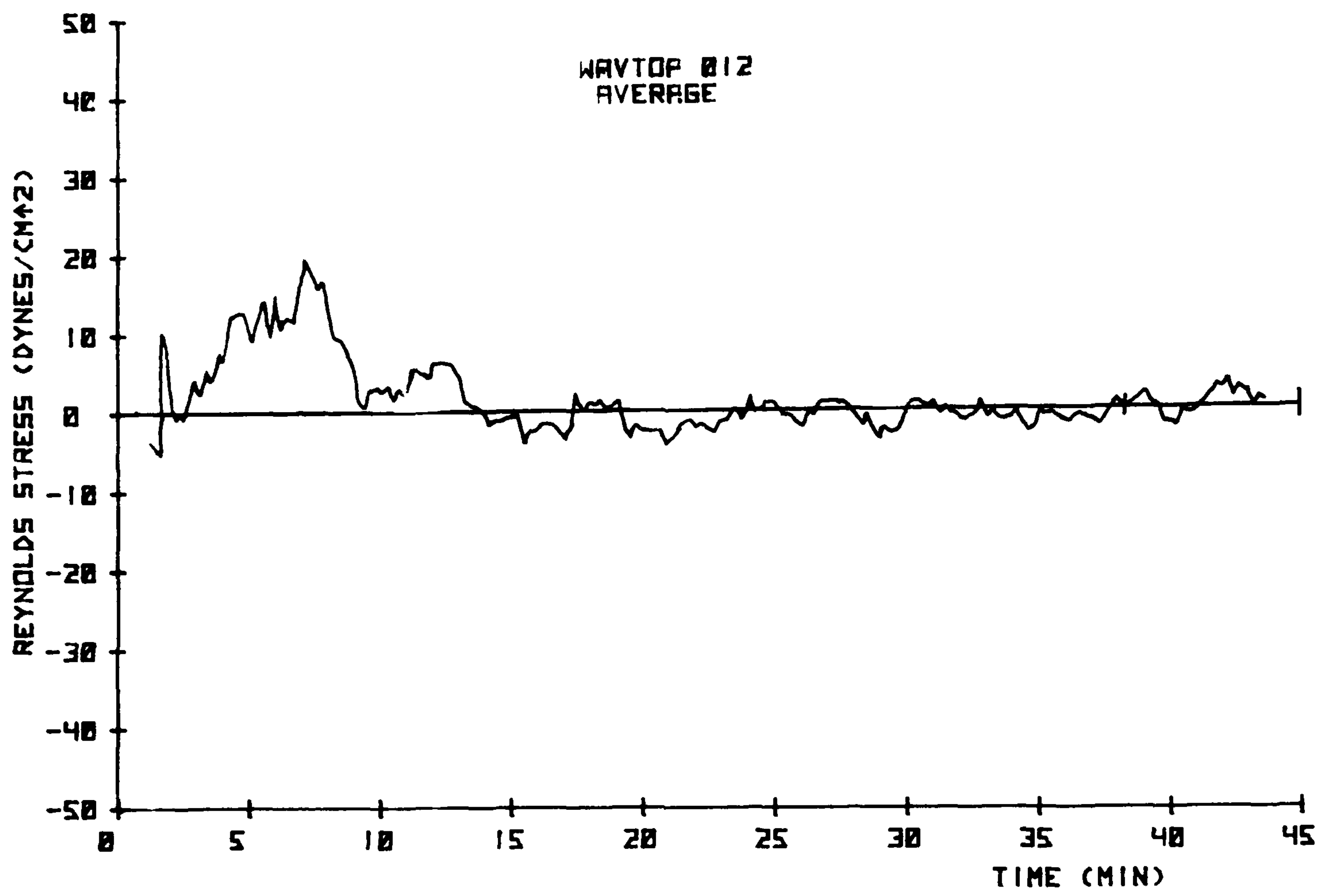

Figure 37: Filtered data of the Reynolds stress estimates for WAVTOP 012.

believed to be a non-linear function (roughly proportional to the square) of the wind speed,thus averaging values squared rather than averaging squared values,which further reduces the values (Shaw, Watts, and Rossby, 1978). Clearly though, it appears that the Reynolds stresses estimated are produced by the waves themselves and not by the fine structure high wave number turbulence.

VII. WHITECAP STUDIES

A. Background

We have established in Section III that, according to wave tank experiments, whitecaps in the presence of an oil slick appear instrumental in the vertical mixing of the oil through the free surface. This implies that the rate of mixing of oil should be related to the population of whitecaps present at a given instance (i.e., number per unit area or population density) and also possibly to total area of whitecapping observed (i.e., the average size of the whitecaps). Both of these statistics relate to the total energy input by the wind per unit sea surface area and hence the rate of energy dissipation in the generating wave spectrum. It is obvious that a whitecap observation program would be appropriate to accompany our wave measurements; such experiments however, must be conceived only in light of the results of previous whitecap studies.

There is a dearth of whitecap literature apparent in both theoretical and experimental areas. (This situation is underscored by the fact that Kinsman, in his extensive treatise on wind waves (1965), devotes apparently only a single comment to the subject, i.e., "(whitecaps) seem to be formed by wind blowing off the tops of the waves." Coincidentaly, one of the most thorough investigations of wind waves at short fetches and low wind speed was done in Chesapeake Bay by Kinsman (1960). Cinema photography of the wave profiles and whitecaps was planned to supplement the observations made from an array of wavestaffs mounted upon a fixed tower. Unfortunately, instrument problems prevented the photographic observations.

Cardone (1969) in his summary of whitecap observations renders the definition, i.e., "Whitecaps are manifestations of wave breaking, which may be thought of as a process whereby energy transferred through wave generation processes to spectral components that are fully developed is made unavailable

to wave motion." This energy "transfer" ostensibly from low wave number (i.e., wind wave) to high wave number (i.e., whitecaps and turbulence) motions is mainly due to an instability mechanism which, if associated with Miles (1965) and Phillips (1966) instability theories (pertaining to spectral growth of wind waves), is related to the stability of the atmospheric lapse rate (near the water). The transfer also must depend upon the spectra and hence, upon factors such as fetch and duration.

The few field observations of whitecaps made suggest the following:

1. Whitecaps appear to form when wind speeds exceed 5-6 m/s (Munk, 1955) and are associated with dynamic instability of air flow over the waves. Once formed, the whitecap population expands rapidly - maybe even as the square of the wind speed (Blanchard, 1963).

2. Observations in the North Atlantic (Cardone, 1969) indicate that with wind speeds (V) from 4-10 m/s the maximum areal fraction (%) covered by whitecaps (W) can be estimated by

$$W = 1.35 \times 10^{-3} V^{3.4} \quad (24)$$

(e.g., for V - 4 m/s, W = 0.15% and for V - 10 m/s, W = 3.4%).

3. Whitecaps persist longer in salt water than fresh water apparently because of the abundance of salts and organics which (in the ocean) tend to preserve bubbles and foam longer (Cardone, 1969). This may cause bias in estimates of whitecap population density obtained by photographic methods when comparing salt versus fresh water environments.

4. Whitecap coverage (i.e., production) for a given wind speed is higher for unstable than for stable lapse rates in the air column directly over the ocean (Cardone, 1969). This seems logical since in unstable conditions wind stress (momentum flux) should be enhanced, more strongly energizing the sea surface.

To give a physical feeling of whitecap phenomena, Figure 38 summarizes data (from Cardone, 1969) of the percentage of surface coverage by whitecaps over a wide range of wind speeds and air-sea temperature differences and stabilities. Superimposed are results of (Munk, 1955) and Blanchard, 1963). The scatter in fractional coverage is large at high speeds but there clearly appears a threshold of wind speed to produce whitecaps (i.e., 6-7 m/s). This brief discussion of whitecap phenomena suggests that if, in fact, the rate of surface oil mixing were strongly dependent upon the number of whitecaps per unit area or the percent coverage, then it is obvious from Figure 38 that the uncertainty especially at higher wind speeds might approach factors of two or even three. Clearly, we must enhance our understanding of whitecap production which at present lacks a theoretical base, but more importantly requires a solid data base.

Another factor for which we have heretofore not mentioned is the possible effects of an oil slick upon the production of whitecaps themselves. It is well known that a certain damping occurs at least of smaller waves by the presence of a surface oil slick, a phenomenon related to the alteration of surface tension (between oil, water and air interfaces). Field experiments are needed to examine the relation of whitecap density with the presence of different concentrations of surface oil.

B. Preliminary Experiments

During the course of the WAVTOP observations, preliminary studies were made of possible techniques of recording whitecaps. Personnel from Eastman Kodak, Rochester, NY were contacted for information about aerial photography of whitecaps. A special film "Linograph Shellburst", was recommended which is a high contrast (medium speed) with ASA-500.

Our desire was to analyze the photos for the number, percent of total area and intensity of whitecaps. Discussions were held with scientists

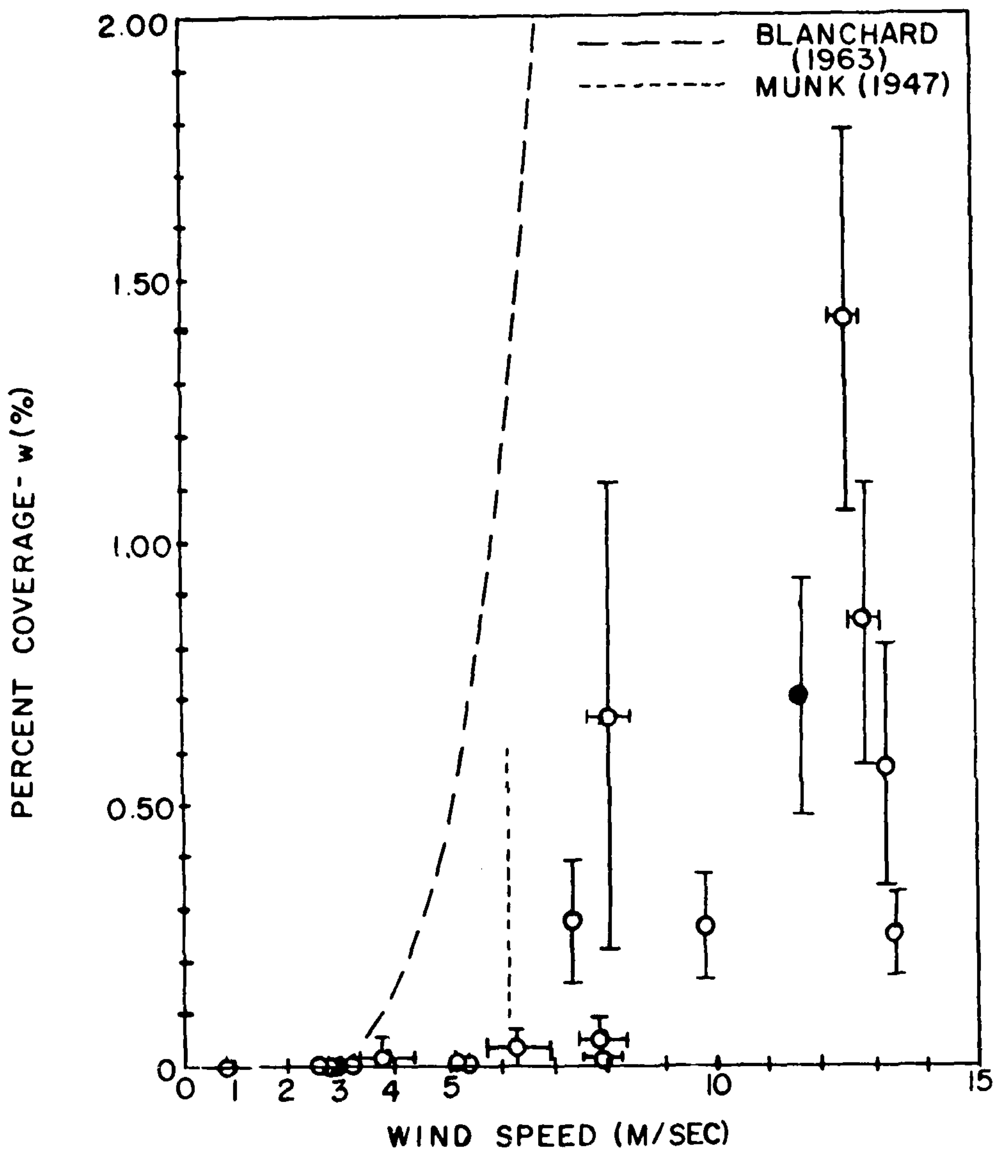

Figure 38: A summary (from Cardone 1969) of observations of percent whitecap coverage (w) versus wind speed. Black circles represent unstable lapse rate and open circles represent stable conditions. Superimposed are curves of Munk (1947) and Blanchard (1963) suggesting onset of whitecaps. (From Shonting, Petrillo and Temple 1979).

from ITEK, Cambridge, MA. We reviewed the possibility of using an optical densitometer to scan photographs to both map the locations and size estimate the whitecaps on each photo. The use of new automatic scanning densitometers were discussed. Plans were made to utilize optical densitemetric scanning devices available from NASA Goddard Space Flight Center, Green Belt, MD.

Aerial observations made at an altitude of about 600 m of whitecap populations were made from a 180 Cessna aircraft around Brenton Reef Light Station (41°25.6 N, 71°23.3 W) where the water depth is about 19 m. The photographs (Figure 39) were taken with a Tri-X Pan #6049-ASA-320 using red filters and with a Hasselblad Model 500 CM with an 80 mm lens. The photos show the crosshatched seas produced by 7.5-10 m/s (15-20 knots) southwest winds mixed with a slight swell from the southeast.

The Brenton Reef Light Station provides a Cartesian coordinate system. Here a count can be made at time intervals to provide density and coverage variation of whitecaps in a 40,000 m^2 area during WAVTOP observations. The tower legs at the lower crosspipe have about 12 m separation, providing a convenient measure for delineating a Cartesian grid as is shown.

Several aerial photos were also made using Kodak 2481 infrared film. Unfortunately, focusing was difficult because the reflex focusing adjustment was set for normal visible black and white film. The infrared film, however, appears to enhance the brightness of the whitecaps, possibly due to the warm air mixing in the foam radiating much more than the smooth sea surface between the whitecaps. It is clear that certain films created better visibility of whitecaps than others. Further in-flight practice could provide better techniques to optimize the whitehead clarity by taking advantage of azimuth, sun altitude, altitude of plane, type of film and filters used.

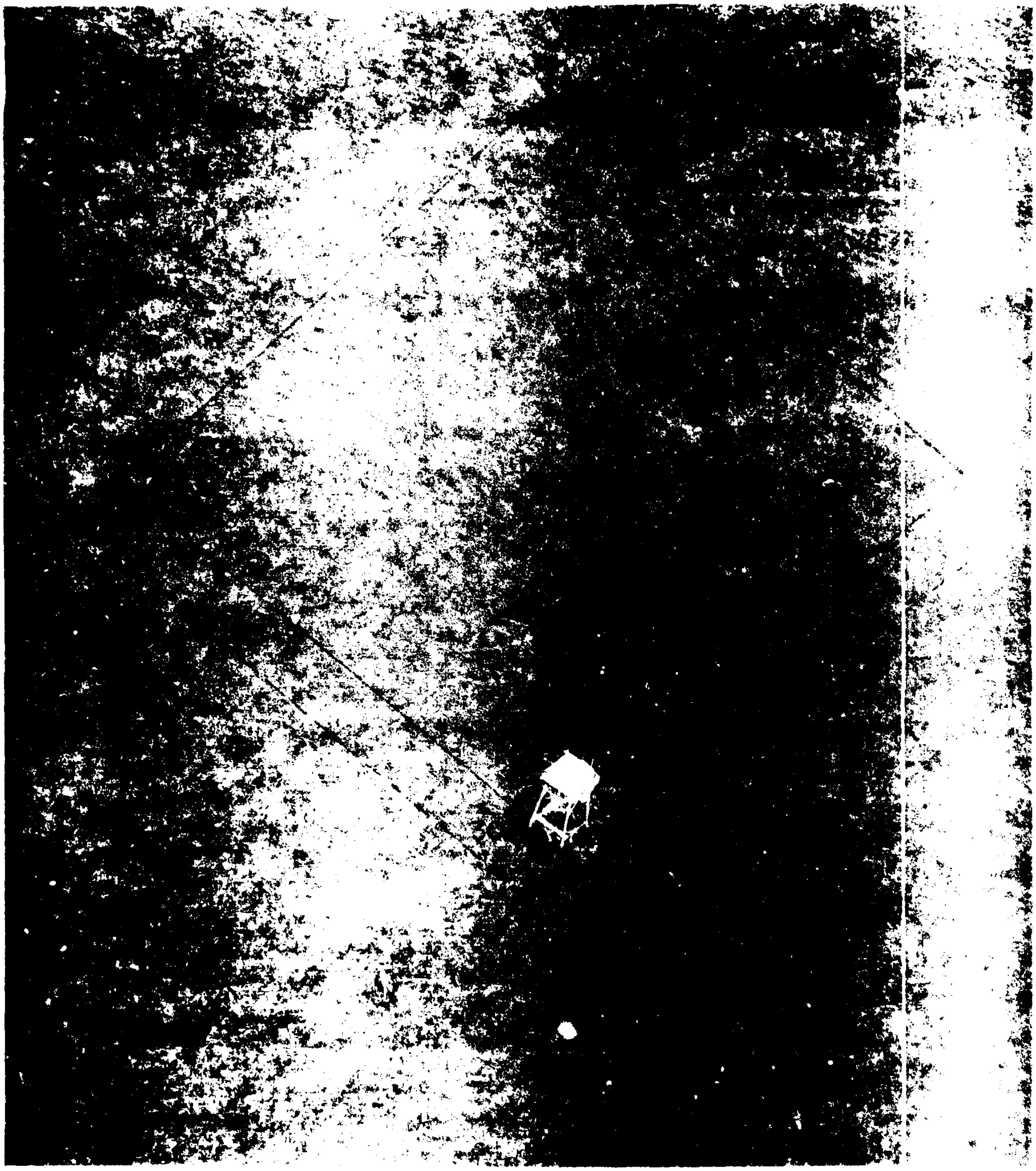

A final set of wave-whitecap observations were made using cinema photography. Records of time variation of whitecaps densities were made from Gould Island Pier. A preliminary experiment was performed to view a fixed area of Narragansett Bay looking due west of the pier. Time lapse movies were made from the roof of the pier building using a Bell and Howel 16 mm cinema camera (model 70-HR) positioned about 9 m above sea level and aimed at 30^{0} downward from the horizon (Figure 40). A time lapse Lafayette Motor System was used to make 1 s interval exposures, this interval allowing sequential viewing of changes since each whitecap has about a 3-5 s life span. This technique strikingly displayed the evolution of whitecap density as it follows the changing wind velocities.

Figure 40: The cinema photography [illegible] mounted for viewing the wave and whitecap field [illegible] of Gould Island. Unfortunately this day the [illegible] capping finished up early.

VIII. CONCLUSIONS

From the results of the Wind and Turbulence Observation Program the following can be concluded.

1. Review studies indicate oil slicks are mixed downward by breaking waves coupled with the subsurface wind wave and turbulent motions, the degree of vertical mixing being dependent upon whitecap density and the kinetic energy of the fluctuating subsurface motions. Both of these parameters are inherently associated with wind generated surface waves.

2. Equations were derived which define the balance of the time rate of change of mean and fluctuating kinetic energy relative to dynamic stress and pressure terms. These equations, when integrated vertically, provide a physical framework from which observed values of wave motions and dynamic pressure may be evaluated in terms of energy and momentum flux budgets associated with wind stress.

3. The Smithometer ducted impeller systems developed at the University of Washington mated with the NUSC developed microprocessor data logger (BLT) provide a tool to make a variety of observations of wave motion velocity, and with added available sensors, also can register free surface fluctuations and dynamic pressure.

The BLT system, when used in conjunction with the AESOP stable spar buoy, provides a sophisticated and unique self-contained data gathering system. The entire system, including buoy sections, damping disks, pressure cases, batteries and instruments, weighs less than 200 kg. The basic sensors, extensively calibrated in a ship towing tank, are capable of registering wave motion from 4 mm/s to 200 cm/s and velocity fluctuations up to a frequency of 5 Hz. The sensors can portray orbital motion and turbulent components having scales down to 10-20 cm and can resolve orthogonal velocity components to estimate Reynolds stresses in the wave

field.

The AESOP can be packed in 5 m sections for easy air freighting, and assembly time is of the order of one hour. Hence, the BLT/AESOP system can, at short notice, be flown anywhere in the world for oil spill or other pollution dynamics monitoring. An appropriately mounted BLT system can be used to make basic observations of dynamic motions both in sea surface and bottom geophysical boundary layers.

4. The BLT system has been used in Narragansett Bay mounted from the AESOP stable spar buoy and from the Gould Island pier facility on a 15 m extension boom.

Preliminary observations of wave motions show the exponential decrease of the vertical distribution of wave kinetic energy and the interrelationship of the total energy integral to the local wind and wave field. Further, the actual phase shift of energy flow from the surface indicates a downward speed of propagation of wind imparted kinetic energy of roughly 3-5 mm/s. Auto-spectra of the velocity records demonstrates the capability of the impeller sensors to both resolve and record the wave motions. Strong narrow spectral peaks of the ambient waves display the high monochromaticity of short fetch wind-generated waves. Finally, the BLT system has been used to observe orthogonal velocity pairs which were used to estimate the Reynolds stresses. Values ranging from 1-5 dyn/cm^2 indicate a proper downward momentum flux imparted by the wind at the sea surface.

5. Investigation was made of historical observations of whitecaps. Preliminary photographic and cinema studies were made to establish techniques of whitecap monitoring during further wave observations.

In conclusion, since the raw field data can be analysed to show the changes in these preliminary observations presenting results of kinetic

AD-A083 014 NAVAL UNDERWATER SYSTEMS CENTER NEWPORT RI F/G 8/3
THE WINDWAVE AND TURBULENCE OBSERVATION PROGRAM (WAVTOP). THE M--ETC(U)
MAY 79 MIPR-Z-70099-7-71825-A
UNCLASSIFIED USCG-D-68-79 NL

2 OF 2
AD
A083014

END
DATE
FILMED
5-80
DTIC

energy and spectra with depth, together with Reynolds stresses and their variation with surface wind and wave condition, the BLT system has been demonstrated as a valuable tool with which to measure and quantify the energetics of wind waves in the upper oceanic layer.

IX. RECOMMENDATIONS AND PLANS FOR FUTURE STUDIES

We now have a tested BLT/AESOP system for the measurement of the wind generated wave and turbulence parameters which govern the degree of vertical mixing of oil slicks. These preliminary results of the study of the wind generated kinetic energy content in the upper layer offer encouraging results. Further analyses of our present data set, improvement on our measuring technique and finally more observations will provide information on the important Reynolds stresses as a function of the local wind field and the sea state. These measurements should explore the relationship of the wave orbital motions to the momentum and energy transfer of the wind downward through the water column. Observations should be similar to those reported by (Shonting, 1971) and by (Cavaleri et al., 1977). A dynamic pressure sensor is planned to be added to the present Smithometer sensor systems and wave staff. With this array of systems, a step-by-step evaluation of the terms of energy equations can commence. Once the validity of the energy and stress relations is demonstrated, these parameters can be used to verify oil mixing models and theory.

A catalog of data is now required to obtain statistical samples of wave observations which can be related to wind energy input. Much more data is needed to fill out the curves of energy versus depth at different wind speeds, fetches, and duration. Open sea measurements must be made to enlarge the samples to cover higher wind speeds (up to 15-20 m/s) and larger waves (1-3 m wave heights).

Opportunities exist for making measurements on various platforms, namely:

1. Gould Island Facility for small wave amplitudes but rapid changing conditions of wave generation over short fetches.

2. Brenton Reef Light Station used for high sea conditions with

short crested steep waves from NW winds up to 15 m/s.

3. Oil rig platform WESTERN PACESETTER II has been offered for use by Shell Development Corp as a platform. With it moored at an open ocean station we can make wave measurements under a large variety of sea conditions associated with winds from 10-30 m/s.

4. The French Bouee Laboratoire (BOHRA II), recently moored in the Western Mediterranean. Has been utilized by NUSC for several Eulerian temperature experiments.

5. Wave Tower in the Northern Adriatic Sea off Venice is used to conduct measurements for CIESM Physical Oceanography Committee to study vertical pollution from surface slicks.

6. The R/V LIMNOS of the Canada Centre for Inland Waters will be the stage for observations planned for Lake Erie in summer and fall 1979.

This new data obtained under different wind and wave conditions will provide kinetic energy values to predict the typical energy levels as a function of wind speeds and sea states. Further experiments should be made in conditions which produce the minimum energy values necessary to mix oil downward against the buoyant forces.

Another technique of assessing wind stress on waves is under consideration, that of recording the ambient acoustic noise from 1 kHz associated with wind turbulence (i.e., pressure fluctuations) and also from spray of whitecapping. Work by Shaw, Rossby, and Watts (1978) has strongly suggested that noise is a direct manifestation of wind stress on the sea surface. As it turns out, the precise parameters measurable with the BLT system and a dynamic pressure sensor are thought to be responsible for much ambient noise generation in the sea (Wenz, 1971, and Yen and Perrone, 1979).

In order to face up to the real problem, actual on-site observations should be made of oil spills and of the ambient wind/wave conditions pre-

vailing. It is from data gathering, analysis and on-site observations that one can evaluate the best methods of oil spill contorl, their potential and limitations with respect to sea state conditions.

Ultimately, we should develop techniques to deploy the BLT-AESOP system in planned oil spills where actual measurements are being made of vertical mixing of oil. This data can thus be correlated with wind and wave data obtained from the BLT system. Figure 41 suggests and interesting, if not amusing, conglomerate of oceanographic activity needed to best monitor and analyze the time history of environmental conditions and of the actual spill. (Not shown in the Figure would likely be the armada of clean-up craft frantically trying to control and recover our spilled oil.)

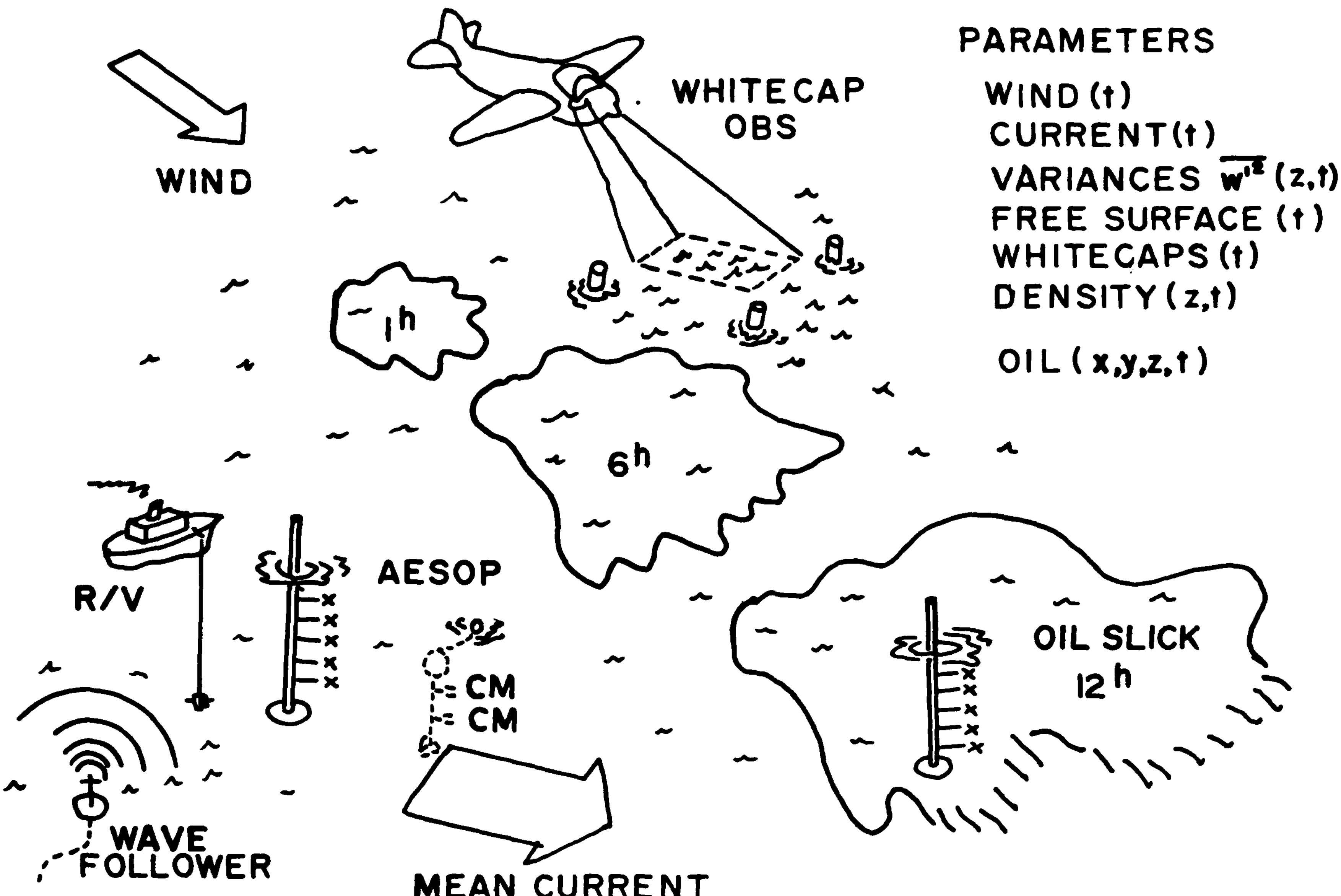

Figure 41: Intentional (or not) oil spill scenario observations. Research vessel (left) profiles temperature/salinity to obtain $\rho(z)$ and profiles oil droplet concentrations with bottlecasts and oil concentration with profiling fluorimeter. Wave follower system records surface waves to obtain spectra of sea and swell. The AESOP/BLT system records particle motions and dynamic pressure records, current meters (cm) define advecting motions of surface and bottom (subsurface floats reduce wave effects on mooring).

REFERENCES

Bendat, J.S. and Piersol, A.G., 1971. Measurement and analysis of random data. John Wiley & Sons Inc., New York, N.Y., 2nd Ed. 390 pp.

Blanchard, D.C., 1963. The electrification of the atmosphere by particles from bubbles in the sea. Progr. Oceanog., 1, 71-202.

Cardone, V.J., 1969. Specification of the wind distribution in the marine boundary layer for wave forecasting. Geophys. Sci. Lab. TR-69-1, New York University Dept. Metor. and Oceanogr. 131 pp.

Cavaleri, L., Ewing, J., and Smith, N., 1977. Measurements of the pressure and velocity field below surface waves. NATO Symposium: Turbulent fluxes, through sea surface. Wave dynamics and prediction. Ile de Bendor, France 12-16/Sep/77.

Denman, R., 1973. A time-dependent model of the upper ocean. J. Phys. Oceanog., Vol. 3, No. 2.

ENDECO, 1978. Measurement of dynamics of oil-in-water concentrations during the "AMOCO-CADIZ" oil spill. Data Report Environmental Devices Corporation, Marion, Massachusetts, 14 pp.

Hinze, J.O., 1959. Turbulence an introduction to its mechanism and theory, McGraw-Hill Book Co., New York, 586 pp.

Kinsman, B., "Surface waves at short fetches and low wind speeds - a field study." Chesapeake Bay Institute, Baltimore, Maryland (unpublished manuscript). Tech. Report XIX. 1960.

Kinsman, B., "Wind waves: there generation and propagation on the ocean surface," Prentice Hall, Englewood Cliffs, N.J., 1965.

Lin, J.T., Gad-el-Hak, M., and Ta-Liu, H., 1978. A study to conduct experiments concerning turbulent dispersion of oil slicks. Flow Research Corporation for the Department of Transportation (U.S. Coast Guard) No. 65 (DOT-CG-61688-A).

Miles, J.W., 1965. A note on the interaction between surface waves and wind profiles. J. Fluid. Mech., 22, 823-827.

Milgram, J.H., Donnelly, R.G., Van Houten, R.G., and Camperman, J.M., 1978. Affects of oil slick properties on the dispersion of floating oil into the sea. Massachusetts Institute of Technology (for U.S. Coast Guard) Report No. CG-D-64-78, 374 pp.

Munk, W.H., 1955. Wind stress on water: a hypothesis. Quart. J. Roy. Meteor. Soc., 81, 320-332.

Phillips, O.M., 1966. The dynamics of the upper ocean. Cambridge University Press, London., 261 pp.

Raj, P.K., 1977. Theoretical study to determine the sea state limit for the survival of oil slicks in the ocean. Arthur D. Little Corporation, Final Report No. CG-D-90-77, Task No. 4714.21, For the Department of Transportation (U.S. Coast Guard), 276 pp.

Shaw, P.T., Watts, D.R., and Rossby, H.T., 1978. On the estimation of oceanic wind speed and stress from ambient noise measurements. Deep Sea Res., Vol. 25. pp. 1225-1233.

Shonting, D., 1964. A preliminary investigation of momentum flux in ocean waves. Pure and Applied Geophysics, Vol. 57, No. 1, p. 149.

Shonting, D., 1967. Measurement of particle motions in ocean waves. Journal of Marine Research, Vol. 25, p. 152.

Shonting, D., 1968. Autospectra of observed particle motions in wind waves. Journal of Marine Research, Vol. 26, No. 1, p. 43.

Shonting, D., 1970. Observations of Reynolds stresses in wind waves. Pure and Applied Geophysics., Vol. 281, No. IV, p. 202.

Shonting, D. and Barrett, A.H., 1971. A stable spar-buoy platform for mounting instrumentation. Journal of Marine Research, 29/2:191-196.

Shonting, D. and Temple, P., 1978. The NUSC windwave and turbulence observation program (WAVTOP); a status report, from Marine forecasting, J. Nihoul, Ed., Elsevier Scient. Pub. Co., Amsterdam. pp 161-181

Shonting, D., Petrillo, A. and Temple, P., 1979. Windwave and turbulence observations related to oil mixing parameters. Workshop on the physical behavior of oil in the marine environment, Princeton Univ., Princeton, N.J., 8-9/May/79, pp. 663-690.

Smith, J.D., 1978. Measurement of turbulence in ocean boundary layers. Proceedings of a working conference on current measures. University of Delaware, Newark, Delaware, pp. 95-128.

Starr, V.P. and Newell, R., 1963. Pilot calculation of the flux of angular momentum in a spiral galaxy. Publ. Astron. Soc. Pacific, Vol. 75 pp. 239-247.

Starr, V.P., 1968. Physics of negative viscosity phenomena. McGraw-Hill Book Company, N.Y., 256 pp.

Sutton, O.G., 1953. Micrometeorology. McGraw-Hill Book Company, N.Y., 33 pp.

Wenz, G.M., 1972. Review of Underwater Acoustics Research: Noise. J. Acoust. Soc. Am., Vol. 51, pp. 1010-1024.

Yen, N.C. and Perrone, A.J., 1979. Mechanisms and Modeling of Wind-Induced Low-Frequency Ambient Sea Noise. NUSC Technical Report 5833, Naval Underwater Systems Center, Newport, RI, 34 pp.